SAPIENZA
UNIVERSITÀ DI ROMA

Use of Metamodels in Uncertainty Analysis of Concrete Arch Dams

Faculty of Civil and Industrial Engineering

Ph.D. in Structural and Geotechnical Engineering

Candidate
Rodrigo Rivero
ID Number 1724190

Supervisor
Prof. Rosario Gigliotti

September 2019

Use of Metamodels in Uncertainty Analysis of Concrete Arch Dams
Ph.D. thesis - Sapienza University of Rome

Author's e-mail: rodrigo.m.rivero13@gmail.com

This research has been conducted thanks to a grant provided by the ELARCH Project from the Erasmus Mundus Programm

To my wife Astrid, for all the care and patience during these long years,
and for all the happiness in those about to come

Abstract

Uncertainty analysis of large coupled systems, such as those formed by concrete arch dams, their reservoirs and surrounding foundations, is typically addressed with Monte Carlo simulations in literature. Although it is a robust method, the high computational effort required makes it impractical for everyday engineering. This research investigated the applicability of the so called *metamodels*, specifically of the Response Surface Method, as a more efficient alternative. The goal was to develop polynomial surrogate models that could estimate diverse structural responses with acceptable precision, allowing for uncertainty quantification at a much cheaper computational cost. For that end, two case studies located in Italian territory were taken into consideration, namely the *Lumiei* dam (cupola) and the *Pertusillo* dam (arch-gravity). Starting from original documentation, linear and non linear numerical models of both of them were developed. Cantilever joints were introduced in the non linear models, located in their real positions, and modelled with a hard-contact formulation. Material and rock foundation were considered as linear elastic materials. Dynamic interaction between the main structure and the reservoir was accounted for with the aid of acoustic finite elements. Their use and precision were evaluated in detail, comparing the method with classic approaches such as those of Westergaard and Zangar. Five Design of experiment techniques were adopted, and the resulting metamodels precision/ computational cost ratio analyzed. Finally, it was concluded that metamodels are a valid an efficient alternative for the task proposed, and furthermore can be used in other applied sciences as well.

Keywords: Arch dams, uncertainty, metamodels.

Contents

Figures

Tables

Nomenclature

g Gravitational acceleration.

t Time.

ρ Water density.

k Water bulk modulus.

P Water pressure.

P_{dyn} Hydrodynamic pressure in excess over hydrostatic pressure.

P_{sta} Hydrostatic pressure.

H Height of the dam.

u Vector of displacements along the x coordinate.

v Vector of displacements along the y coordinate.

x Horizontal Cartesian coordinate.

y Vertical Cartesian coordinate.

c Speed of sound in the water.

Q Resultant hydrodynamic thrust.

M Resultant hydrodynamic moment.

S Amplification factor of the resultant hydrodynamic thrust over the dam.

K Amplification factor of the hydrodynamic pressure at the lower point of the dam.

E_c Nominal elastic modulus of concrete.

E_{cm} Average elastic modulus of concrete.

f_{ck} Characteristic compression strength of concrete.

R_{ck} Characteristic cubic compression strength of concrete.

f_{ctm} Average tensile strength of concrete.

ρ_c Concrete density.

α_c Thermal expansion coefficient of concrete.

ν_c Poisson's ratio of concrete.

h Dimensionless elevation as a fraction of the dam height.

ω Imposed angular vibration frequency.

f Imposed vibration frequency.

T Imposed vibration period.

α Imposed vibration amplitude as portion of g.

f_s Resonant frequency of empty dam.

ω_w Angular resonant frequency of the reservoir.

Ω_w Dimensionless vibration frequency as portion of f_w.

Ω_s Dimensionless vibration frequency as portion of f_s.

L_e Length of the reservoir.

H_e Depth of the reservoir.

q_s Acoustic impedance of reservoir sediments.

α_s Wave reflection coefficient of reservoir sediments.

ρ_s Reservoir sediments density.

c_s Speed of sound in the reservoir sediments.

k_d Seismic coefficient.

ϕ Fluid velocity potential.

b Size of the water mass that influences dam behavior.

Q_0 Hydrodynamic thrust at the at the lower point of the dam.

M_0 Hydrodynamic moment at the at the lower point of the dam.

C_z Amplification factor of pressures in the theory of Zangar.

C_m Tilt coefficient in the theory of Zangar.

θ Inclination angle of the dam respect to the vertical.

Introduction

This document describes the process of a research work carried on as part of a Structural PhD course at the Sapienza University of Rome.

It is articulated in the following way: in Chapter 1, the problem of uncertainty valuation is described, its antecedents and the difficulties involved. The state of the art and international regulations related to dams assessment are carefully reviewed. Main difficulties related to dynamic simulation of large coupled systems are also revised. In Chapter 2 the methodology of the procedures followed, the applicability of the proposed method and its limitations are presented. In Chapter 3 the obtained results are reported and the reliability of metamodels is discussed, as well as the effect of different factors associated to the problem under study.

Two case studies were taken corresponding to two different dam typologies, *Lumiei* (arc dam) and *Pertusillo* (arc-gravity dam), both located in Italian territory. After developing numerical models for both, the Response Surface Method is successively applied to them in order to verify its adequacy and observe differences in their structural behaviour.

This research is part of a structural monitoring scheme for large dams, focusing on the dynamics of dam-reservoir systems. The aim is to develop a reliable and precise method that allows dealing with more complex problems arising from non-linear behaviour and aging of this type of structures.

Research Motivation

Dams have an important role in human society fulfilling a variety of functions, such as energy generation, flood regulation, water consumption and irrigation. According to the International Commision of Large Dams, *ICOLD*, over 45,000 large dams have been built worldwide [1]. The Italian normative for dams and water holding structures, *"Norme tecniche per la progettazione e la costruzione degli sbarramenti di ritenuta"* (NTD14) [2], defines "Large Dams" as those of at least 15 m height or $1 \times 10^6\,\mathrm{m}^3$ of reservoir volume. There are over 500 of them on Italian territory, most of which were designed and built more than 50 years ago using empirical formulas and static deterministic analysis, applying the structural knowledge of the time. Given the severe operating conditions, both the main dikes and their complementary facilities are subjected to a process of deterioration that must be properly monitored. A failure event of a dam of significant size, entails extensive economic and life losses, as well as ecosystem damage. In that sense, a National Law issued in 2004 [3] establishes that the structural performance of all large dams must be examined in the light of the new seismic territory classification.

Structural analysis of water holding structures is a complex task. Throughout their long lifespan, they are subjected to a wide range of chemical and physical phenomena that may occur simultaneously. For this reason, traditionally dikes performance assessment is accomplish through numerical multhi-physics deterministic analysis. Extensive research related to the efficiency and precision of these techniques has been carried out in the structural engineering field in recent years. Particularly, dams response is highly influenced by non-linear mechanisms that arise from geometric discontinuities and material behaviour. In top of that, both the environmental actions and the structure characteristics themselves can change over time. This variability have been accounted for trough reliability analysis, using a large number of deterministic simulations to estimate the probability of failure of the structure. However, the computational cost associated with this approach is so high that makes it practically impossible for everyday engineering.

This thesis focuses on the applicability of an alternative approach for the evaluation of uncertainties related to structural assessment of arch dams. The concept of *Metamodeling* have been introduced on the context of probabilistic engineering design. Applied to the topic under study, the basic idea is to establish a mathematical structure that can estimate the responses of the structure with an acceptable precision, employing a much lower computational effort than the finite element technique would. Once this is achieved,

probabilistic analysis can be performed on the metamodel instead of the original numerical model, thus reducing by several orders of magnitude the amount of time needed to asses the reliability of dams.

The procedure for validating metamodels requires a high number of deterministic simulations. This leads to the second main objective of this research, namely the study of critical aspects related to simulation of large water-structure coupled systems, with the goal of developing numerical models of optimized precision/ computational cost ratio, which are essential in the present investigation.

To the best of the authors knowledge, there is only one previous research focused on the applicability of mathematical metamodels for uncertainties valuation in the dam field. Hariri-Ardebili and Amin [4] analyzed a gravity dam with linear behaviour, using surface metamodels and considered the uncertainties distribution of several material parameters and characteristic values of seismic ground motions. However, there are other examples of the use of the metamodeling technique for civil structures in literature. These previous work will be referenced to for the problem under study.

1. State of the art

1.1 Uncertainties in Dam Engineering

In this section, basic concepts relevant to the subject under study are presented as introduction to the state of the art. Most of the information presented is extracted from the book [5] dedicated to Probabilistic Design.

Uncertainty refers to imperfect and/or unknown information, related both to input and output data of a given system. In the Structural Engineering field, input is conformed by all the external and internal phenomena (known also as *stressors*) that can affect the output data, i.e. dam response. There are 2 main sources of uncertainty:

- **Aleatory** or **stochastic** uncertainty, linked to the intrinsic randomness of nature processes. E.g.: Earthquakes events (intensity, duration time, return period), hydrological events (rain intensity, return periods, run-off coefficients), temperature variation, etc. Aleatory uncertainty is irreducible.
- **Epistemic** uncertainty, originated from the lack of information about the system, given that characterization processes are imperfect (measurements, laboratory tests). E.g.: Material properties, geometry of the structure, joints positions, etc. Epistemic uncertain can be reduced, acquiring more knowledge and collecting more data.

  Model uncertainty, is an special kind of epistemic uncertainty, associated to the use of mathematical models to simulate physical phenomenon. E.g.: Validity of assumptions, numerical approximations, precision of CPU round calculations, etc.

It is known that uncertainty cannot be accounted for in a comprehensive way through classical deterministic analysis, as they only provide the

response of the structure for a unique set of material parameters and stressors. For this reason, concepts and techniques that were originally developed in the context of Probabilistic Engineering Design will be used for uncertainty modelling of existing dams. These ideas will be described briefly in the following paragraphs.

1.1.1 Basics of random variables theory

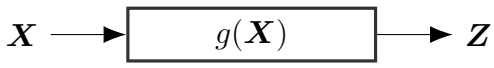

Fig. 1.1: Generic engineering system

Let $\boldsymbol{X}$ be a vector of input variables, and $\boldsymbol{Z}$ a vector of output variables of a given system, represented in Figure 1.1. Its *performance function* $g(\boldsymbol{X})$, transforms $\boldsymbol{X}$ into $\boldsymbol{Z}$.

In the context of the problem under study, $\boldsymbol{X}$ can contain both stressors and model parameters (temperature, module of Young of concrete, water level, etc.), and $\boldsymbol{Z}$ the responses of the structure, which from now on will be referred as *Engineering Demand Parameters (EDPs)*. In general, the performance function is not known as it does not have a closed form formula, given the complex behavior of large coupled systems under multi-physics phenomena. For this reason, the numerical simulation techniques typically used are described as *black box* models.

According to the theory of functions of random variables, any $g(\boldsymbol{X})$ that accepts random input variables will produce random output variables as well. The task of Uncertainty modeling is to quantify the uncertainty of the performance function of an engineering system, given the uncertainty of its inputs. In practice, this translates into determination of the probabilistic characteristics of $\boldsymbol{Z}$ provided those of $\boldsymbol{X}$.

Two fundamental concepts associated to probabilistic frameworks are *Population* and *Sample*. The former is defined as any entire collection of objects of interest and which data may be collected from. It is also known as a *universal set*. Because often a population is too large to study in its entirety, usually a group of units is selected from it and used to draw conclusions about the original set. This is called a sample. The fundamental requirement for sampling is that every group extracted should be representative of the general population. This is generally best achieved by random sampling.

The probabilistic characteristics of a population can be described by the following functions:

- Probability density function (PDF).
- Cumulative distribution function (CDF).

The PDF describes the chance property of a random variable. If the PDF of a random variable X is represented with f, then $f(x)dx$ is the probability of the value of X to be located in the interval $[x, x + dx]$. Probability of X over a finite interval $[a, b]$ can be determined by:

$$P(a \leq X \leq b) = \int_a^b f(x)dx \tag{1.1}$$

Also, a PDF of a continuous variable satisfies the condition

$$\int_{-\infty}^{\infty} f(x)dx = 1 \tag{1.2}$$

which reflects the capability of X of taking any real value.

The CDF, represented here with F, is defined as the probability of X of being less than or equal to a constant a. So:

$$F(x) = P(X \leq a) = \int_{-\infty}^{a} f(x)dx \tag{1.3}$$

The relationship between PDF and CDF is defined by:

$$f(x) = \frac{d[F(x)]}{dx} \tag{1.4}$$

For convenience, usually moments of PDF and CDF are use for describing a variable distribution. The most common are *mean* and *variance*.

Mean is defined as the first moment measured about the origin:

$$\bar{m}_X = \int_{-\infty}^{\infty} xf(x)dx \tag{1.5}$$

if there are n observations (samples) of the random variable X, $(x_1, x_2, ..., x_n)$, the sample mean is the average of the observations:

$$\bar{X} = \frac{1}{n}\sum_{i=1}^{n} x_i \tag{1.6}$$

As the sample size increases, the sample mean $\bar{X}_i$ converges to the population mean $\bar{m}_X$. This implies that the sample mean can be used to estimate the population mean.

Variance is the second moment about the mean. It indicates how the individual measurements scatter around it. It is defined as:

$$\bar{s}^2 = \int_{-\infty}^{\infty} (x - \bar{m}_X)^2 f(x) dx \tag{1.7}$$

when there are n observations, the variance of sample is:

$$s^2 = \frac{1}{n-1}\sum_{i=1}^{n} (x_i - \bar{X})^2 \tag{1.8}$$

Again, as the value of sample variance will converge to population variance when n approaches infinity. The square root, known as the *Standard deviation*, is widely used as its interpretation is straight forward, since it has the same unit of measure as the variable.

Furthermore, the *median* of a population is the point that divides the distribution of the random variable in half. This implies that half of the measurements in a population will have values that are equal to or larger than the median. At the median, the CDF of a variable is 0.5.

A *percentile* value X_a is defined as a value below which probability of the values less than X_a of the random variable is a. I.e.:

$$P(X \leq X_a) = F(X_a) = \int_{-\infty}^{X_a} f(x) dx = a \tag{1.9}$$

1.1.2 Functions of several random variables

When two or more random variables are being considered simultaneously, their joint behavior is determined by their joint probability distribution function.

Let X and Y be two random independent variables. The joint CDF of both is defined as:

$$F_{X,Y}(x,y) = P(X \leq x, Y \leq y) = \int_{-\infty}^{x}\int_{-\infty}^{y} f_{X,Y}(x,y)dxdy \tag{1.10}$$

And the joint PDF:

$$f_{X,Y}(x,y) = \frac{\partial F_{X,Y}(x,y)}{\partial x \partial y} \tag{1.11}$$

If the joint PDF is known, the individual PDFs, called *marginal* PDFs, can be obtained:

$$f_X(x) = \int_{-\infty}^{\infty} f_{X,Y}(x,y)dy \tag{1.12}$$

and,

$$f_Y(y) = \int_{-\infty}^{\infty} f_{X,Y}(x,y)dx \tag{1.13}$$

Similar to the variance of a single random variable, the *covariance* of two random variables, denoted as $Cov(X,Y)$, is the second moment about their respective means $\bar{m}_X$ and $\bar{m}_Y$.

$$Cov(X,Y) = \int_{-\infty}^{\infty}\int_{-\infty}^{\infty} (X-\bar{m}_X)(Y-\bar{m}_Y) f_{X,Y}(x,y)dxdy \tag{1.14}$$

The covariance provides a measure of how the random variables are linearly correlated, and it hence indicates the linear relationship between them. The derived dimensionless quantity *correlation coefficient* is given by:

$$r_{X,Y} = \frac{Cov(X,Y)}{s_X s_Y} \tag{1.15}$$

Values of $r_{X,Y}$ range between -1 and 1, with following interpretation:

- $r_{X,Y} = 0$ there is no linear relationship between X and Y.
- $0 < r_{X,Y} < 1$ there is a positive relationship between X and Y, when X increases, so does Y.
- $-1 < r_{X,Y} < 0$ there is a negative relationship between X and Y.
- $r_{X,Y} = 1$ there is a perfect positive linear relationship between X and Y, Y increases linearly with X.
- $r_{X,Y} = -1$ there is a perfect negative linear relationship between X and Y, Y decreases linearly with X.

Considering a function of several random variables, $\boldsymbol{Z} = g(X_1, X_2, ..., X_n)$, if the joint PDF of $\boldsymbol{X} = (X_1, X_2, ..., X_n)$ is $f_{X_1,X_2,...,X_n}(x_1, x_2, ..., x_n)$, then the CDF of g is given by:

$$F_Z(z) = P(Z \leq z) = \int_{x_1}^{x_1+dx_1} ... \int_{x_n}^{x_n+dx_n} f_{X_1,X_2,...,X_n}(x_1, x_2, ..., x_n) dx_1 dx_2 ... dx_n \tag{1.16}$$

Additionally, if all random variables are independent,

$$f_{X_1,X_2,...,X_n} = \prod_{i=1}^{n} f_{X_i}(x_i) \tag{1.17}$$

Replacing the independent variables $X_1, X_2, ..., X_N$ in Equation 1.16, the complete CDF of the performance function can be obtained, and from it other probabilistic characteristics. For a general non-linear function $g(\boldsymbol{X})$, the integration boundary is non-linear as well. Given that multidimensional integration is involved, it is in general very difficult and often impossible to use the above equation to obtain the CDF of the response variable. In the context of this research, the performance function (Finite Element Analysis) is a black box and a closed form of $g(\boldsymbol{X})$ is not available.

1.1.3 Approximate probability integration

As explained on the previous section, the primary task of Uncertainty analysis is to find the probabilistic characteristics of the output responses, or EDPs, given those of the input variables. Because direct integration of the jointed CDF equation is not possible in general, numerical approximation methods have been developed. There are three categories of them.

The first originated from structural reliability analysis. In the design context, *Reliability* is the probability of a product performing its intended function over its period of usage, and under specified operating conditions. In the structural context, it is defined as the probability of a structure to not exceed a defined Limit State (LS) of performance. When the performance function $g(\boldsymbol{X})$ reaches certain threshold, the state of the structure changes, from one LS to another. If this threshold is defined as LS_i, then $\boldsymbol{Z} = LS_i$ divides the random variable space into safe and failure (or unsafe) regions. Because of this, performance function is also called a limit-state function. For convenience, a threshold of zero is usually used. In that case, the limit state function becomes $g(\boldsymbol{X}) - LS_i$.

Then, Reliability is expressed by:

$$R = P(g(\boldsymbol{X}) - LS_i) \leq 0) \tag{1.18}$$

and the *Probability of failure*:

$$p_f = 1 - R = P(g(\boldsymbol{X}) - LS_i) > 0) \tag{1.19}$$

Two of the most commonly used methods for approximating the probabilistic integral are the First Order Reliability Method and the Second Order Reliability Method. They operate simplifying the performance function and transforming the integration boundary, thus reducing the difficulty of straight integration. Nevertheless, this methods are not applicable for the problem under study in this research, since $g(\boldsymbol{X})$ is not known.

1.1.4 Monte Carlo Simulation

The second category corresponds to the Monte Carlo Simulation (MC), which is a widely used numerical scheme. The process involves performing random sampling of the input variables, according to their distributions, and conducting a large number of experiments on them. After the outputs are observed, conclusions about $\boldsymbol{Z} = g(\boldsymbol{X})$ can be drawn based on statistical inference. Three steps are required in the process:

1. Sampling random input.
2. Evaluating model input.
3. Statistical analysis on model output.

The purpose on sampling in the input random variables X is to represent distributions of the of input CDFs. There are two steps involved for this purpose:

1. Generation of random variables that are uniformly distributed between 0 and 1. Normally this is performed with computer algorithms. Variables generated in this way are called *pseudo-random* numbers.
2. Transforming the samples of the previous step into values of random variables X_i that follow given distributions $f_{X_i}(x_i)$. This is a numerical transformation.

In the context of this research, evaluation of the sampled inputs are to be carried out through finite element simulations. Assuming that there are N samples, simulations yields N deterministic points of $\boldsymbol{Z}$.

The final step is the extraction of probabilistic information of output variables.

The mean:

$$\bar{Z}_i = \frac{1}{N}\sum_{i=1}^{N} z_i \tag{1.20}$$

The variance:

$$s_z^2 = \frac{1}{N-1}\sum_{i=1}^{N}(z_i - \bar{Z})^2 \tag{1.21}$$

If failure is defined by the event $g \geq 0$, the probability of failure is:

$$p_f = \int_{\boldsymbol{x}}^{\boldsymbol{x}+\boldsymbol{dx}} f_{\boldsymbol{X}}(\boldsymbol{x}) d\boldsymbol{x} \tag{1.22}$$

where $\boldsymbol{X}$ encloses all the input variables $X_1, X_2, ..., X_n$ and $\boldsymbol{x}$ contains the corresponding space variables $x_1, x_2, ..., x_n$.

The equation can be rewritten as

$$p_f = \int_{-\infty}^{\infty} I(\boldsymbol{x}) f_{\boldsymbol{X}}(\boldsymbol{x}) d\boldsymbol{x} \tag{1.23}$$

where I is an indicator function, defined as

$$I(\boldsymbol{X}) = \begin{cases} 1, & \text{if } g(\boldsymbol{x}) > 0 \\ 0, & \text{otherwise} \end{cases} \tag{1.24}$$

According to 1.5, the integral of the right side of 1.23 is equal to the expected value or average of $I(\boldsymbol{X})$. Therefore, p_f can be estimated by the average value of $I(\boldsymbol{X})$:

$$p_f \approx \bar{I}(\boldsymbol{X}) = \frac{1}{N} \sum_{i=1}^{N} I(\boldsymbol{X}) = \frac{N_f}{N} \tag{1.25}$$

where N_f is the number of samples that have performance function less than or equal to zero, i.e. $g > 0$.

Reliability can be estimated by

$$R = 1 - p_f = \frac{N - N_f}{N} \tag{1.26}$$

Similarly to the calculation of p_f, CDF is given by:

$$F_Z(z) = P(g \leq z) = \frac{1}{N} \sum_{i=1}^{N} T(x_i) \tag{1.27}$$

where:

$$T(\boldsymbol{X}) = \begin{cases} 1, & \text{if } g(\boldsymbol{x}) \leq z \\ 0, & \text{otherwise} \end{cases} \tag{1.28}$$

PDF can be obtained by numerical differentiation of CDF.

Accuracy of Monte Carlo Simulation depends on the number of simulations N. The higher the number of simulations is, the more accurate the estimate will be. As the number of simulations N approaches infinity, the solution of Monte Carlo simulation will converge to the true probability that is under estimation. The percentage error of the estimate of the probability failure is given by:

$$e = u_{1-a/2}\sqrt{\frac{(1-p_f^r)}{Np_f^r}} \tag{1.29}$$

where p_f^r is the true value of the probability of failure. The equation gives the error under the $(1-a)$ confidence. It indicates that there is a probability of $(1-a)$ for the p_f^r to be in the range $p_f \pm ep_f$.

Experience indicates that Monte Carlo method is a robust computational method. Yet, the required number of samples is often so high that it makes its applicability for large coupled systems not feasible. For this reason, focus will be put in alternative sampling methods, in an attempt to reduce the amount of inputs required to estimate the properties of Y.

1.1.5 Reductive sampling techniques

Several techniques were developed to reduce the number of simulations required by MC method. Three of them will be analyzed in this research.

The first of them is the *Latin Hypercube Sampling* (LHS). It is based on a problem studied by Leonard Euler, which consists on calculating in how many ways Latin letters can be arranged in a matrix, under the condition that each letter appears once and only once on each column and row. The Hypercube is the generalization of this concept, for an arbitrary number of dimensions. Thus, every sample is the only one for each variable axis in the hyperplane containing it. Unlike MC, each sample point generated by LHS depends on the previously generated points. The first algorithm for the procedure was first described by McKay [6].

The other two are the low discrepancy sequences developed by Halton in 1964 [7] and Sobol in 1967 [8]. Their scope is to reduce the high dispersion obtained by random sampling, covering the design space more uniformly and thus requiring less data points to do so.

1.1.6 Metamodeling

Assuming that there is a precise but unknown relationship between the input vector $\boldsymbol{X}$ and the output a generic system $\boldsymbol{Z}$, in the form of:

$$\boldsymbol{Z} = g(\boldsymbol{X}) + \epsilon \tag{1.30}$$

where ϵ refers to the noise with zero mean and variance σ^2.

As the evaluation of the performance function is computationally expensive, for an uncertainty analysis purpose a simplified version can be created to replace it.

A *metamodel*, *surrogate model*, or model of a model, is then a mathematical approximation of the implicit simulation code. It represents a closed form function of the input parameters. If the metamodel is symbolized with $\tilde{g}$, then the objective is to minimize the error of its estimations, expressed as:

$$E = (\boldsymbol{Y} - \tilde{g}(\boldsymbol{X}))^2 \tag{1.31}$$

Construction of metamodels have three steps:

1. Design of experiments
2. Metamodeling
3. Modeling fitting

There are multiple techniques in every step involved. Each combination of them refers to a specific metamodeling environment. The most used are the *Response Surface Method*, *Kriging*, *Inductive learning* and *Neural Networks* with *Machine Learning algorithms*. This research will investigate the applicability of Response Surface metamodels.

1.1.6.1 Design of experiments

In this step, the basic idea is to perform a number of experiments (numeric simulations) at different design points (or inputs), and then use the corresponding outputs to fit the simplified surrogate model. This process is called Design of Experiments (DOE), or more precisely, Computer Design of Experiments. Once a surrogate model is established, the uncertainty analysis methods such as Monte Carlo Simulation, FORM, and SORM, etc. can be applied for uncertainty analysis.

There are several tasks in DOE, including identifying design points where the experiments will be performed, and solving the unknown coefficients of the surrogate model. Generally, metamodels that can accurately represent the original function with a small number of experiments are favourable. There are some principles that govern DOE procedures. Ronald Fisher described these principles in his book *The Design of Experiments* in 1935 [9].

There are three central concepts related to DOE:

- Factors: Input variables that influence the output. There are different categories of them, the primary factors impact the response in a relevant manner, the secondary factors do not.
- Design space: Range of variability of each factor.
- Levels: Amount of discrete points of each factor that are to be considered in the DOE process.

There exist diverse DOE techniques. They differentiate on the combination of the three characteristics above cited. Those investigated in this research will be described next.

1.1.6.2 Full Factorial Design

Full Factorial Design (FFD) is the most common and intuitive technique. It takes every possible permutation of each level of each factor. Usually it is performed with two or three level of them. If L represents the number of levels, and k the number of factors, then the sample size is:

$$N_{DOE} = L^k \tag{1.32}$$

FFD is an orthogonal method, because the scalar product of the columns of any two factors equals zero. Two level FFD, represented in Figure 1.2 allows for a multi-linear polynomial interpolation, while three level FFD, depicted in Figure 1.3 allows for a multi-quadratic form.

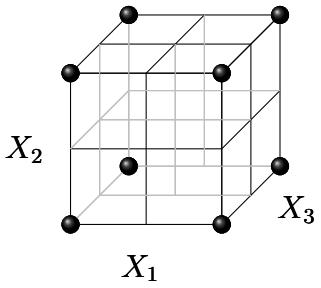

Fig. 1.2: Two level Full Factorial Design for 3 variables

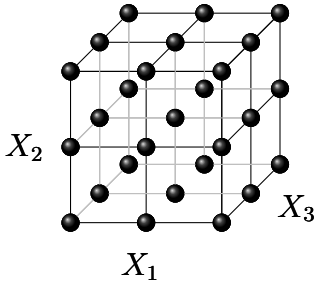

Fig. 1.3: Three level Full Factorial Design for 3 variables

1.1.6.3 Box-Behnken experimental design

The Box-Benhken experimental design (BBED) [10] is an incomplete three levels FFD. It takes the combination of all possible two-factor, two-level, full-factorial designs, with, for each 2^2 design, all other factors held constant at the reference point, plus one or more center points. In this way, this method allows an estimation of quadratic therms of a response surface. The authors of the method gave special tables for its application. [11]. The number of required experiments are resumed in the Table 1.1. The distribution of sample points for three variables is depicted in Figure 1.4.

1.1.6.4 Central Composite Design

Central composite design (CCD) utilizes three sets of experimental points:

k	N_{DOE}
3	13
4	25
5	41
6	49

Table 1.1: Number of experiments required by the Box-Behnken experimental design

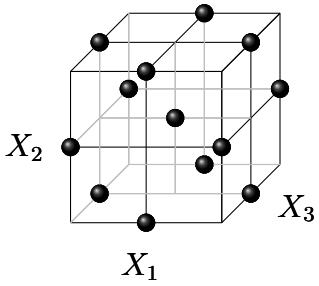

Fig. 1.4: Box-Behnken Design for 3 variables

- Two level fractional factorial.
- Center points, whose values are the medians of the values used on the previous set.
- Axial points outside the design space.

The goal of this technique is to estimate the curvature of the response function. The outside points are taken symmetrically respect to the center of the design space. Figure 1.5 depicts the distribution of sample points. The amount of experiments required in this method are resumed in the Table 1.2. The distribution of sample points for three variables is depicted in Figure 1.5.

k	N_{DOE}
3	15
4	25
5	43
6	77

Table 1.2: Number of experiments required by the Central Composite Design

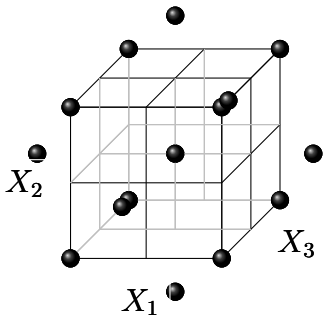

Fig. 1.5: Central Composite Design for 3 variables

1.1.6.5 Plackett-Burman experimental design

Plackett-Burman experimental design (PBD) [12] is a economical DOE with a number of experiments multiple of four. They are well suited for screening purposes, that is, for detecting the large effects factors. The goal is that each combination of levels for any pair of factors appears the same number of times. The number of experiments required is given by:

$$N_{DOE} = L + k - MOD(k, 4) \tag{1.33}$$

where MOD is the remainder of the division of k by 4. In this way, N is always a multiple of 4. The distribution of sample points for three variables is depicted in Figure 1.6.

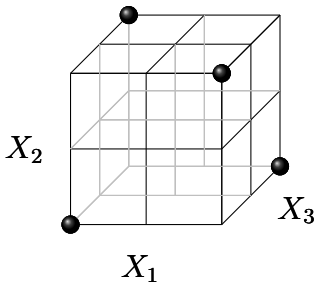

Fig. 1.6: Plackett-Burman Design for 3 variables

1.1.7 Response Surface Method

Response Surface Method (RSM) was introduced by George Box and his collaborators in 1951 [13]. The main idea is to use the outputs produced by experimentation at DOE established points, and then fitting the observed responses to the input data through a least squares approximation. The most common empirical models take either a linear form or quadratic form. A linear model with two factors, X_1 and X_2, can be written as:

$$Z = \beta_0 + \beta_1 X_1 + \beta_2 X_2 + \beta_{12} X_1 X_2 + \epsilon \tag{1.34}$$

where Z is a given EDP, for the given levels of the main factors X_1 and X_2, and the therm $X_1 X_2$ accounts for the interaction between them. ϵ is called the residual difference or error, obtained subtracting the observed responses from the predicted. The constant β_0, known with the name of *interception* therm, is the response of the metamodel when the inputs are 0. A linear model with three factors would be:

$$Z = \beta_0 + \beta_1 X_1 + \beta_2 X_2 + \beta_3 X_3 + \beta_{12} X_1 X_2 + \beta_{13} X_1 X_3 + \beta_{23} X_2 X_3 + \beta_{123} X_1 X_2 X_3 + \epsilon \tag{1.35}$$

A second order, quadratic model adds three more terms to the linear model, namely $\beta_{11} X_1^2 + \beta_{22} X_2^2 + \beta_{33} X_3^2$.

Frequently, the interaction effects are not considered in design purpose DOE applications, because the information they add is low for to the cost of experimenting.

RSM can be used with a number of objectives, such as:

- Response optimization
- Variability reduction
- Regression modelling

RSM has three important properties, namely:

- Orthogonality: Individual effects of each factor can be estimated independently, with a minimal noise of interaction effects. It implies for minimum variance, keeping the factors correlation to a minimum.

- Rotatability: Design points can be rotated around the center of the factors space. This allows for multiple combinations of factors levels, keeping a constant input distribution. Given that the experimenter does not have any prior information about the characteristics of the surface, a design that provides equal precision of estimation in all directions is desired.
- Uniformity: As a result of the first two properties, RSM estimation capability is uniform across the design space.

For convenience, factor and responses are coded before fitting the RSM. This kind of normalized factors is suited for efficient computer algorithms, specially for a high number of factors.

$$v_i = \frac{u_i - (u_i^U + u_i^L)/2}{(u_i^U - u_i^L)/2} \tag{1.36}$$

where u_i^U is the upper limit of the X_i factor, u_i^L its lower limit, v_i a generic value and x_i its coded value. The linear regression version of polynomial metamodels is:

$$z = \beta_0 + \sum_{i=1}^{m-1} \beta_i x_i + \epsilon \tag{1.37}$$

where m depends on the degree of the polynomial, through $n = (k + n)!/n!k!$ and β_i are the coefficients of the polynomial. In a matrix form:

$$\boldsymbol{Z}_{N\times 1} = \boldsymbol{X}_{N\times m}\boldsymbol{\beta}_{m\times 1} + \boldsymbol{\epsilon}_{N\times 1} \tag{1.38}$$

The unknown parameters can be estimated by least-squares regression method, minimizing the sum of squares of the differences between the observed and estimated outputs. From Equation 1.37 it becomes clear that the number of coefficients grows quickly with the degree of polynomial used to represent the RSM. Given that at the number of outputs required for fitting has to be at least equal to the number of unknown coefficients, a low degree polynomial is preferred in general.

1.2 Arch dams

In this section, concepts related to arch dams and their structural analysis will be introduced. The most important problems will be described and the corresponding state of the art will be revised.

Arch dams are constituted of an important mass of concrete with relatively few steel reinforcements within, built in a narrow cannon and supporting the water thrust and other external forces fundamentally through three structural mechanisms, i.e., an arch effect in the horizontal direction, and cantilever effect in the vertical direction, and a torsional diagonal effect. The combination of them allow to carry the forces to the rock foundations through the abutments.

1.2.1 Loads

Dams are subjected to a wide range of external and internal stressors within their long life span. Here the most important are summarized:

- Gravitational: Formed by the sum of the weight of the dike and the complementary structures built on top of it. Some dam codes [14], [2], require the complete construction process to be considered, taking into account the closing sequence of the expansion joints.
- Hydrostatic thrust: Its value depends on the level of the reservoir, which in turn is a function of the operating conditions and the hydrological characteristics of the tributary basins upstream. The thrust on the downstream face is usually neglected, in favour of slip safety.
- Thermal load: The construction process is to place independent concrete blocks that set at a certain temperature and then grouting the joints between them. Whenever the temperature of the structure is different from the set temperature, stresses will be generated inside the material. There is also a thermal absorption in the reservoir, which implies a significant temperature difference between the upstream face and the downstream face. This effect is more important the smaller the separation between the two, that is, for curved dams. There is also a phenomenon of solar radiation on the face downstream, which depends on its altitude and orientation, and the time of year.

- Creep and shrinkage: Rheological phenomena of concrete. They result in displacements imposed on the material, often simulated as an added thermal load.
- Uplift: Pressures due to interstitial water at points of discontinuity such as thermal joints, cracks and foundation joints. They are particularly important in gravity dams, since they reduce the contact area between the structure and the rock, affecting sliding and overturning safety.
- Sediment thrust: The maximum level of sediment deposition is established in design phase, depending on the solid transport and the management of the reservoir. Its mechanical effects are three: Hydrostatic thrust on the face upstream, reduction of water pressure (as a result of a lower depth of fluid) and refraction of incident hydrodynamic waves.
- Dynamic actions: Generated by seismic events, dynamic tests, local effects or other events that generate an important effect in a short period of time, activating the inertia forces.

Experience indicates that the most influential of this phenomenons in dam structural safety is the last of this list. The spectrum of factors by which a dam can vibrate is wide; seismic movements, explosions, dynamic characterization tests, waves generated by floods, landslides on the reservoir, collisions, local effects of sinks or floodgates, among others.

When this happens, the independent movement of the structure generates waves of hydrodynamic pressure in the reservoir, which travelling along its domain, are reflected in its bed and in turn influence the deformations of the dam. To these two phenomena a third is added; the flexibility of the foundation rock. The simultaneous exchange of energy is represented in the Figure 1.7.

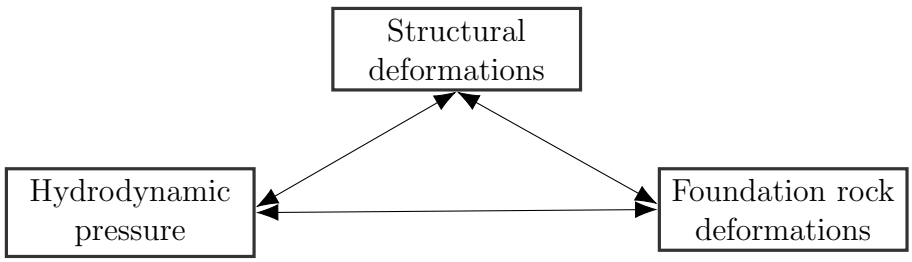

Fig. 1.7: Components of the dam-reservoir-terrain coupled system

Consequently, there exists a closed process of interactive type, which must be solved considering at the same time the three phenomena as parts a dynamically coupled system. This type of problems is characterized by its complexity, both from classical physics and numerical approach.

This work focuses the precise and efficient simulation of Fluid Structure Interaction phenomenon (FSI). To do this, numerous sources of information have been consulted in the scientific literature, and international safety regulations regarding dams, their construction conditions, analysis and operation have been compared. A summary of the most important advances is presented below.

1.2.2 Analytic Methods for FSI Simulation

1.2.2.1 Theory of Westergaard

The first researcher to take an interest in the problem was Harold Westergaard, in 1933, on the occasion of the construction of the Hoover Dam, in the USA [15].

In his study, a two-dimensional model of a gravity dam with a full reservoir is considered, as schematized in the Figure 1.8, to which the following calculation hypotheses are applied:

- Infinitesimal in plane movements.
- Rigid dam rigid, with a perfectly vertical face.
- Rigid foundation.
- Compressible, irrotational fluid with no viscosity.
- Full reservoir, with a free surface located at the dam crest level, and infinite length in the upstream direction.
- Negligible surface waves, ruling out the possibility of overflowing over the crest.
- Harmonic horizontal acceleration, in a perpendicular to the structure direction, with a frequency lower than 1 Hz.

The rigidity of the structure implies that each point of it has the same acceleration at every moment, simplifying the formulation of the problem,

allowing for it to be decomposed into two other fundamentals; the inertial effect of the structural mass acting on itself, and the hydrodynamic pressure in excess over the hydrostatic thrust, due to the pressure waves generated inside the reservoir.

Bearing in mind that the fundamental period of vibration of a gravity dam is of the order of fractions of a second, the last hypothesis guarantees that the phenomena of amplification will be non-existent.

The author analyses the problem by defining the equations of movement in the fluid and transforming them into stresses applied to the main structure. First, the potential velocity function ϕ is defined for all points in the compressible fluid domain:

$$\frac{\partial u}{\partial t} = -\frac{\partial \phi}{\partial x} \tag{1.39}$$

$$\frac{\partial v}{\partial t} = -\frac{\partial \phi}{\partial y} \tag{1.40}$$

where, according to Figure 1.8, x e y are orthogonal coordinate directions, u and v the corresponding displacement vectors and t the time.

The pressure wave function is established according to the velocity potential:

$$\frac{\partial^2 \phi}{\partial x^2} + \frac{\partial^2 \phi}{\partial y^2} = \frac{\rho}{k} \frac{\partial^2 \phi}{\partial t^2} \tag{1.41}$$

where ρ is the density of the fluid and k its compressibility module. The constitutive equation of the environment relates the pressure P with the velocity potential through:

$$P = \rho \frac{\partial \phi}{\partial t} \tag{1.42}$$

The boundary conditions for the solution of the wave equation are the following:

- No hydrodynamic pressure on the surface of the reservoir.
- Null vertical movement at the bottom of it.
- Homogeneous harmonic acceleration for all points on the face of the dam in contact with the fluid.

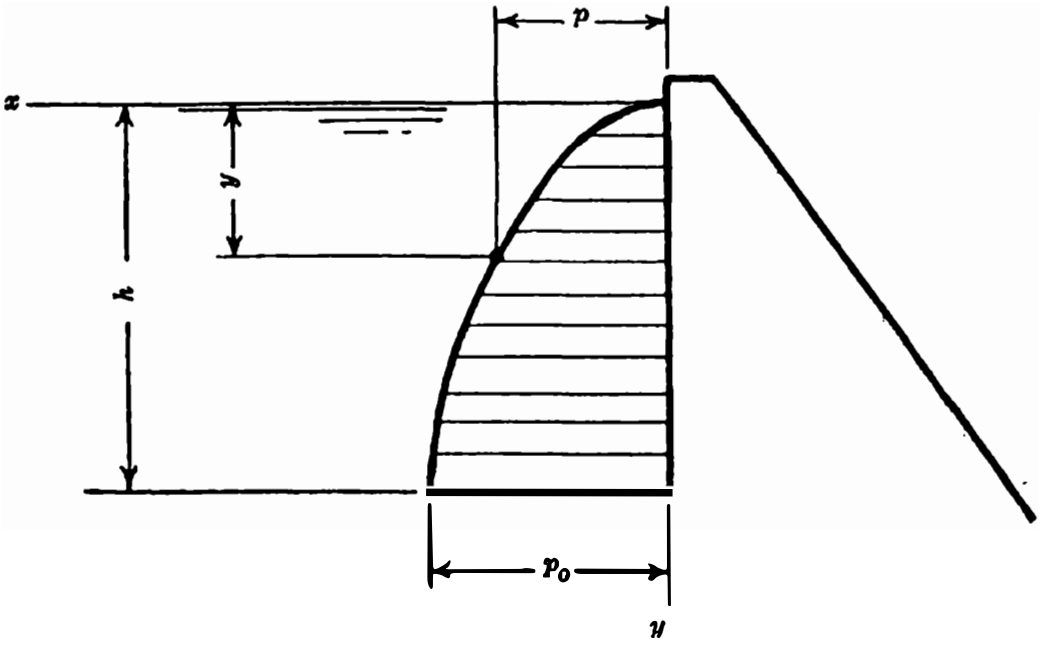

Source: Westergaard article [15]

Fig. 1.8: Westergaard model

- Convergent pressure to a null value for sufficiently large x values.

Which, mathematically equivalent to:

- $P = 0$, for $y = 0$
- $v = 0$, for $y = H$
- $u = -\left(\alpha g T^2/4\pi^2\right)\cos\left(2\pi t/T\right)$, for $x = 0$
- $\lim_{x\to\infty} P = 0$

where H is the height of the dam, g the acceleration of gravity, α the amplitude of the acceleration expressed as a fraction of g (known also as *"seismic coefficient"* [16]) and T the period of the harmonic movement imposed on the structure.

Solving the system of differential equations with the boundary conditions

described, the pressure distribution on the upstream face of the dam is expressed as:

$$P(y,\omega) = \frac{8\alpha\gamma H}{\pi^2} \sum_{1,3,5,...}^{n} \frac{1}{n^2 C_n} sin \frac{n\pi y}{2H} \tag{1.43}$$

$$C_n = \sqrt{1 - \frac{16\gamma H^2}{n^2 g k T_f 2}} \tag{1.44}$$

where $\omega = 2\pi/T$ is the circular frequency of the imposed harmonic motion and $\gamma = \rho g$ is the specific weight of the fluid.

From Equation 1.43 the following characteristics of the hydrodynamic pressure distribution are deduced:

- The pressure curve is tangent to the horizontal on the free surface and tangent to the vertical at the bottom of the reservoir, as shown in Figure 1.8.
- The maximum pressure occurs at the foot of the dam, where $y = H$, and is:

$$P_0 = \frac{8\alpha\gamma H}{\pi^2} \sum_{1,3,5,...}^{n} \frac{-1^{\frac{n-1}{2}}}{n^2 C_n} \tag{1.45}$$

- The maximum pressure occurs when $t = 0, T, 2T, ...$

The last point implies that the responses of both components; the inertial forces and the overpressure forces, occur in phase. This allows a different physical interpretation of the inertial effect of the reservoir. The author calls this concept "added mass", imagining that a part of the fluid is added to the main structure, increasing its mass but not its rigidity, thus elevating the fundamental period of the system. Equaling the force of inertia produced by this imaginary mass, with the resulting hydrodynamic pressure, is possible to calculate the distance b, measured from the dam, to which the mass of water is added to the structure, for each dy of it:

$$b = \frac{7}{8}\sqrt{Hy} \tag{1.46}$$

On the other hand, the solution diverges when the frequency of the harmonic movement $f = 1/T$ approaches the natural frequency of the reservoir, defined as:

$$f_w = \frac{c}{4H} \tag{1.47}$$

$$c = \sqrt{\frac{k}{\rho}} \tag{1.48}$$

The factor c is known as the speed of sound in the fluid, in the case of water $c \approx 1440\,\mathrm{m/s}$.

From a engineering application point of view, it is interesting to know the resultants of pressures, to be applied on the cantilever section of the gravity dam, both for the design and verification phase. These are, the total thrust and the overturning moment over the section under study. Their values are obtained from Equation 1.43, making the pertinent integrations, and are expressed per unit of width of the structure. Thus, the thrust Q has magnitude of force per unit width, and the moment M force magnitude per distance per unit width:

$$Q(y,\omega) = \frac{16\alpha\gamma H^2}{\pi^3}\left(q - \sum_{1,3,5,\ldots}^{n} \frac{1}{n^3 C_n} cos\frac{n\pi y}{2H}\right) \tag{1.49}$$

$$Q_0 = \frac{16\alpha\gamma H^2 q}{\pi^3} \tag{1.50}$$

$$M(y,\omega) = \alpha\gamma H^3\left(\frac{16qy}{\pi^3 H} - \frac{32}{\pi^4}\sum_{1,3,5,\ldots}^{n} \frac{1}{n^4 C_n} sin\frac{n\pi y}{2H}\right) \tag{1.51}$$

$$M_0 = \alpha\gamma H^3\left(\frac{16q}{\pi^3} - \frac{32}{\pi^4}\sum_{1,3,5,\ldots}^{n} \frac{-1^{\frac{n-1}{2}}}{n^4 C_n}\right) \tag{1.52}$$

$$q = \sum_{1,3,5,\ldots}^{n} \frac{1}{n^3 C_n} \tag{1.53}$$

Westergaard described a simplified way of calculating pressures, replacing the shape of the exact distribution represented in the Figure 1.8 with that of a parabolic curve, represented in the Figure 1.9.

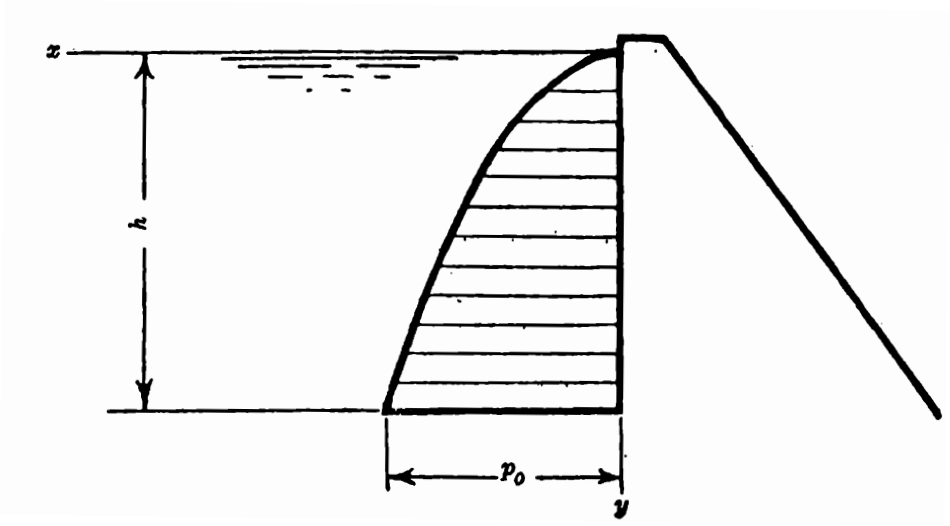

Source: Westergaard article [15]

Fig. 1.9: Approximate pressure distributions in the Westergaard model

In this way, the following expressions are deduced:

$$P = C\alpha\sqrt{Hy}\ ;\ P_0 = C\alpha H \tag{1.54}$$

$$Q = \frac{2}{3}C\alpha y\sqrt{Hy}\ ;\ Q_0 = \frac{2}{3}C\alpha H^2 \tag{1.55}$$

$$M = \frac{4}{15}C\alpha y^2\sqrt{Hy}\ ;\ M_0 = \frac{4}{15}C\alpha H^3 \tag{1.56}$$

The coefficient C is calculated by replacing the value of M_0 in Equation 1.56 with the one obtained in Equation 1.52, so that the maximum overturning moment of both distributions be the same.

1.2.2.2 Theory of von Karman

The next significant work is the one of Theodore von Karman [17]. The main difference with that of Westergaard, is based on considering the reservoir water as an incompressible fluid. This allows an important simplification of the pressure equations in the fluid medium. As Westergaard did, he used the

concept of "added mass" to obtain the following expressions at the foot of the dam:

$$P_0 = 0{,}707\,\alpha\,\rho\,H \tag{1.57}$$

$$Q_0 = 0{,}555\alpha\rho H^2 \tag{1.58}$$

$$M_0 = 0{,}236\alpha\rho H^3 \tag{1.59}$$

This model was adopted by the Italian regulation of 1959 [18]. The percentage difference with the results of Westergaard theory is of the order of one digit.

1.2.2.3 Theory of Zangar

In 1952, Carl Zangar [19] used an electrical model, analogous to the two-dimensional mathematical model of the dam and its reservoir, schematized in the Figure 1.10. To incompressible fluid hypothesis of von Karman, he added the variable tilt of the face upstream.

The equation that governs the phenomenon is:

$$\frac{\partial^2 P}{\partial x^2} + \frac{\partial^2 P}{\partial y^2} = 0 \tag{1.60}$$

Which is analogous to the Laplace equation for ideal electrical systems. Considering pertinent boundary conditions, the pressure distribution is given by:

$$P(y) = \alpha C_z \gamma H \tag{1.61}$$

$$C_z = \frac{c_m}{2}\left[\frac{y}{H}\left(2 - \frac{y}{H}\right) + \sqrt{\frac{y}{H}\left(2 - \frac{y}{H}\right)}\right] \tag{1.62}$$

where c_m is a coefficient that depends on the inclination of the structure upstream, point to point along its height. It is obtained from:

$$C_m = -0{,}0073\theta + 0{,}7412 \tag{1.63}$$

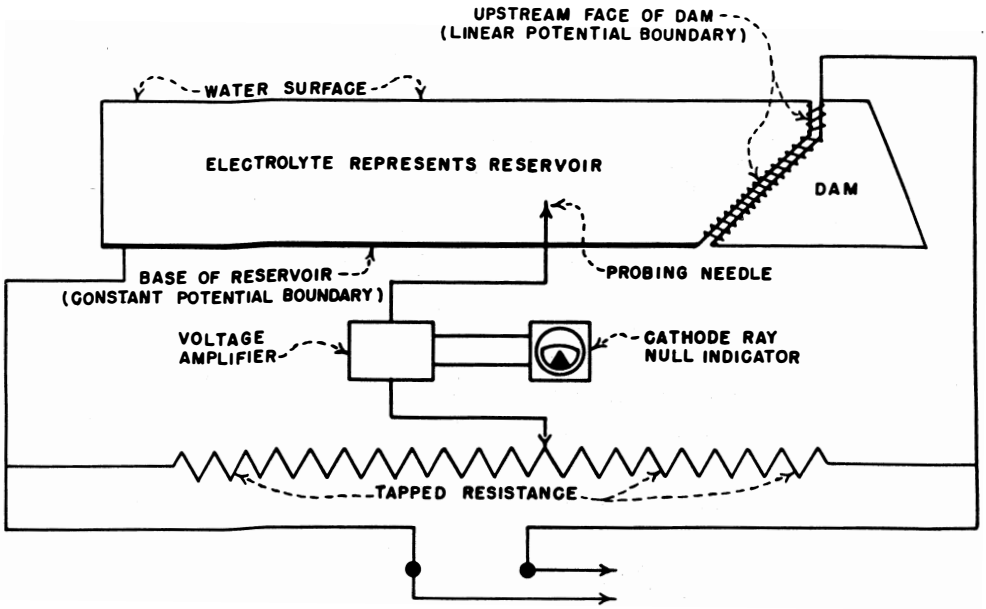

Source: Zangar article[19]

Fig. 1.10: Zangar analogous model

In this way, considering the maximum values on the section, doing $y = H$:

$$P_0 = \alpha c_m \gamma H \tag{1.64}$$

$$S_0 = 0{,}726 \alpha c_m \gamma H^2 \tag{1.65}$$

$$M_0 = 0{,}299 \alpha c_m \gamma H^3 \tag{1.66}$$

This model was adopted by the Italian regulation of 1982 [20].

1.2.2.4 Theories derived from Westergaard

George Housner, in 1957 [21] carried out a study to determine the hydrodynamic pressures in circular and rectangular containers, and later extended those results for inclined gravity dams. The hypotheses considered are:

- Subdivision of the fluid in thin vertical membranes without mass.
- Movement of the membranes in the direction of soil movement.

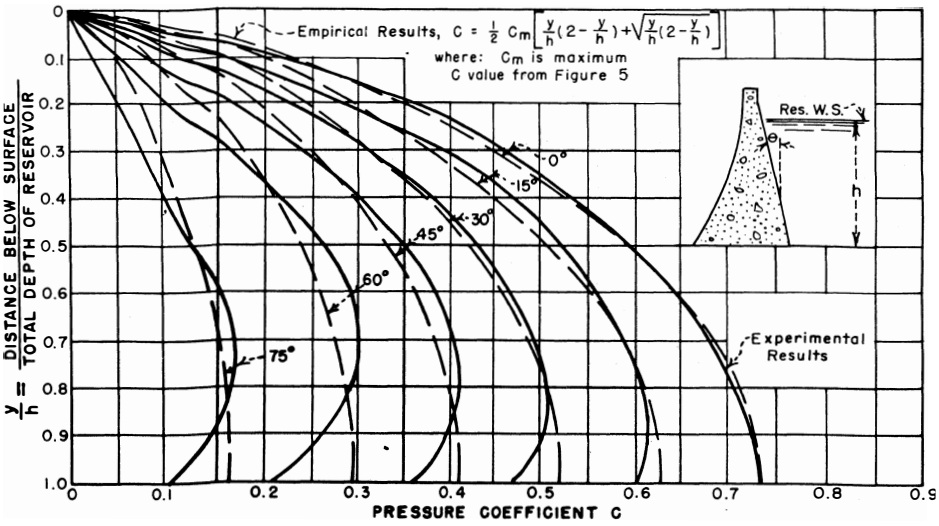

Source: Zangar article [19]

Fig. 1.11: Pressures for different values of θ. Zangar model

- Incompressible liquid.
- Infinitesimal movements.

In this way, the distribution of pressures is influenced by the inclination value of the dam. The results obtained are similar to those from Zangar.

Housner himself, together with Chwang in 1978 [22], starting from the work of von Karman, and using the balance of the momentum to solve the pressure equations, arrived at a result similar to that of Zangar and the previous one from Housner.

In 1963, Kulmaci [23] considered the hypothesis of random movements in any direction within the plane of the analyzed section. From this study it is concluded that the most unfavourable situation is that of horizontal movement perpendicular to the dam, which corresponds to the original hypothesis assumed by Westergaard.

1.2.2.5 Theory of Chopra

Beginning in 1967, Anil Chopra and his collaborators [24] developed a procedure known as the "substructure method", with the aim of removing the most restrictive boundary conditions existing in the state of the art so far.

He considered both domains, fluid and structure, as independent systems, seeking the simultaneous solution of two independent problems:

- The response of the isolated structure.
- The hydrodynamic pressure in the fluid, supposed the dam as rigid.

In this way, hydrodynamic pressure forces are obtained first, to be added later to the mass and force matrices of the first problem.

The first important novelty comes from introducing a wider range of soil movement frequency f, that until this point was considered as lower than 1 Hz. As a result of the evolution of the theory of seismic movements, for the time in which Chopra began his research, it was discovered that such hypothesis is not always fulfilled, and therefore was incomplete. The researcher managed to overcome this limitation, obtaining the solution to the second problem for the full range of oscillation frequencies of the system. The solution is expressed as follows:

$$P(y,t,\omega) = \frac{-4\alpha\gamma}{\pi}\left[\sin\omega t \sum_{n=1}^{n_1-1} \frac{(-1)^{n-1}}{(2n-1)\sqrt{\frac{\omega^2}{c^2}-\lambda_n^2}}\cos\lambda_n y + \cos\omega t \sum_{n=1}^{\infty} \frac{(-1)^{n-1}}{(2n-1)\sqrt{\lambda_n^2-\frac{\omega^2}{c^2}}}\cos\lambda_n y\right] \tag{1.67}$$

$$\lambda_n = \frac{\pi(2n-1)}{2H} \tag{1.68}$$

$$\Omega_w = \frac{f}{f_w}\ ;\ \omega = 2\pi f;\ \omega_w = 2\pi f_w \tag{1.69}$$

where n_1 is the minimum value of n such that $\lambda_n^2\ \omega^2/c^2$. Equation 1.67 is reduced to Equation 1.43 when $n_1 = 1$, that is, if $\omega < \omega_w$, since the term containing the expression $\sin\omega t$ disappears. This means that the Westergaard solution is valid only when the oscillation frequency is lower than the fundamental frequency of the reservoir, which was already demonstrated by Kotsubo [25]. When $\omega > \omega_w$ the sinusoidal term does not disappear, and represents the response of the system out of phase with the forces of inertia. In this case, the hydrodynamic pressure can no longer be represented by the concept of added masses.

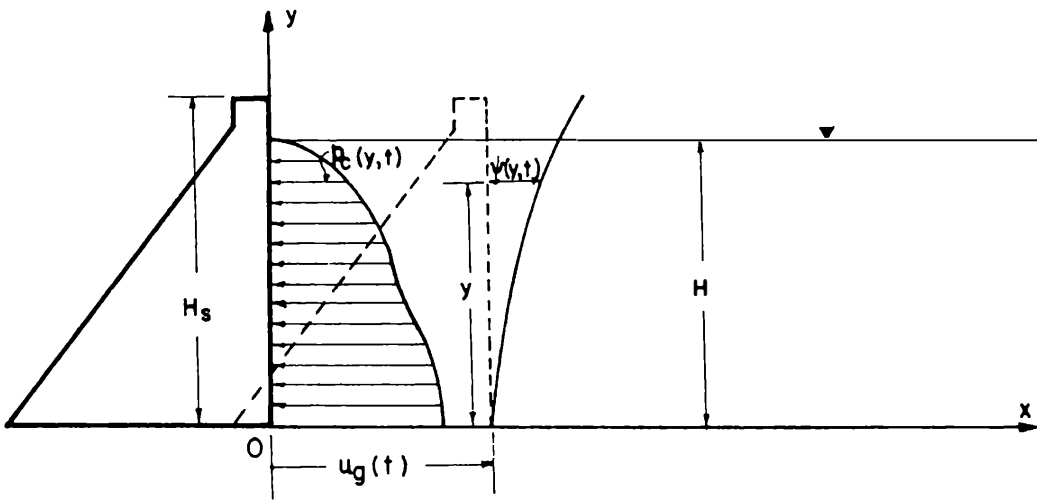

footnotesize Source: Chopra article citechopra1968earthquake

Fig. 1.12: Chopra model

From these equations it follows that the pressure in the Chopra model is a function of the frequency of soil movement. Being expressed as a *complex response function*, it allows to calculate the response of the system coupled to any input strong motion record, in the time domain, from a convolution integral of the Fourier transform of the *unit response function*. No dissipation of energy is contemplated, so the response is unlimited for a certain value of Ω_w that does not correspond to the unit, since the frequency of the deformable coupled system is different from that of the rigid coupled system.

1.2.2.6 Effect of boundary conditions

1. Fluid compressibility: The only authors that have included this effect are Westergaard and Chopra. It is of fundamental importance, considering that it is the mechanism that allows to evaluate the interaction of the dam and the reservoir. Under the incompressible fluid hypothesis, the response of the system is independent of the oscillation frequency, canceling the coupling.

2. Length of the reservoir: In analytical methods, the reservoir is considered as a semi-infinite plane, starting at the dam and extending upstream. However, Brahtz and Heibron in 1933 [26] and later Bustamante in 1963 [27] showed that a reservoir length equal to or greater than 3 times the height of the dam is sufficient to simulate the phe-

nomenon with adequate precision.

3. Surface wave: According to Chen's studies in 1961 [28] and Bustamante in 1963 [27], the error that is made when ignoring surface waves is of the order of 5 %, this value being a function of the height of the dam and the reservoir period. In general, the effect of waves can be neglected without introducing major errors.

4. Vertical aspect: The most important study in this regard is that of Zangar. It is concluded that if the dike is vertical in more than half of its height, the solution is identical to that of a completely vertical dam. Otherwise, the inclination introduces important modifications and can not be ignored.

5. Deformability of the dam: It is the most influential factor, together with the compressibility of the water. A realistic analysis can not do without this hypothesis, because the characteristics of the coupled system change with it.

Through the work of Chopra and his collaborators during the following decades, the method of substructures has been evolving continuously.

The first improvement introduced is the consideration of the flexibility of the dam, considering it as deformable in the first problem, expressing its displacements in the modal space as a function of the first mode of vibration of the isolated structure. Subsequently, it was added to the foundation considered as elastic, with mass and radiation of energy. The researchers demonstrated [29] that the radiation mechanisms play a key role in the response of the dam.

Another interesting aspect is that of the spatial variation of soil movements [30], which was also important in the response of the coupled system. However, to be able to consider it, accurate records of previous seismic events are needed at different points of the foundation and structure, which are often not available. A complementary source of energy dissipation was added later; the absorption of energy through the sediments of the riverbed [31]. It is modeled as a one-dimensional mechanism that refracts the incident wave at the base of the reservoir, such that only a portion of the incident energy is reflected. The fundamental parameter that characterizes the absorption effect of hydrodynamic pressure waves is the admittance coefficient q_s, which depends on the intensive properties of the sediments. The reflection coeffi-

cient α_s is defined as:

$$\alpha_s = \frac{1 - q_s c}{1 + q_s c} = \frac{1 - (\rho c / \rho_s c_s)}{1 + (\rho c / \rho_s c_s)} \tag{1.70}$$

where ρ and c refer to the density and speed of sound in water, respectively, and ρ_c and c_s those corresponding to the sediments.

The reflection coefficient energy absorption and can be interpreted as the ratio of the amplitude of the reflected wave to that of the incident wave. Its value can vary between 1 and 0. A value of 1 represents a non-absorption condition, where all the incident energy is reflected within the reservoir, while a value of 0 implies a total absorption. Field investigations [32] have identified values of α_s in a wide range, consistently between 0.5 and 0.75.

1.2.3 Numerical methods for FSI simulations

1.2.3.1 Lagrangian Methods

Although the method of substructures is an accurate and robust tool for the structural analysis of dams, its main disadvantage is that it has limited application to linear systems. This excludes the possibility of considering non-linear phenomena, such as the opening / closing and sliding of expansion joints through non-linear contact, cracking concrete, cavitation in the reservoir, large deformations, non-linear constitutive equations, chemical reactions, etc.

For this reason, alternative numerical methods have been developed. A set of them corresponds to the Lagrangian approach, which makes use of the finite fluid elements based on the displacement vector. Its main advantage is that when using this type of finite elements, any generic structure simulation software can be adapted to use them, provided that the movement is infinitesimal, defining a material with zero shear modulus. However, this last factor generates vibration modes of zero energy (due to the use of reduced integration methods [33]) and tendency to numerical instability of type *hour-glass* that increase with the fineness of the mesh [34], which generates problems of difficult approach, as the solution diverges with the convergence of the mesh. This greatly complicates the computational effort necessary for the extraction of the modes of vibration of the coupled system and their associated frequencies, which are fundamental in the identification of the dynamic characteristics of the model.

1.2.3.2 Eulerian Methods

Gladwell [35] introduced in 1965 the finite elements based on scalar pressure. Its main advantage is the fact of having only one unknown for each node of the mesh (pressure, instead of the three displacements present in the Lagrangian methods). According to Craggs [36], the order of the matrices of the elements is reduced by two-thirds, maintaining an equivalent precision.

The method proposed in this research work is of the Eulerian type. Its characteristics will be described in the Chapter 2.

1.2.4 International regulations

The regulations for calculating and operating dams in the following countries were reviewed: Italy, Switzerland, the United States and Japan. These were selected for their known seismic activity and their locations (Europe, America and Asia), in order to obtain a broad panorama, both from the technical and historical and geographical point of view, of the solutions currently adopted worldwide. The following documents are cited below:

- Italy: *"Norme tecniche per le costruzioni"* [37], *"Norme tecniche per la progettazione e costruzione degli sbarramenti di ritenuta (dighe e traverse)"* (NTD14) [2].
- Switzerland: *"Documentation de base pour la verification des ouvrages d'accumulation aux sèismes""* [38].
- USA: *"Best Practices in dam and Leeve safety risk analysis "* [39], *"Federal Guidelines for safety"* [40], *"Time-history dynamic analysis of concrete hydraulic structures"* [14].
- Japan: *"The River Law"* [16], *"Draft of Guidelines for seismic safety evaluation of Dams"* [41]

As mentioned in the section 1.2.2.3, the Italian code NTD14 adopts the theory of Zangar as a reference for the evaluation of the dynamic effect. It is recalled that, since the compressibility of the water in it is ignored, the resulting pressures are constant for any value of the oscillation frequency.

The Swiss regulation, following the Westergaard theory, adopts the following expression for the coefficient C to be introduced in the equation 1.54:

$$C = \frac{7}{8}\rho \tag{1.71}$$

The added mass is calculated in a similar way, according to the theory described in Section 1.2.2.1.

On the other hand, the American norms dictate the possibility of using three modalities: added masses (according to Westergaard's theory), incompressible finite elements and compressible finite elements. However, it does not provide particular indications for the use of the last two methods.

Finally, Japanese regulations, particularly the *River Law* [16], introduce the concept of *" Seismic hazard coefficient"*, symbolized as k_d:

$$P = \frac{7}{8}\rho k_d \sqrt{Hy} \tag{1.72}$$

The value of k_d varies between 0.20 and 0.24 for arc dams and between 0.10 and 0.12 for gravity dams.

In the most recent Japanese regulation, of 2005 [41], no indication is found regarding the subject under treatment.

With this analysis it is evident that in all cases the adopted solutions are of the independent type of the oscillation frequency of the structure. This fact, as will be seen later, results in underestimates of the tensional state of the dams, both in the design and evaluation phases.

1.2.5 Fluid-structure-foundation interaction

Another important aspect of dams modeling is the interaction that occurs between the main structure and the surrounding foundation rock under dynamic load. There are several ways of accounting for this interaction that have been investigated.

The first attempt was made by Chopra [42], in which the author considered a massless flexible foundation rock, treating it as a sub domain in the substructure method. He found that dam-foundation interaction effects:

- Depend on the ratio E_f/E_c of the foundation elastic modulus and dam material elastic modulus. As this ratio decreases, the fundamental

resonant frequency of the dam decreases, and the response of the dam decreases as well.

- Are quite similar whether the reservoir is full or empty.
- Increase by a small amount the maximum tensile stresses computed for the dam on rigid foundation, but does not significantly alter the distribution of stresses over the dam faces.
- Hydrodynamic effects are smaller if dam-foundation rock interaction is considered [43].

Other authors have also researched on this topic, mainly using FE models [44], [45] [46], [47]. The results converge into the conclusions above reported. The effect of a massless model vs a massed model is of importance [29]. Presence of mass allows also for a damping radiation condition similar to that established at the end of acoustic domain. This implies sense that a massless model results in overestimation of stresses over the structure. Yet, the wave transmission mechanism must be precisely defined, in a deconvolution analysis [48], [49]. In this way, ground motion can be applied at the contours of the terrain model, resulting in the recorded ground motions at the free field surface.

1.2.6 Expansion joints

The main structure of an arch dam is built by casting blocks of an approximate cubic form of 20 m of height, that are placed one at a time. After the initial shrinkage due to the internal chemical reactions, the space between them is grouted, leading the independent cantilevers to be in contact. Consequently, there are three types of geometric discontinuities within the body of the dam [50], namely, the "foundation contact" formed by the perimeter between the rock and the abutments; the "lift lines", horizontal planes between adjacent blocks within the same cantilever, and the "contraction joints", designed to allow for relative movement between adjacent monoliths. These discontinuities cause the whole structure to have an important non-linear behavior.

Under dynamic load, if the amplitude of motion is big enough, tensile strength of grout may be exceeded, and the joint may be open. Thus, the joints can carry a very limited amount of tensile stresses. To account for this effect, several contact formulations have been introduced through extensive research. Lau [51] defined a "Hard contact" formulation that allowed

accounting for shear keys effects indirectly. Hariri-Ardebili et al. [52] used a similar approach.

Alembagheri and Ghaemian [53] used an exponential "Soft contact" formulation that also allowed for modeling discrete cracks. According with this formulation, contact is composed of two characteristics behaviors, tangential and normal. Normal behavior is considered as an exponential function of clearance between the surfaces, meaning that the surfaces begin to transmit normal pressure once the distance between them is equal or less than a critical value c_0, and rise to a maximum of σ_0, when the joints are completely close. This behavior diminishes numerical problems related to hard contact formulations. Tangential behavior is related to normal forces through a classical Coulumb friction model. A maximum allowable shear exists across the interface of the joint, and when this value is reached, relative sliding begins. The three variables of the model are μ (material characteristic), σ_o and c_o.

1.3 Summary of State of the art

To the best of the authors knowledge, there is only one previous research focused on the applicability of mathematical metamodels for uncertainties valuation in the dam field. Hariri-Ardebili and Amin [4] analyzed a gravity dam with linear behavior, using surface metamodels and considered the uncertainties distribution of several material parameters and characteristic values of seismic ground motions. However, there are other examples of the use of the metamodeling technique for civil structures in literature.

Aleatory uncertainty, specifically to ground motion variability has been extensively studied in term of the seismic fragility analysis. Epistemic uncertainty in the material and modeling, on the other hand, is reported in a limited amount of studies. De Araujo and Awruch [54] carried out the first published research related to probabilistic seismic analysis of concrete dams. Material properties and the seismic input were considered as random variables (RVs) for a gravity dam. MC simulation was used to evaluate the fragility of the factor safety against sliding. Elingwood and Tekie [55] used the LHS scheme to sample material and seismic RVs in analysis a concrete gravity dam. Dam foundation interface was modeled with a perfectly plastic Mohr-Coulumb law. Recorded ground motions were de-convoluted and applied to the base of the foundation. Uplift pressure was modeled as a linear distribution. A two-parameter Darbre's model (nodal masses in series with dampers) was used for FSI. Normal distribution was used for compressive strenght of concrete, and uniform distribution for other 11 parameters. A total of 12 earthquake records were used for fragility analysis. Mirzahosseinkashani and Ghaemian [56] considered only aleatory uncertainty for the Pine Flat gravity, using a non linear material model. No joints were modeled. The foundation was assumed as massless, and pressure based FE elements were used for the reservoir. Two LS were defined: Crack length at the base, and the total cracked area on the dam face. Ghanaat et al. [57], [58], [59] developed a series of investigations for a concrete gravity dam, investigating different seismic and epistemic RVs, using both 2D and 3D models. Alembagheri and Seyedkazemi [60] studied three material parameters for a gravity dam (Elastic modulus, tensile strength and ultimate tensile strain), using a damage model. Pushover and dynamic incremental analysis were employed. Hariri and Saouma [61] performed a sensitivity analysis of a gravity dam with an interface joint. Fifteen RVs were identified in a "Tornado diagram" is developed for the system subjected to an intensifying stochastic acceleration. LHS was used for sampling.

Yao, Elnashai and Jiang [62] studied only seismic input variability for a 305 m high arch dam. The dam was modeled with 3 contraction joints, while the concrete was taken as linear. The added masses approach from Westergaard model was used to model FSI. 18 ground motions were selected as RVs. Zhong, Li and Bao [63] considered both seismic and material uncertainties using MC simulations, for a high arc dam. Non linearity of concrete was modeled. Kadkhodayan et al. took a 203 eter high arc dam as a case study, with a linear material and the peripheral joint modeled. Foundation was considered massless and linear. Nine three-component ground motion record were used as RVs. Hariri et al. [64] selected a high arc dam with pressure based FE for the reservoir and massless foundations. Nine ground motions were selected as Rvs, and epistemic variability was neglected. Non linearity of both joints and materials were modeled. Fragility seismic curves were derived for the dam.

Simpson et al. [65] summarized the metamodels options for computer based engineering design. They analyzed polynomial. kriging, artificial neural networkd and support vector machines, among other procedures. Faravelli, in 1989 [66] was the first to apply RSM in structural engineering. Rajashekhar and Ellingwood in 1993 [67] applied RSM for a cantilever beam, and stated that RSM is much computationally cheaper than MC. RSM have been widely used for structural reliability and seismic fragility for other kind of civil structures, such us base-isolated storage tanks [68], masonry bridges [69], nuclear power plants [70] and for railways bridges [71]. It also has been successfully applied for rockfills [72] and concrete faced rockfill dams [73].

2. Methodology

2.1 Research main work flow

In order to achieve the first objective of this research, namely to verify the applicability of RSM metamodel for non linear arch dams, a series of analysis were be performed. These steps required are summarized next.

- Deterministic Analysis (DA)
- Sensitivity Analysis (SA)
- Design of Experiments (DOE)
- Metamodeling fitting
- Metamodeling comparison against multi-sampling classical approaches

The first step is related to the second objective of this research. Critical modelling aspects are appointed in this stage. Two study cases are adopted. FE models were developed from the original documentation. Simulation of FSI, terrain interaction and joints non linearity were investigated.

After that, in the second step the most influential factors were identified through sensitivity analysis. Ranges and adequate EDPs were chosen as well.

In the third step, five DOE techniques were be applied, in order to study different possibilities of number experiments / estimation precision ratio. The resultant polynomial models were fitted in the step four through the least squares method.

Finally, a high number of deterministic analysis, executed on points obtained through different sampling procedures were used to find out the precision of metamodels developed in the previous stage.

2.1.1 Factor Analysis

Through classical FE deterministic analysis, using the results of the first step, and with a review of the theory available in literature, factors that influence on the EDPs are identified.

The loads considered acting in the dam are three: Own weight, hydrostatic thrust (with a full level reservoir) and a ground motion record. The first 30 s of the *Dinar* event are applied to the terrain. A bounding variation of $\pm 20\%$ is considered for each input factor. Keeping all their mean value, one factor at a time is modified to take, once its maximum possible value (thus, 1.2 times its mean value), and once its minimum possible value (0.80 times its mean value). By doing so, a tornado diagram is built at the end and the influence of factors is read from it.

The rest of the steps are of straight forward application, and details will be explained in Chapter 3.

2.2 Case Studies

To have a contrast between different structures, two study cases were selected for this research. The first one corresponds to a Cupola dam (double curvature dam), with a rough volume of $10 \times 10^5\,m^3$, and the second to an Arch-gravity dam, with a rough volume $4.7 \times 10^5\,m^3$, much greater that the first case study. Their main characteristics will be described in the next sections.

2.2.1 Lumiei dam

The dam was designed by Eng. Carlo Semenza. The construction began in 1941 and finished in 1948. Is located in the in the Udine district, Friuli Venezia Giulia region, in northern Italy. Between the below foundation plane and the crown there is a difference of 136.15 m. By blocking the Lumiei stream it rises a $73 \times 10^6\,m^3$ reservoir. The artificial lake formed receives the name of *Sauris* Lake. Its main use is generation of hydro-electrical energy, through the *Ampezzo Carnico* energy central.

2.2.1.1 Structure description

It is built as a thick slab with double curvature, that is, both in horizontal and vertical direction. In the bottom foundation it is present an asymmetric plug, which thickness varies between 15.87 m and 14.8 m in its upper level, while the main body is almost perfectly symmetrical, and of variable thickness as well. It has 13.68 m at the lower level, and 3.15 m in the crown. Also, the horizontal arches that form the main body have variable thickness, growing going from the key to the abutments. In coincidence with the bottom plug and the pulvinus, there is a continuous perimeter joint. The radial joints are located with a mean distance of 15 m between each other and has been closed with cementitious injections after the initial shrinkage.

2.2.1.2 Lumiei Concrete Characteristics

Concrete was initially dosed with 300 kg of cement for m^3 with a water/cement ratio of 0.47 until July 1947, for then becoming 279 kg for m^3 and a water/cement ratio of 0.53. Mechanical tests were carried to characterize the material properties, both at the construction site and a laboratory located

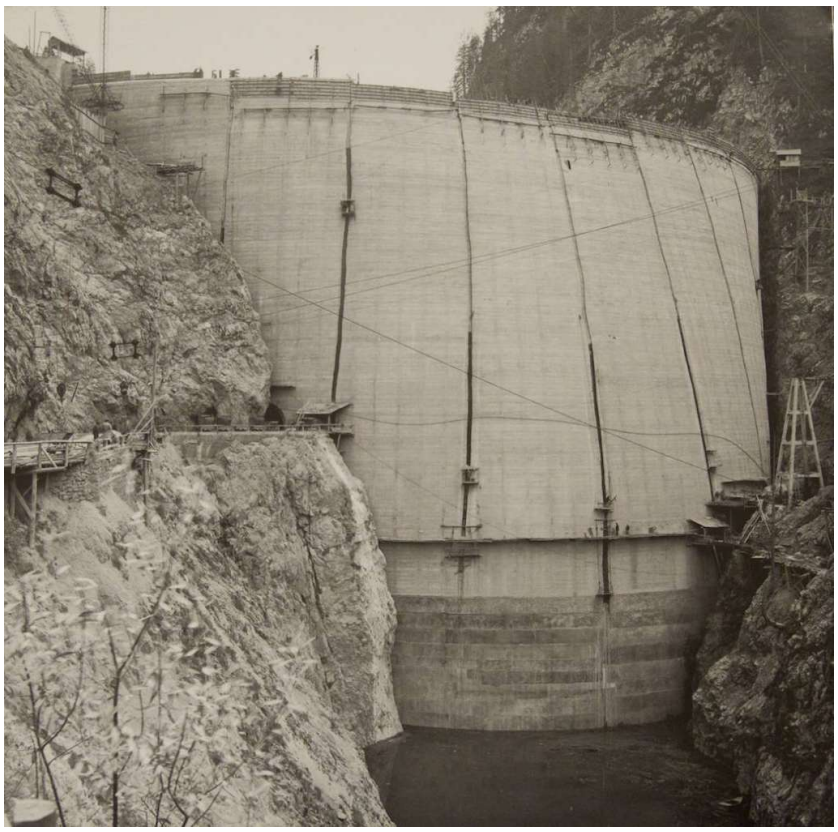

Source: *Progetto Dighe*

Fig. 2.1: Lumiei Dam - Frontal view

in Padova, using specimens of 20 x 20 x 20 cm.

With the strength characteristics reported on the original documents, and in according with the empirical correlations established in the Italian Building Code *"Norme Technique per le costruzioni"* (NTC 08) **NTC08**, the elastic modulus is obtained through:

$$E_{cm} = 22{,}000 \left[\frac{f_{cm}}{10}\right]^{0.3} \qquad \text{[MPa]} \quad (2.1)$$

$$f_{cm} = f_{ck} + 8 \qquad \text{[MPa]} \quad (2.2)$$

$$f_{ck} = 0.83\, R_{ck} \qquad \text{[MPa]} \quad (2.3)$$

where f_{cm} is the concrete elastic modulus, f_{ck} is the mean value of the

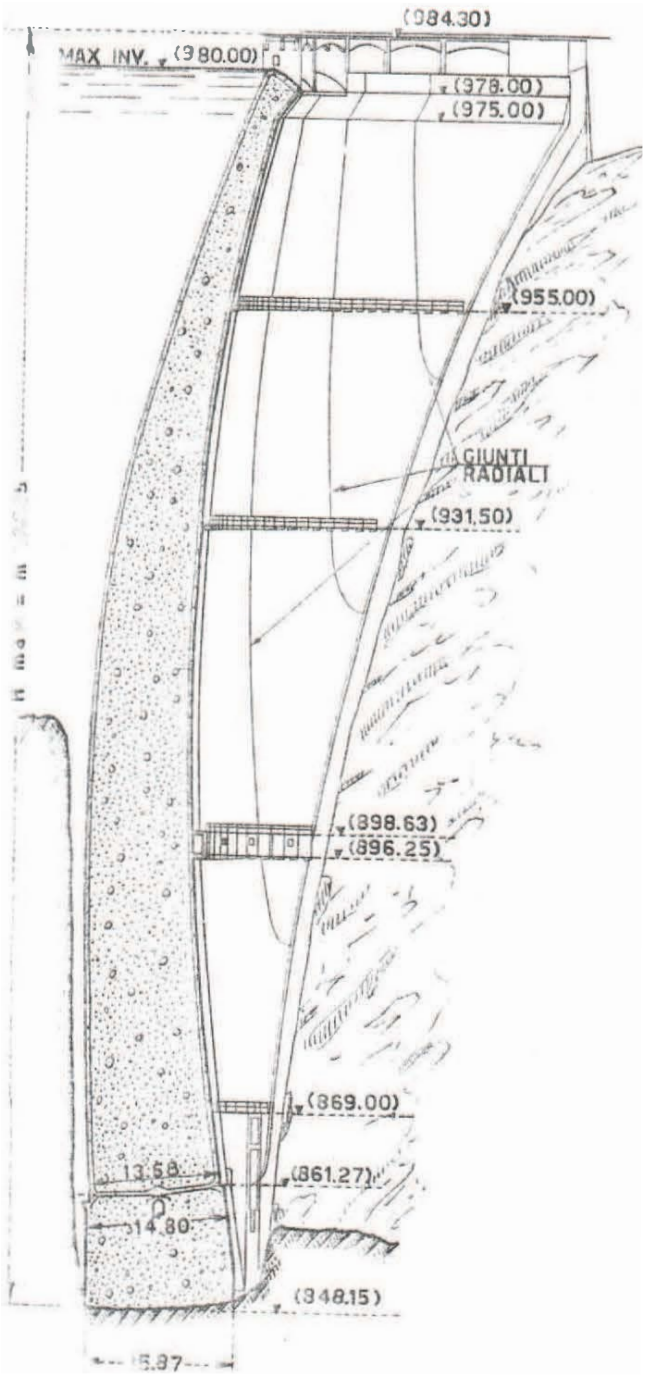

Source: *Ministero delle Infrastrutture e dei Trasporti*

Fig. 2.2: Lumiei Dam - Cross-section view

Condition	Normal use
Use	Hydro-electrical
Structural type	Cupola
End of Construction	1947
Maximum exercise level	980 m s.n.m.
Maximum reservoir level	982 m s.n.m.
Dike height	128 m
Crown length	156 m
Volume of exercise reservoir	$70 \times 10^6\,\mathrm{m}^3$
Volume of full reservoir	$73 \times 10^6\,\mathrm{m}^3$
Area of reservoir surface	$139\,\mathrm{km}^2$
Volume of main structure	$102.62\,\mathrm{m}^3$

Table 2.1: Lumiei Dam - Structural description

compressive strength, and R_{ck} the cubic compressive strength.

Assuming a value of 48.50 MPa for R_{ck}, f_{cm} is 48.26 MPa, f_{ck} is 40.25 MPa and E_{cm} in 35,276.5 MPa, that is, a nominal value E_c of 35,000 MPa.

Also, the tensile strengths are obtained through:

$$f_{ctm} = 0.3\, f_{ck}^{2/3} \qquad \text{[MPa]} \quad (2.4)$$

$$f_{cfm} = 1.2\, f_{ctm} \qquad \text{[MPa]} \quad (2.5)$$

where f_{ctm} is the concrete mean tensile strength and f_{cfm} the flexural strength. The lesser of the two is adopted, in favour of safety, that is, 3.50 MPa.

R_{ck}	48.50 MPa
f_{ck}	40.25 MPa
f_{cm}	40.25 MPa
f_{ctm}	3.50 MPa
E_{cm}	35.28×10^3 MPa
E_c	35.00×10^3 MPa
ρ_c	$2.4 \times 10^3\,\mathrm{kg}/\mathrm{m}^3$
α_c	$1.00 \times 10^{-5}\,^\circ\mathrm{C}^{-1}$

According to *NTC08*, a value of de $1.00 \times 10^{-5}\,^\circ\mathrm{C}^{-1}$ is adopted for thermal expansion coefficient α_c, and $2400\,\mathrm{kg}/\mathrm{m}^3$ for material density ρ_c.

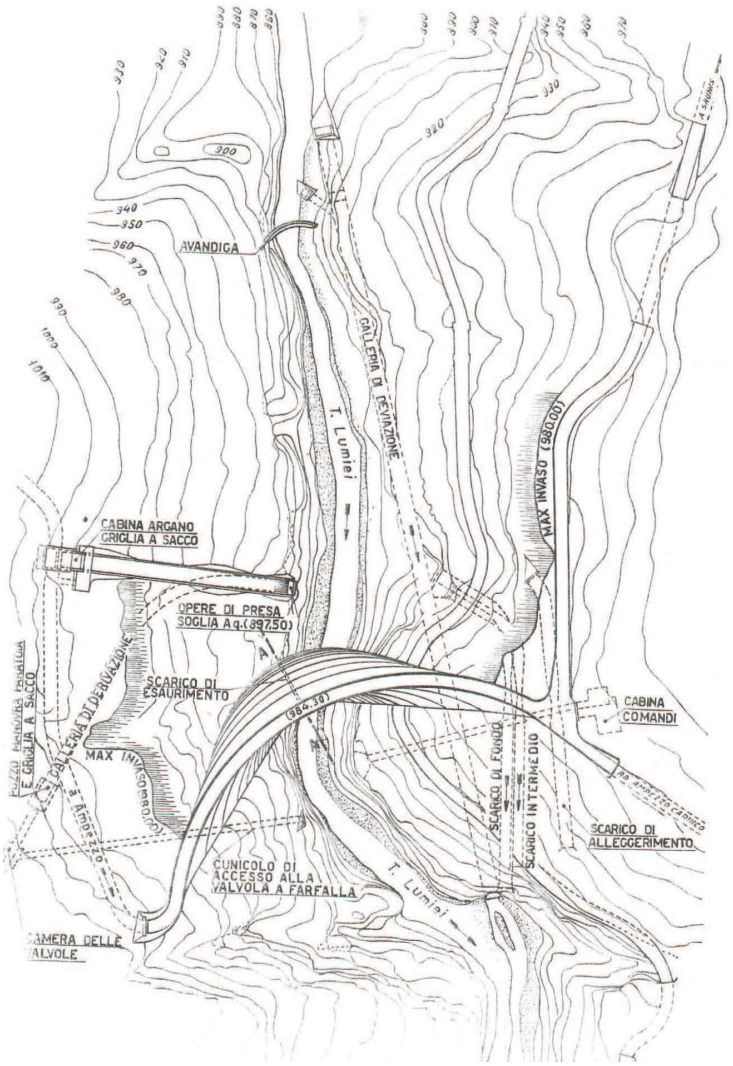

Source: *Ministero delle Infrastrutture e dei Trasporti*

Fig. 2.3: Lumiei Dam - Top view

2.2.1.3 Lumiei Rock characteristics

The cannon upon which the dam rests has been originated from the erosion of a calcareous rock from. On the river bottom, a modest thick of alluvion sits. The foundation rock presents optimum compactness and solidness attributes. The value of the elastic modulus is not available anywhere in the documentation. There were not carried geotechnical tests, as it was not yet a common practice at the time of the original designing process took place.

2.2.2 Pertusillo dam

The dam was designed by Eng. Carlo Drioli. The construction began in 1957 and finished in 1963. Between the bottom foundation plane and the crown there is a difference of 105 m. It is located in the in the *Spinoso* district, *Potenza* region, in southern Italy. By blocking the *Agri* stream it rises a $105 \times 10^6\,\mathrm{m}^3$ reservoir. The artificial lake formed receives the name of *Pertusillo* Lake. It has multiple uses, serving as a departure point for the *Pugliese* aqueduct, one of the biggest systems of drinkable water in Europe. It is also used for hydroelectric energy generation, and well as for irrigation.

Source: *Ministero delle Infrastrutture e dei Trasporti*

Fig. 2.4: Pertusillo Dam - Air view

2.2.2.1 Structure description

The structure presents a "V" profile, extended through the rather wide canyon. The predominant curvature is on the arch direction, thus horizontally. The pulvinus is almost symmetrically built and totally fixed into the rock foundation. It has a mean thickness of 10 m. The main body is also symmetrical. Also, the horizontal arches that form the main body have variable thickness, growing going from the key to the abutments.

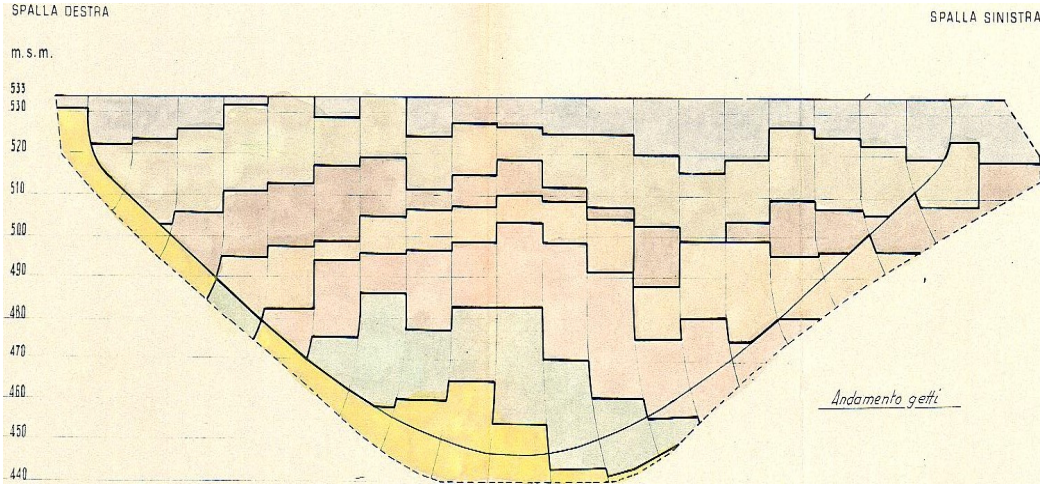

Source: *E.I.P.L.I.*

Fig. 2.5: Pertusillo Dam - Frontal view

In coincidence with the the pulvinus, there is a continuous perimeter joint. The radial joints are located with a mean distance of 15 m between each other and has been closed with cementitious injections after the initial shrinkage.

2.2.2.2 Pertusillo concrete characteristics

Concrete was design with low heat concrete dosed with 235 kg of cement for m^3, and then becoming 275 kgfor m^3. Some steel reinforcements have been placed through the independent monoliths, in coincidence with the expansion joints locations, both on the upstream and downstream faces. Through an analogous process used for the Lumiei Dam, the following characteristic values were obtained:

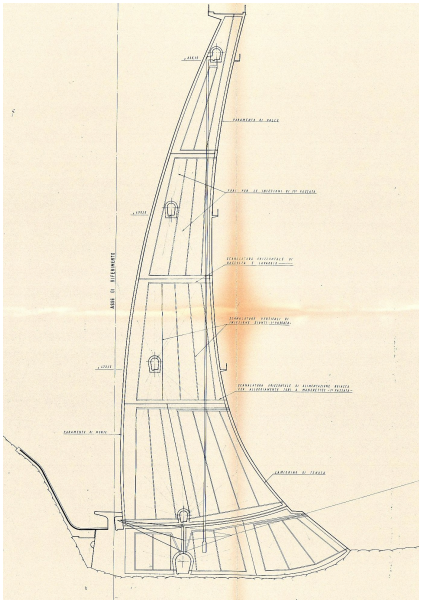

Source: *Ministero delle Infrastrutture e dei Trasporti*

Fig. 2.6: Pertusillo Dam - Cross-section view

2.2.2.3 Pertusillo Rock characteristics

The dam sits upon a clayey-marly-arenaceous formation. At the time of construction, injections of impermeabilization and strengthen have been made. There were not carried geotechnical tests, as it was not yet a common practice at the time of the original designing process took place.

2.2.3 Finite element models developing

In order to perform the series of deterministic analysis that uncertainty valuation requires for validation of the metamodels, finite element technique will be used in this research.

Taking the original documentation of the 2 cases study as starting point, using computer aided design software (CAD), geometric models were developed. The process is quite iterative, since the only available information are a few arcs at different discrete heights. These arcs were first built, and after that, the curved surface were interpolated between the known points.

For developing the CAD model of the rock terrain, Lidar satellite images were employed. These were obtained from the United States Geological

Condition	Normal use
Use	Aqueduct, Hydroelectrical, Irrigation
Structural type	Arch-gravity
End of Construction	1963
Maximum exercise level	531 m s.n.m.
Maximum reservoir level	532 m s.n.m.
Dike height	95 m
Volume of exercise reservoir	$142 \times 10^6\,\mathrm{m}^3$
Volume of full reservoir	$155 \times 10^6\,\mathrm{m}^3$
Area of reservoir surface	$630\,\mathrm{km}^2$
Volume of main structure	$476.25\,\mathrm{m}^3$

Table 2.2: Pertusillo Dam - Structural description

R_{ck}	60.00 MPa
f_{ck}	50.00 MPa
f_{cm}	58.00 MPa
f_{ctm}	3.51 MPa
E_{cm}	31.24×10^3 MPa
E_c	32.00×10^3 MPa
ρ_c	$2.40 \times 10^3\,\mathrm{kg}/\mathrm{m}^3$
α_c	$1.00 \times 10^{-5}\,^{\circ}\mathrm{C}^{-1}$

Table 2.3: Pertusillo Dam - Concrete characteristics

Survey (USGS) [74] service, and processing them a Geographic information system software (GIS), Digital elevation models (DEM) were obtained. Using this DEM models in combination with the original documentation allowed to develop a quite detailed CAD model of the terrain around the dam.

From this point, the Finite Element Software *Abaqus* was used to create the FE models for analysis. The CAD files were imported, and the mesh created with the meshing tools available within the software.

The Lumiei dike is modelled as symmetric around its main cross section. The asymmetry of the bottom plug has been ignored. The main dam has 9 independent monoliths, and the expansion joints that are located between them have important shear key forms. The terrain is also symmetric in the valley. The reservoir is considered to have the exact form of the terrain in the points were the river bottom and water are in contact. However, no direct interaction is considered between rock and water.

The Pertusillo Dam has 19 independent cantilevers, as it is a much bigger dam than Lumiei in terms of volume and length of crown. It is almost perfectly symmetric, except for a segment of the pulvinus on its upper part. This asymmetry has been ignored as well. The terrain does not present sharp curves near the dam and does not present strong asymmetries.

For both study cases, mesh sensitivity analysis were performed, under static and dynamic loads. After that, FSI were studied in deep, as it was known to be a critical aspect of modelling. The methodology of FSI investigation will be summarized next.

2.3 FSI study methodology

The dynamic coupling between a dike and its reservoir can be considered as an acoustic-structural problem, in which the dam is modelled with classical Lagrangian finite elements and the fluid with the so-called *acoustic finite elements*, which have a single degree of freedom; the scalar pressure. Both domains exchange energy through a layer of special elements called *of interface*.

2.3.1 Problem equations

The equilibrium equation for a compressible fluid, in the hypothesis of small pressure variations, for the more general case, is defined as [75]:

$$\frac{\partial P}{\partial \boldsymbol{x}} + \gamma_d(\boldsymbol{x}, \psi_i)\dot{\boldsymbol{u}} + \rho(\boldsymbol{x}, \psi_i)\ddot{\boldsymbol{u}} = 0 \tag{2.6}$$

with the constitutive equation:

$$p = k(\boldsymbol{x}, \psi_i)\frac{\partial \boldsymbol{u}}{\partial \boldsymbol{x}} \tag{2.7}$$

where $\boldsymbol{x}$ is the spatial position of the fluid particle, $\dot{\boldsymbol{u}}$ is the velocity of the fluid particle, γ_d is the drag function representing the losses of energy by viscosity and ψ_i allows to consider eventual variables of the medium, such as salinity, humidity, temperature, etc.

2.3.2 Calculation hypothesis

The assumptions assumed for the fluid medium are the following:

- Linear, compressible and non-viscous medium (γ_d is null).
- Small pressure variations.
- Constant physical properties throughout the domain geometry (independence of ψ_i).
- Non-existent surface wave.
- Impossibility of cavitation phenomena.

- Variable reservoir length.

In this way, the equations of the movement are reduced to expressions analogous to those of the classical solutions, allowing a direct comparison between these and the proposed numerical method.

2.3.3 Boundary conditions

For the domain of the reservoir, a special condition must be defined at its end upstream, in order to avoid reflection of the waves (simulating an infinite reservoir). For finite element models, boundary elements have been used successfully [76], [47], [77].

Another condition commonly used in the field of research software is the condition of Sommerfield [78]. The impedance condition at the edge of the domain of the acoustic medium is governed by:

$$\dot{\boldsymbol{u}}_{\boldsymbol{sal}} = \frac{1}{k_1}\dot{p} + \frac{1}{c_1}p \tag{2.8}$$

where $\dot{\boldsymbol{u}}_{\boldsymbol{sal}}$ is the velocity of the acoustic particle in the normal direction outgoing from the surface of the acoustic medium, $\dot{p}$ is the rate of change of the pressure, k_1 the coefficient of proportionality between the pressure and the normal displacement to the surface and c_1 the coefficient of proportionality between the pressure and the normal velocity to the surface.

In addition to simulating the infinity of the reservoir in the upstream direction, this condition can be used to model partial energy absorption in the bed of the reservoir.

The other boundary conditions of the acoustic domain are:

- No pressure on the free surface of the fluid.
- Dynamic coupling in the water-dam interface. It is simulated by a pair of surfaces *master-slave*, whose degrees of freedom are linked through the equation

$$\boldsymbol{n}\ddot{\boldsymbol{u}} = \boldsymbol{n}\frac{1}{\rho}\frac{\partial p}{\partial x} \tag{2.9}$$

For all the simulations of the present investigation, where it is not stated otherwise, these are the boundary conditions used.

2.3.4 Implicit solution vs. explicit solution

The main difference between both methods is found in the integration technique of the motion equations. In the first case, implicit operators are used, while in the second case, central difference methods are used.

The use of implicit operators implies that the matrix associated with the system must be formed and inverted at each time increment, solving the equations of motion. On the contrary, in the central difference methods, the displacements and velocities are considered as input data at the beginning of each interval, so that the mass and stiffness matrices should not be calculated for each increment, resulting in this methodology in a much lower computational cost.

However, this advantage has an important disadvantage, related to the stability of the method, which is not always guaranteed. This is linked to the time necessary for the propagation of the pressure wave in the smallest elements of the calculation mesh.

In this way, with the propagation speed being relatively high, it will be necessary to use more detailed calculation meshes and intervals much smaller than those necessary for the implicit solution. **For this reason, implicit integration methods will be used in this study**.

2.3.4.1 Integration method

The integration method used is that of Hilbert-Hughes-Taylor [79], which is an expansion of the Newmark method (known as β method) [80]. In each increment, the matrices of mass and rigidity, and their respective inverse, are calculated through an iterative process, known as Newton's method, which is unconditionally stable. In it, there is a dissipation of energy linked not to the physical damping of the system, but to the process of numerical integration itself. In particular, the magnitude of such dissipation varies according to three factors, α_d, β_d and γ_d, related through:

$$\beta_d = \frac{1}{4}(1 - \alpha_d)^2 \tag{2.10}$$

$$\gamma_d = \frac{1}{2} - \alpha_d \tag{2.11}$$

with the set ranges $-\frac{1}{2} \leq \alpha_d \leq 0$, $\beta_d \geq 0$ and $\gamma_d \geq \frac{1}{2}$.

The dissipation of energy varies in inverse proportion to the value of α_d, such that, in the limit of minimum energy dissipation:

$$\alpha_d = 0 \; ; \beta_d = \frac{1}{4} \tag{2.12}$$

similarly, in the limit of maximum dissipation $\alpha_d = -1/3$.

3. Results

In this section, the main results from this research are presented and discussed.

First, modelling aspects are studied, and the most interesting results are reported. In particular, the use of acoustic finite elements is highlighted. Reservoir dam interaction is studied in deep, defining the problem from the basic ideal conditions and removing constrictive contour conditions one by one, in order to have an idea of their individual effects. A comparison with classic solutions is performed as well.

After that, the probabilistic flowchart is used to assess the applicability of metamodels to the problem under study. Different DOE techniques and their resulting metamodels are presented and their capability to estimate structural responses compared.

For the sake of space, not all the produced results are shown in detail. When and if it has been considered appropriate, some of them are mentioned without going into detailed plots and other data showing tools.

3.1 Models for FSI analysis

As a first approach, a two-dimensional master section is studied for each case of study. These are obtained by cutting the structures in space with a vertical plane. Subsequently, simulations are performed with three-dimensional models.

Additionally, a simple two-dimensional ideal model of 1 m height is introduced, used for the comparison of the calculation method with the classical solutions of literature. The models used in the present investigation are summarized in Table 3.1.

Code	**Dam**	**Dimension**
I_0	Ideal	2D
L_2	Lumiei	2D
L_3	Lumiei	3D
P_2	Pertusillo	2D
P_3	Pertusillo	3D

Table 3.1: Codes of used models for FSI

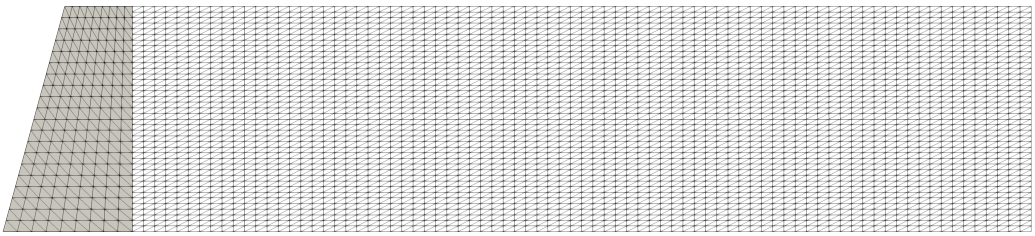

Fig. 3.1: Model I_0 - Dam and reservoir mesh

3.2 Validation of acoustic elements against classic approaches

The bidimensional idealized model I_0 was used, with the objective of evaluating the accuracy of the method, comparing the obtained results with those corresponding to the closed solutions of literature. In particular, the study conditions established by Westergaard in his research are used.

Model	I_0
α	0.10
T	1.00 s
E_c	32.00×10^3 MPa
ρ_c	2.40×10^3 kg /m^3
ν_c	0.16
k	2.15×10^3 MPa
ρ	1.00×10^3 kg /m^3
H	1.00 m
H_e	1.00 m
L_e	4.00 m

Table 3.2: Acoustic FE validations conditions

The dam and the terrain are considered rigid. The response to a simple harmonic movement with an amplitude acceleration $\alpha = 0.1$, that is, $a = 0.981m/s2$, for a reservoir depth H_e equal to the height of the structure.

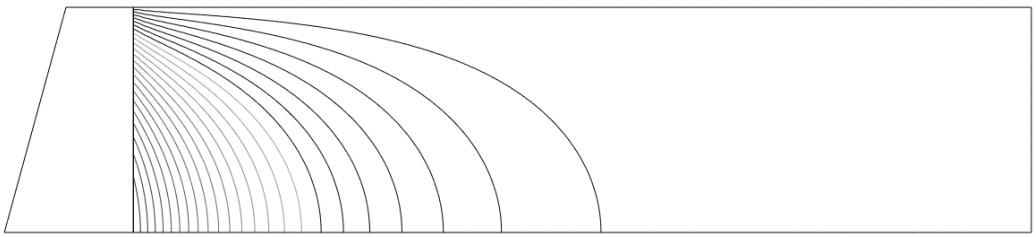

Fig. 3.2: Model I_0 - Pressure waves transmission within the reservoir

Figure 3.3a shows the distribution of maximum pressures generated by the vibration described, when $t = T = 1s$. The pressures of the Westergaard model are identical to those of Chopra and are superimposed. The solutions of Zangar and von Karman present slight variations, due to the hypothesis of incompressibility of the fluid. Those corresponding to the simulation approach the theoretical solutions in an acceptable manner. The amplification

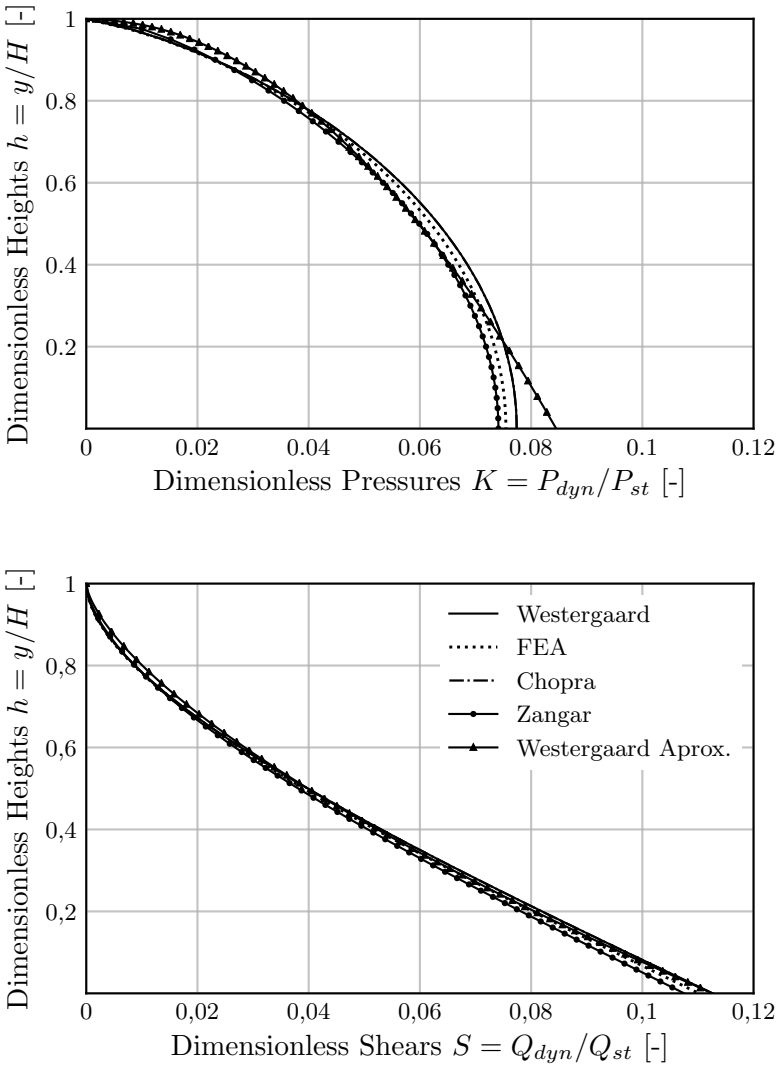

Fig. 3.3: Model I_0 - Comparison of solutions for ideal conditions

with respect to the hydrostatic pressure is of the order of 9 %. Figure 3.3b shows the distribution of the resulting thrusts on each longitudinal section of the structure. The amplification of the thrusts is greater than the pressures, because the integrals of the pressure functions do not maintain a linear relationship.

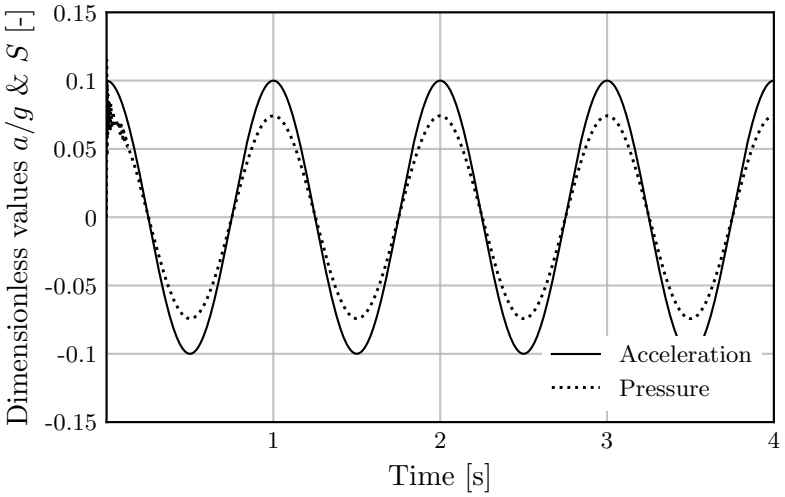

Fig. 3.4: Model I_0 - Maximum pressure over time - Harmonic oscillation

The variation in time of acceleration and maximum pressure, which occurs at the foot of the dam, are represented in Figure 3.4. It is appreciated that the dynamic amplification is not activated, because the relationship between the period of vibration and the resonance of the reservoir $4H/c$ is very small. The transient component of the hydrodynamic response is characterized by a rapid variation caused by the inertia of the resting dam. On the contrary, the permanent component is in phase with the vibration, in accordance with the provisions of Westergaard for the range of frequencies far from the resonance of the structure.

3.3 Dynamic amplification

The eigenvalues of the reservoir and its natural frequencies were calculated. The numerical method under study introduces residual intermediate modes originated by the high amount of degrees of freedom of the calculation mesh. However, it is clear from the distribution of effective masses represented in Figure 3.5 that they do not affect the propagation of dynamic waves to an important extent, since the most important modes coincide with the 1st, 3rd and 5th fundamental frequencies $f_{wn} = c(2n-1)/4$ given by the theory.

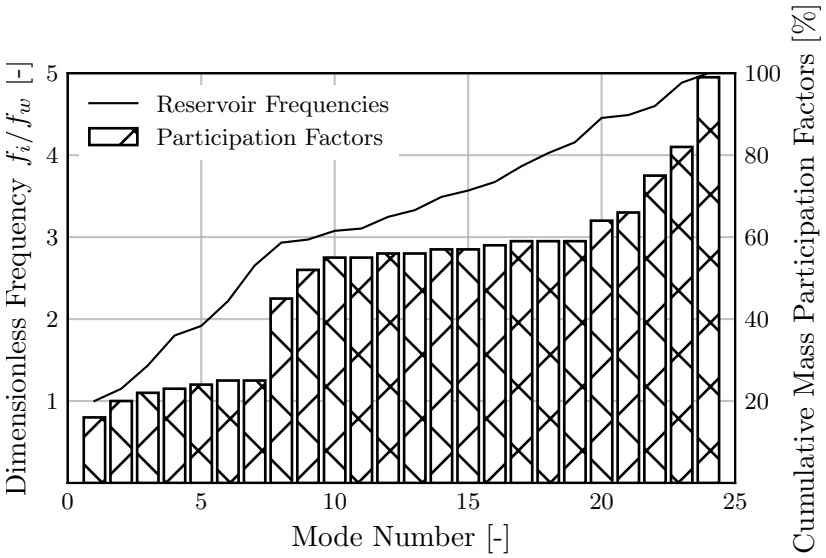

Fig. 3.5: Model I_0 - Reservoir eigenfrequencies

According to the theories of Westergaard and Chopra, the maximum amplification of the hydrodynamic pressure on the face of the dam corresponds to a frequency oscillation f equal to that of the fundamental mode of the reservoir $f_w = c/4H$. To study the phenomenon, an analysis of *Frequency Sweep* was performed. This consists of subjecting the system to a harmonic oscillation of constant amplitude ($a = 0.981\ \mathrm{m\,s^{-2}}$) and variable frequency in the study range, recording the maximum response of interest, in this case the pressure at the foot of the dam.

The result is reported in Figure 3.6, in which the variable $\Omega_w = f/f_w$ is defined. Westergaard's theory allows calculating the answers only for the range $0 > \Omega_w > 1$, as already verified by Kotsubo [25]. The solution of Zangar, adopted by the Italian regulation [2], is independent of Ω_w due to the hypothesis of incompressibility of the fluid, for which no dynamic ampli-

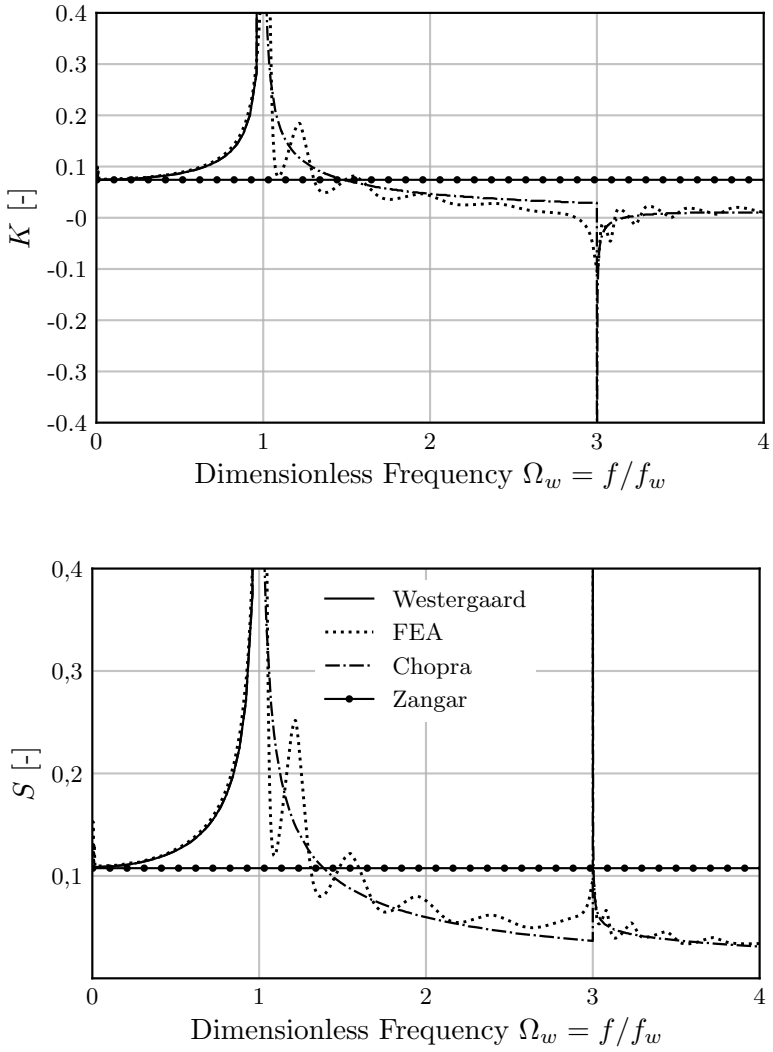

Fig. 3.6: Model I_0 - Sweep Analysis.

fication is provided by the author.

On the other hand, the theory of Chopra extends the results found by Westergaard for the full range of frequencies and provides for an unlimited amplification for $\Omega_w = 1$, and smaller amplifications for $\Omega_w = 3, 5, etc..$ The results of the simulation are in accord with those found by the author, with a difference, the answer in the plane (S, Ω_w) oscillates around the theoretical curve, because of the residual modes described above. This effect is attenuated by the energy dissipated by the deformation of the dam, as will be seen in Section 3.6.3.

From the foregoing, it is concluded that, in the ideal conditions far from resonance, the increase of the hydrodynamic thrust with respect to the static one is of the order of 11 %. For the seismic field, where oscillation frequencies vary in the $3Hz > f > 30Hz$ range, the phenomenon occurs much more often than assumed by classic authors.

3.4 Numeric solution parameters

The effect of the following variables on the proposed numerical solution is studied:

- Δt integration.
- Constant α_d of integration.
- Finite element size.
- Length of reservoir.
- Typology of finite elements (Hexahedral and Tetrahedral).

Through the simulations it is verified that step Δt that allows an accurate simulation is in the range $T/40 > \Delta t > T/30$. The constant α_d influences the numerical stability of the solution, as shown Figure 3.7. For this reason, for the phenomenon under study it is recommended the adoption of values that guarantee a minimum dissipation, in such a way to obtain a more efficient convergence. For the present investigation, a value of -0.5 is adopted.

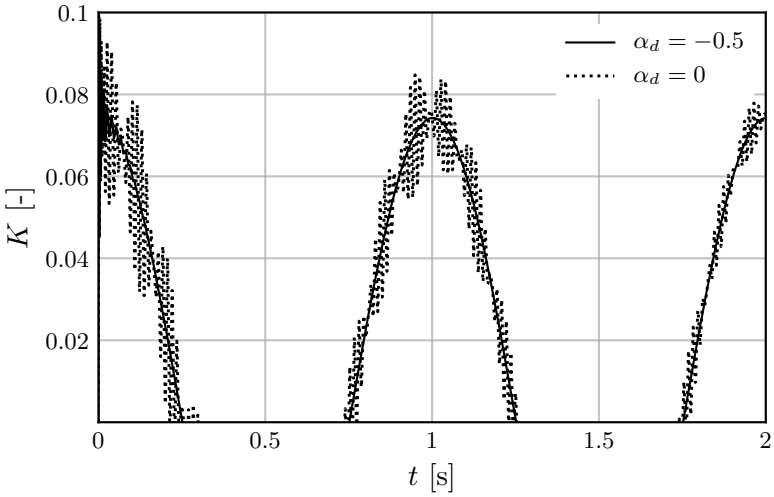

Fig. 3.7: Model A - Effect of constant of integration

A relatively thin mesh is necessary to allow the propagation of dynamic waves in an acceptable manner. Its accuracy depends on the length of the acoustic wave in the middle, related in turn to the period T of vibration. The criterion chosen for the present investigation is to define a minimum

dimension for the acoustic finite elements, based on a wave with a period equal to 0.01 s. Given that the field of frequencies under study is always below the value $f = 1/T = 100Hz$, the correct modelling of the phenomenon under study is assured. In consequence:

$$dim_{min} = c * T \simeq 14m \tag{3.1}$$

Regarding the length of the reservoir, it is found that the response remains fundamentally unaltered for values of the ratio L_e/H_e greater than 3, as shown in Figure 3.8. Lesser values lead to non-stringent solutions, regardless of the energy absorption condition applied to the domain contour.

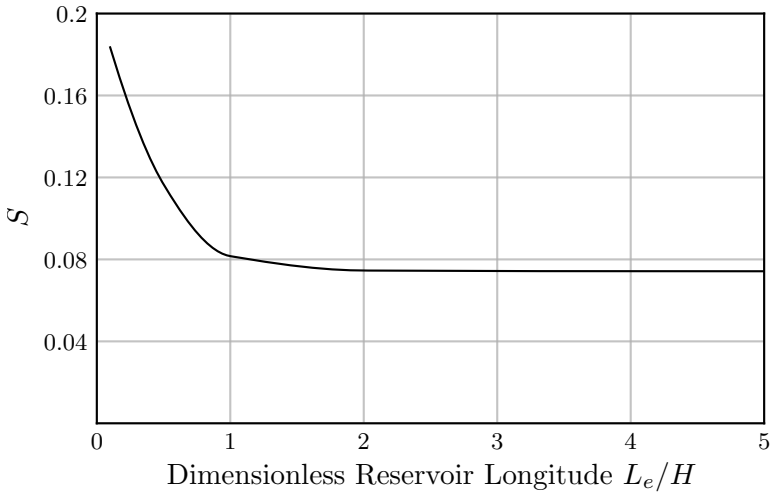

Fig. 3.8: Model I_0 - Effect of reservoir length

Finally, regarding the typology of finite acoustic elements, it is reported that the hexahedral elements with quadratic expansion are those that present a faster convergence. However, in the present investigation, tetrahedral element models will be used, since they allow the modeling of irregular geometry domains with greater adaptability and efficiency.

3.5 Mesh convergency

In order to introduce the elasticity of the dams for the case studies, the convergence of the calculation mesh is analyzed, for all the models to be used. Given that the NTD14 does not give any indications for the finite element model techniques, USA USACE EM 1110-2-6051 [14] was used as guideline for the mesh generation. All materials were considered as linear elastic, and no geometric discontinuities of non-linear mechanism were considered in this stage.

The American normative establishes that for arch dams, 3D models must be used. Also, "a thin or medium-thick arch dam can be modeled adequately using a single layer of shell elements through the dam thickness". A thick arch dam requires three or more layers of solid elements though the dam thickness.

Considering these recommendations, a mesh sensitivity analysis was performed for the dam body, considering it as a monolithic body. First, the effect of the type, amount and disposition of FE elements was investigated, in a parametric analysis, were different values were assigned to these three variables, generating different FE models. Static loads were considered to act upon the structure, the dead weight in a first analysis step, and the hydrostatic thrust in a second one. Crown displacements and stress distribution over the FE elements were monitored, and the effect of the variables were captured.

Secondly, the natural frequencies and the fundamental modes of vibration for the different FE models were determined and compared. Also, crown displacements under harmonic ground motion were analyzed.

In a first instance, the master sections are taken for the three case studies, that is, the L_2 and P_2 models. The effects of the type and finite element disposition are studied, assigning different values to these three variables in a parametric analysis. Static loads are used, the own weight and the hydrostatic thrust, considered the reservoir with a depth equal to the total height of the dam. The displacements of the crest and the distribution of stresses in the structure are monitored. The number of elements necessary for each model were around 600, in order to confine the relative error of calculation to a value lower than 5 %. The elements tend to increase their concentration in areas of greater stress gradient, which for the hypothesis of perfectly rigid foundation, are close to the base considered as fixed.

Through a process analogous to that followed for the two-dimensional

Dam	**Type**	**Model**	**Elements**	**Nodes**
Lumiei	Arc	L_2	618	259
Pertusillo	Arc-gravity	P_2	779	338

Table 3.3: 2D models characteristics

models, the convergence of the mesh for the three-dimensional models of the 3 case studies is also studied. The final models to be used in the investigation are summarized in Table 3.4.

Dam	**Type**	**Model**	**Elements**	**Nodes**
Lumiei	Arc	L_3	6527	1868
Pertusillo	Arc-gravity	P_3	8690	2398

Table 3.4: 3D models characteristics

In Figures 3.9 and 3.10 the calculation meshes corresponding to the models of two and three dimensions, respectively, are observed. Table 3.5 summarizes the amount of structural mass of each model.

Dam	**Type**	**Model**	**Structural mass**
Lumiei	Arc	L_2	3.16×10^6 kg
Pertusillo	Arc-gravity	P_2	4.48×10^6 kg
Lumiei	Arc	L_3	2.56×10^8 kg
Pertusillo	Arc-gravity	P_3	1.20×10^9 kg

Table 3.5: Structural masses of dam models

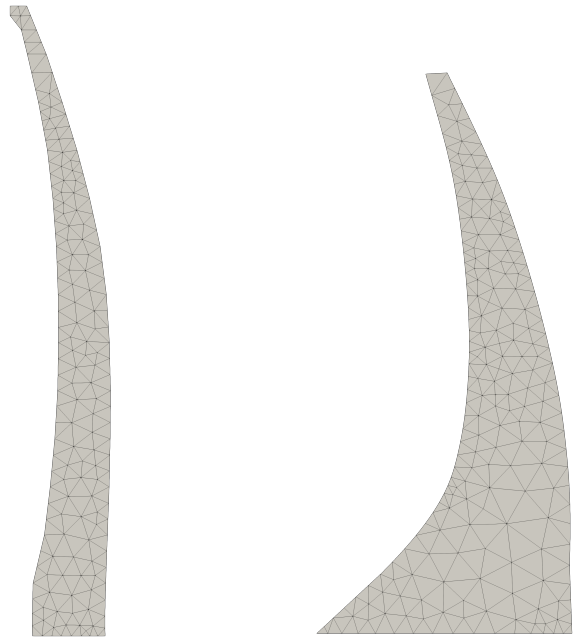

(a) Lumiei Dam

(b) Pertusillo Dam

Fig. 3.9: 2D models

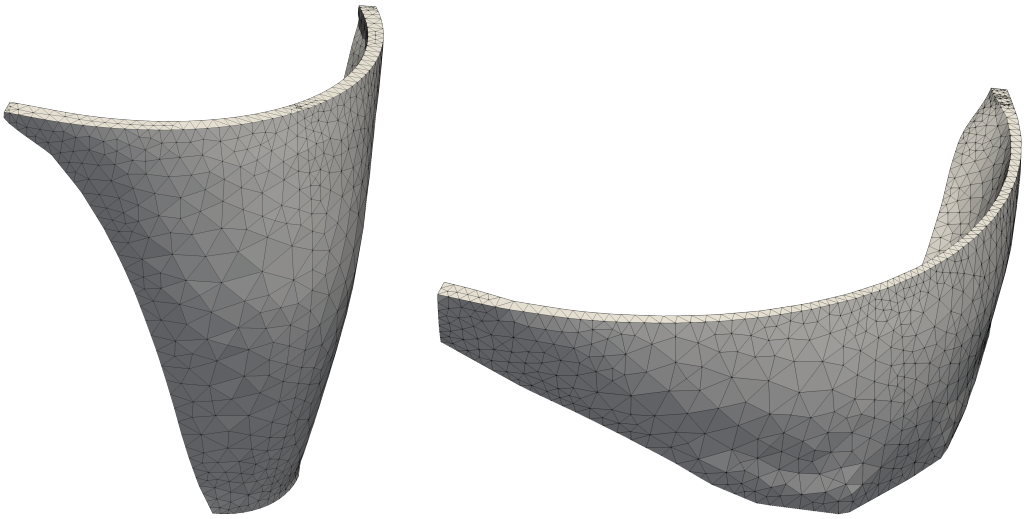

(a) Lumiei Dam

(b) Pertusillo Dam

Fig. 3.10: 3D models

3.6 Effects of flexibility

The results obtained in the simulation are presented below using the method validated in the previous chapter. The restrictive hypotheses assumed in literature will be removed one by one, in such a way to carefully study the effect of each one.

- Elasticity of the structure: It constitutes the most restrictive hypothesis of all. It is established in order to simplify the analysis of the problem, by allowing to equalize the vectors of acceleration and velocity of all the points of the dam. However, despite the structures under study have high rigidity, its behaviour is far from perfectly rigid. In fact, there are different dynamic mechanisms that combine in the dynamic range, as will be seen later.

- Verticality of the face of the dam: Both Westergaard and Chopra study a dam with a perfectly vertical face. This condition, although useful for the formulation of closed solutions, almost does not occur in reality. Zangar introduced the possibility of considering an inclined face, but his theory is incomplete, due to the incompressibility of the fluid, as described in the section 3.6.4.

- Non-damped response: The absence of energy dissipation mechanisms is particularly problematic in numerical simulations. In particular, for the problem under study, the mechanisms of absorption of dynamic waves at the end of the reservoir and the energy dissipated by deformation of the structure are fundamental.

- Horizontal component of the movement: With this hypothesis two effects are neglected: the horizontal thrust of the water due to the horizontal acceleration (for inclined walls), and the vertical acceleration itself, which generates additional tipping moments on the dam.

- Plane problem: In the particular case of curved dams, there are three-dimensional mechanisms that can not be considered in the plane models.

3.6.1 Modal analysis of dams without reservoir

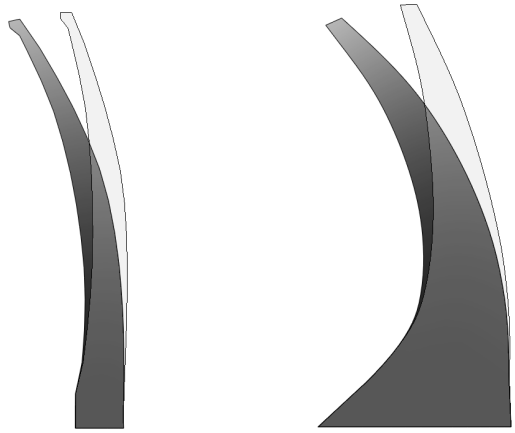

(a) Lumiei (b) Pertusillo

Fig. 3.11: 2D Models - First vibration mode

Dam	**Type**	**Model**	**Frequency**
Lumiei	Arc	L_2	0.663 Hz
Pertusillo	Arc-gravity	P_2	2.102 Hz

Table 3.6: 2D Models - Eigenfrequencies of empty dams

The primordial behaviour of the bracket in the first vibration mode is observed in Figure 3.11. The high slenderness of the section in the model L_2 causes a reduced rigidity and consequently a very low frequency of vibration. Figure 3.12 shows the frequency distribution for the first 100 vibration modes. The trend clearly goes according to the explanation for the fundamental mode.

3.6.2 Acoustic beating

By varying the frequency of the harmonic oscillation of the dam-reservoir system, a very particular phenomenon occurs that demonstrates the nature of the phenomenon, and is a consequence of the interaction of both systems. For values of f/f_s near the unit, where f_s is the fundamental frequency of vibration of the empty dam, the hydrodynamic pressures in the reservoir present an amplitude that grows indefinitely in a linear manner over time. This is known as *beating*.

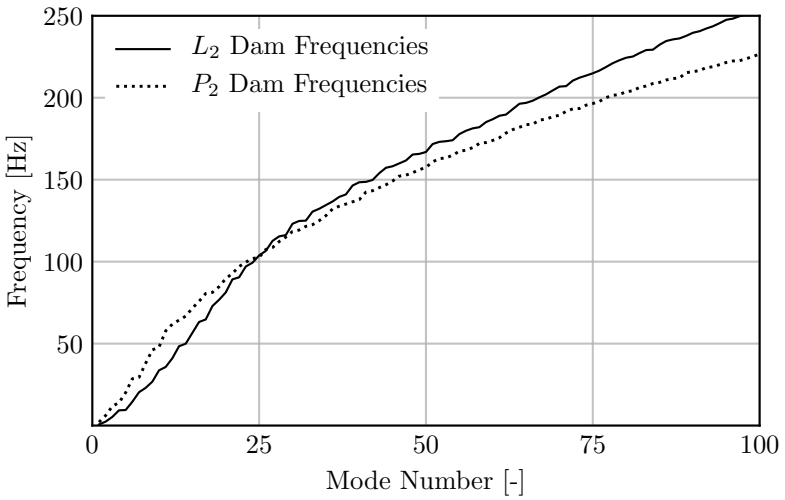

Fig. 3.12: 2D Models - Eigenfrequencies of empty dams

The beat occurs when the pulse of the oscillation is close to that of the structure, initiating an exchange of energy in the coupled system that produces vibrations in the primary system, instead of suppressing them.

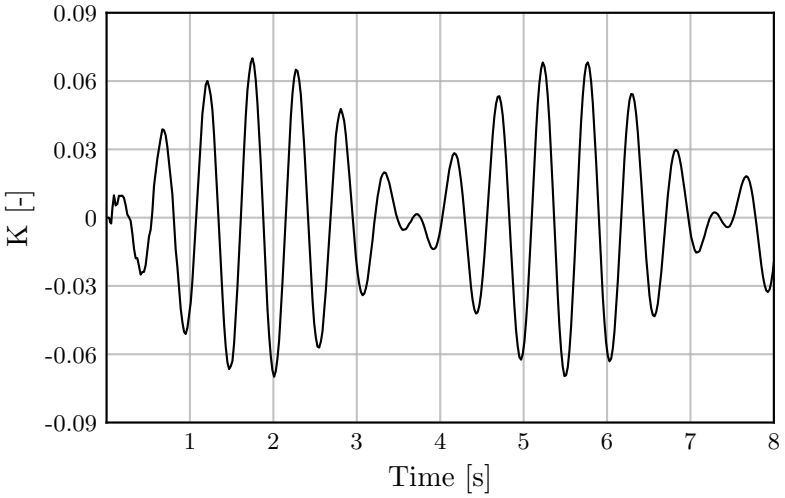

Fig. 3.13: Beating phenomenon

Figure 3.13 reports the pressure at the foot of the dam for a frequency $f \simeq 0.9 f_s$. The oscillations suffer linear amplitude modulation in time. It is possible to plot an envelope of these amplitudes, passing through the zero

response points. This will have its own period defined by:

$$T_b = \frac{2\pi}{1 - (f/f_s)} \tag{3.2}$$

called beating period.

The phenomenon has been extensively studied in the acoustic field, in particular by Den Hartog in 1956 [81], from the superposition of two waves of similar frequencies that join in a different one, called the wave of beat.

3.6.3 Damping

The introduction of this variable is done in order to evaluate the effect of viscous energy dissipation, always present in the structures that deform. Conventionally, damping for concrete structures is set at a 5 % of the critical value, this being a purely indicative value since the factors that influence the phenomenon are so many that it is impossible to consider them directly in practice.

The effect, the quantity and the precise definition of damping, in the case of dams in particular, depend on the constitutive relationship of the materials used, and very especially on the non-linear mechanisms present, such as the opening of joints and cracks in the concrete.

In this research, the dissipation of energy is considered through the classic Rayleigh formulation. This uses a range of frequencies in which the value of the coefficient ζ varies according to the limits defined as input values. To do this, two coefficients are defined, α_r and β_r, according to the equations:

$$\zeta_1 = \frac{1}{2}\left(\frac{\alpha_r}{\omega_1} + \beta_r\omega_1\right) \tag{3.3}$$

$$\zeta_2 = \frac{1}{2}\left(\frac{\alpha_r}{\omega_2} + \beta_r\omega_2\right) \tag{3.4}$$

where ω_1 and ω_2 are the natural frequencies of the system, chosen according to its properties, ζ_1 and ζ_2 the associated critical damping coefficients, generally considered equal.

In this way, the procedure to obtain α_r and β_r is as follows:

1. Choice of values of ζ_1 and ζ_2.

2. Selection of the frequency range to be dampened (from modal analysis).

3. Solution of simultaneous equations.

Analytically, α_r and β_r are linked to the mass and stiffness of the structure, respectively.

To evaluate the effect of damping on the beating of the coupled system, it is decided to compare the dynamic behaviour for different values of $\zeta = \zeta_1 = \zeta_2$.

Figure 3.14 presents the comparison of the response in terms of pressure at the foot of the dam for ζ equal to 0 %, 1 % and 5 %, for a harmonic oscillation with frequency $f = 0.9 f_s$. It is observed how the beat is attenuated proportionally with the value of ζ. It follows that for dam-reservoir systems coupled, the presence of damping, however small, is necessary to avoid the phenomena of the type described here that, although possible in theory, do not occur in real life, due to the action of the multiple energy dissipation mechanisms present in the environment.

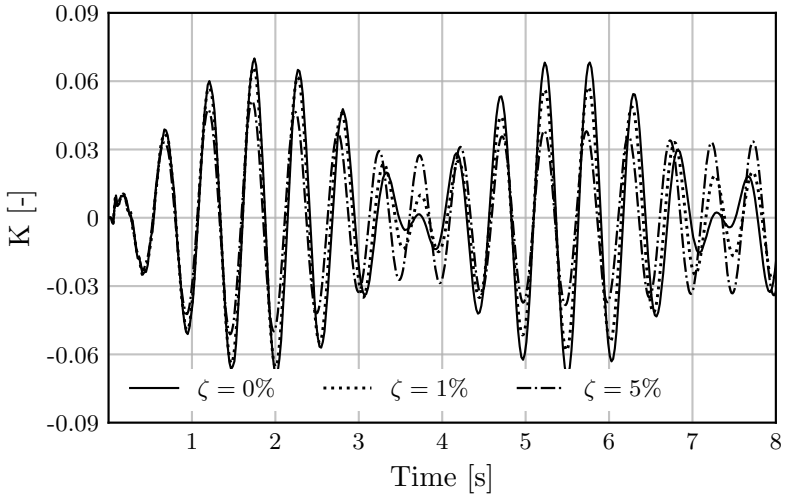

Fig. 3.14: Effect of damping over acoustic beating

3.6.4 Dynamic coupling

Chopra considered the effect of elasticity in his sub-structure method, decomposing the problem into the following two:

1. Response of the dam ignoring the reservoir.

2. Hydrodynamic pressure considered the dam as rigid.

The author used the response in coupled frequencies to take flexibility into account, expressing the field of displacements as a function of the first vibrating mode of the empty dam.

In this study, however, we seek to obtain the response of the coupled system in the time domain, by integrating the dynamic equations step by step, in such a way to include non-linear effects in a later stage. At this point, the first contour condition studied is included; the viscous damping. The starting models are the two-dimensional models for the 2 case studies. The geometries of the corresponding reservoirs are presented, in Figure 3.15.

(a) Model L_2

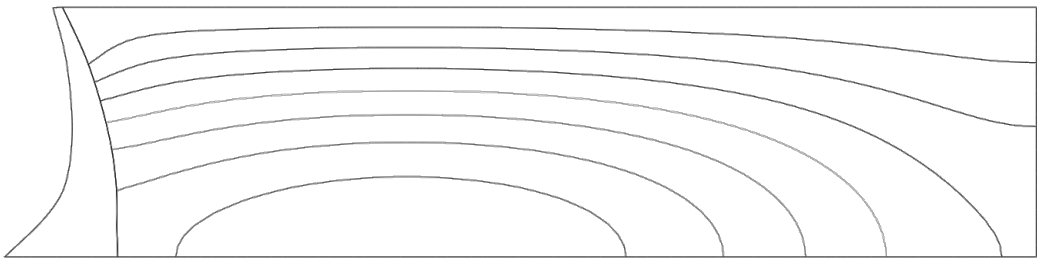

(b) Model P_2

Fig. 3.15: 2D Models - Pressure distributions for flexible dams

A frequency scan analysis is performed, studying the response of the coupled system in the range of interest. Pressures at the foot of the dam are presented in Figures 3.16a and 3.16b, for rigid and flexible dam conditions, respectively. It is observed how, when the flexibility is introduced, the first peaks of pressure are given for values of Ω_w less than 1, and in addition, there are higher amplifications for values greater than Ω_w. From here for the simulations of flexible dams, the quotient $\Omega_s = f/f_s$ is introduced, in order to generalize the solution of the system fully coupled with respect to the dam without reservoir.

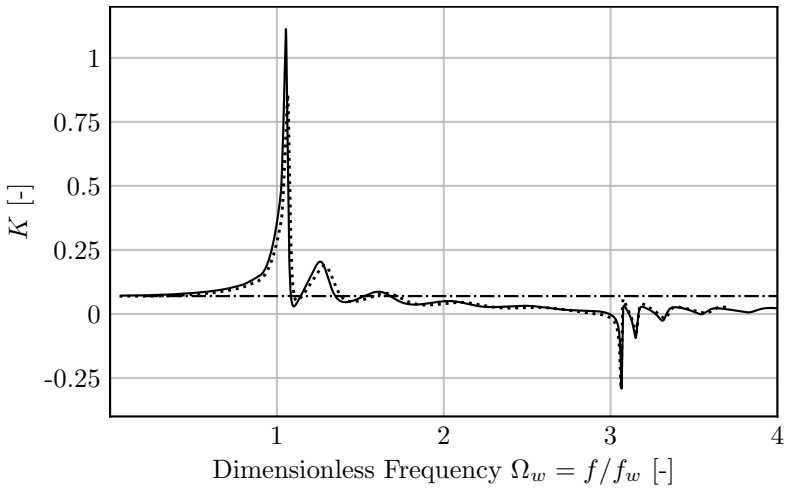

(a) Coupled system with rigid dams

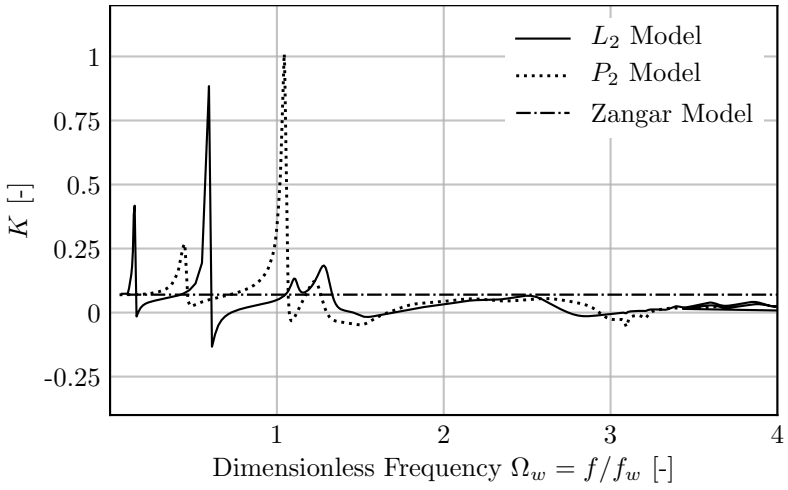

(b) Coupled system with flexible dams

Fig. 3.16: 2D Models - Sweep Analysis - Pressure at dam bottom

It is noticed that the phenomenon is actually more complex than in the case of the rigid dam studied previously. In particular, the distribution of pressures on the section is no longer parabolic for any oscillation frequency. In Figures 3.17g and 3.18g the pressure distributions for the 2 cases are reported for different values of Ω_s.

It is particularly important that for certain situations, points close to the free surface of the fluid can exert greater pressure on the dam than those located below them, in disagreement with the classical results adopted by international regulations. For the specific case of Pertusillo dams, negative absolute pressures are observed on the face of the structure. This implies the possibility of cavitation phenomenon, which will be ignored in this study. However, more in-depth studies are needed in this regard.

From the pressure distributions presented it is evident that not only is it wrong to consider a constant inertial effect of the reservoir on the dam, as suggested by Zangar, but the parabolic distribution suggested in the Italian, Swiss and Japanese regulations is also not on the safety side. Therefore, to describe the increase in stresses on the structure, it is not enough to evaluate the amplification of the pressure at the foot of it. It is necessary to introduce a more significant value, which takes into account the complete distribution of the pressures on the section. The resultant of them is selected, the hydrodynamic thrust $S = \int P(y)$, for it.

In Figure 3.19, the value of S is observed for different values of Ω_s. With the rigid dam hypothesis, the 2 study cases present a similar response, with a maximum amplification around 1.2 times the hydrostatic thrust, for a vibration frequency equal to that of the reservoir resonance. However, this situation changes with the introduction of flexibility. The peaks move to the left and the first amplification is reached for a value less than $\Omega_s = 1$ in both cases. In addition, higher peaks are observed for higher frequencies. In particular, the flexibility of the Lumiei dam introduces higher amplifications for values of f above $2\Omega_s$.

From the foregoing in this section it is concluded that the flexibility of the structure completely modifies the characteristics of the coupled system, making it necessary to consider them, in order to obtain responses close to the real behaviour of the dam-reservoir system.

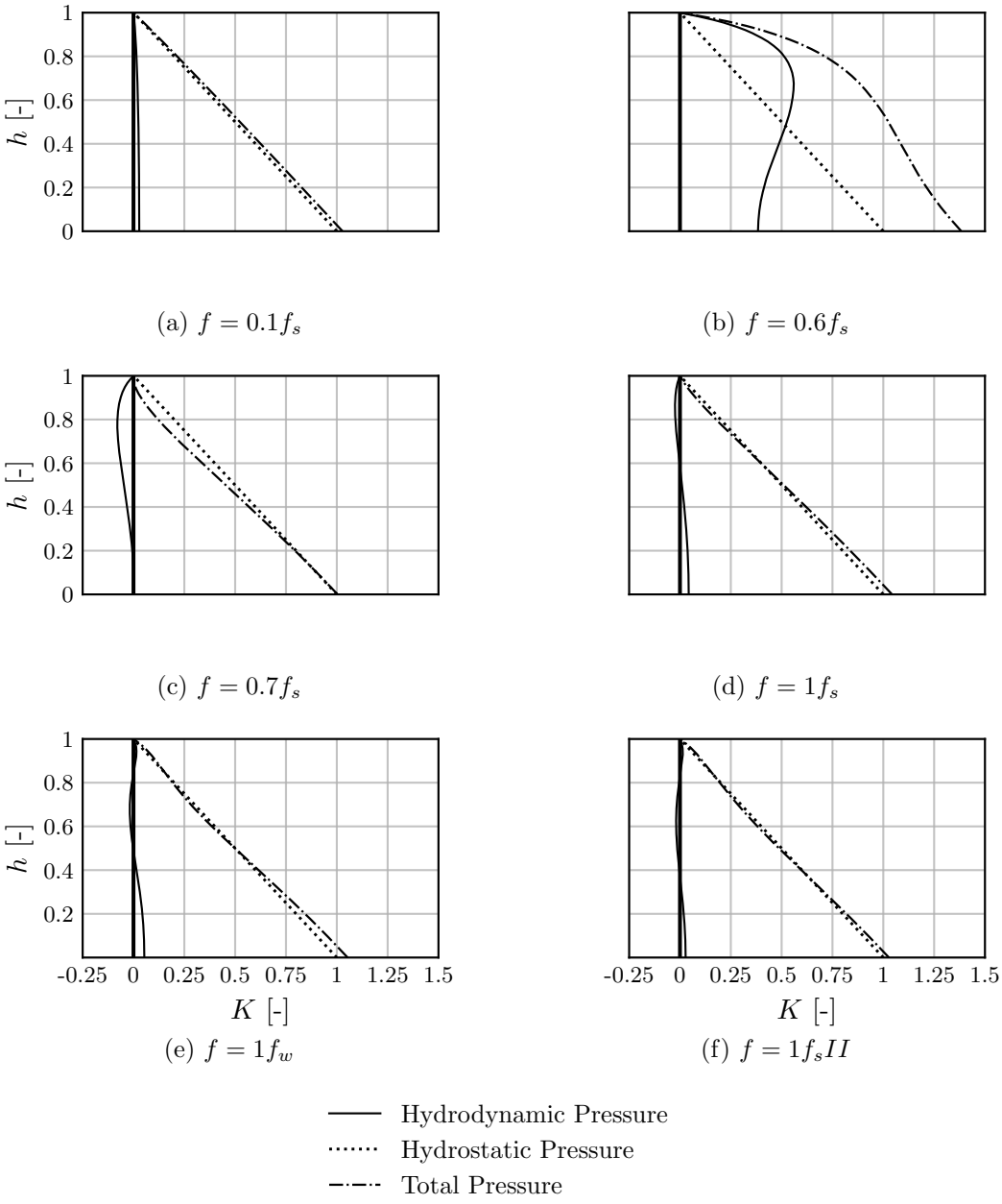

Fig. 3.17: Model L_2 - Pressure distribution for flexible dam

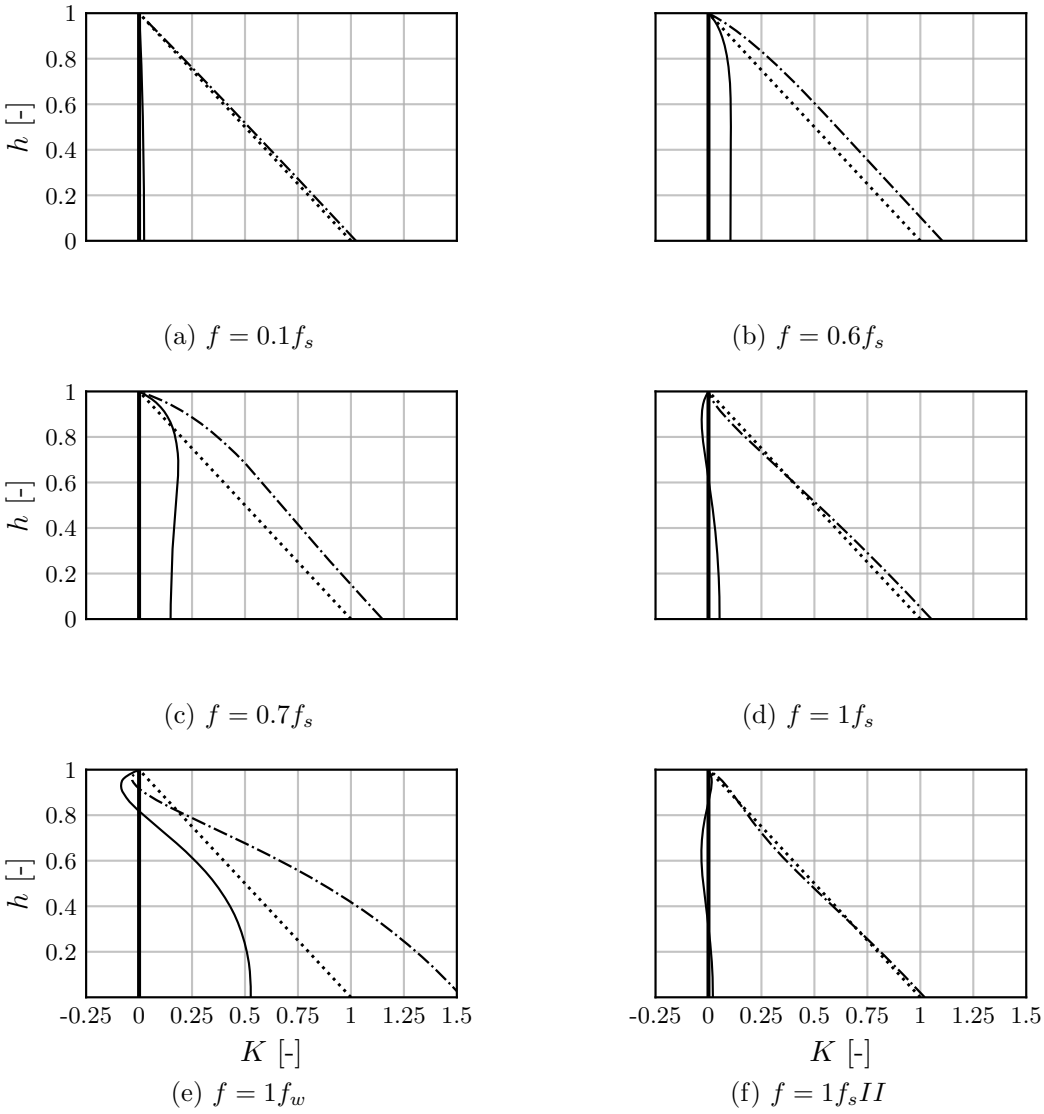

(a) $f = 0.1f_s$ (b) $f = 0.6f_s$

(c) $f = 0.7f_s$ (d) $f = 1f_s$

(e) $f = 1f_w$ (f) $f = 1f_sII$

Fig. 3.18: Model P_2 - Pressure distribution for flexible dam

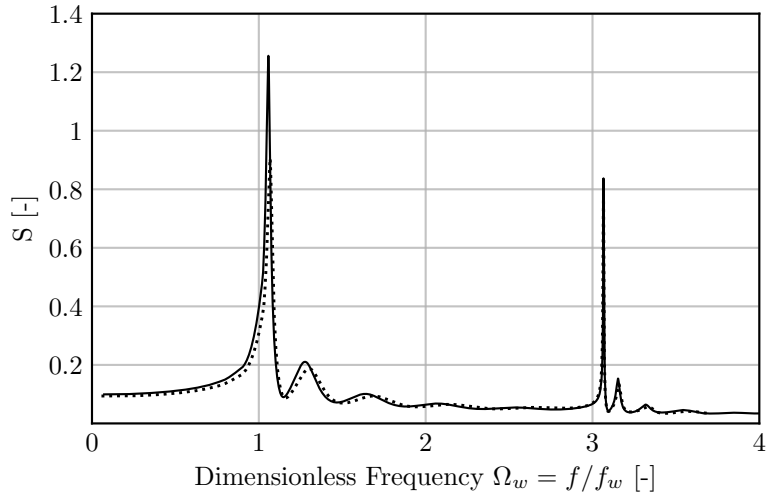

(a) Rigid dams

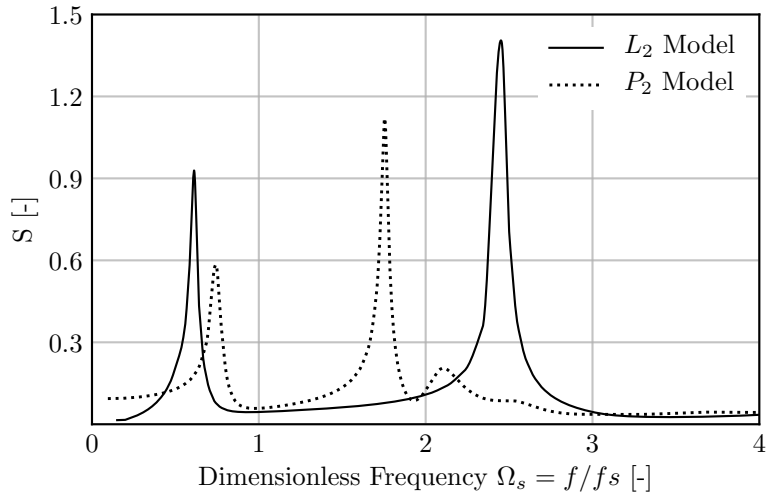

(b) Flexible dams

Fig. 3.19: 2D Models - Hydrodynamic thrusts in Sweep Analysis

3.6.5 Modal analysis of the coupled system

From the previous section, in particular of Figure 3.19, it is understood that the fundamental period of the coupled system is not equal to that of the empty dam, but greater than this. In this section we present the modal analysis of the coupled system and its differences with respect to those of the empty dam.

Dam	**Model**	f_s	f_w	f_a	$(f_s - f_a)/f_s$
Lumiei	L_2	0.663 Hz	2.798 Hz	0.405 Hz	38.91 %
Pertusillo	P_2	2.102 Hz	3.562 Hz	1.570 Hz	28.29 %

Table 3.7: 2D Models - Natural frequencies of the dam-reservoir system

Different increase ratio of system vibration period are observed. This is due to the mass distributions of each case study. In particular, the arch-gravity dam suffers the least variation. Its relatively high stiffness, coupled with its smaller height (103 m against the 131 m of Lumiei), are the causing such situation.

3.6.6 Interpretation of modal coupling

The complete system can be seen as the union of two simple systems with their fundamental periods (elementary oscillators). The set possesses two degrees of freedom, and each of them is associated with its own vibration mode with the corresponding own periods.

For the phenomenon under study, the dam period is known through modal analysis, available through empirical formulations available in literature or any basic software of structures. The reservoir period is obtained through Chopra theory $T_w = 4H/c(2n-1)$. In general:

- $T_1 \neq T_s$
- $T_2 \neq T_w$

where T_1 and T_2 are the first two periods of vibration of the coupled system, T_s the period of the empty dam and T_w that of the reservoir. Two limit cases are identified for the response of the system:

1. $lim_{f_w/f_s \to 0}$: Corresponds to a dam with a frequency much greater than that of the reservoir, that is, relatively rigid with respect to the reservoir. In this case, the problem can be dealt with with the classic solutions, since the lack of flexibility greatly simplifies the interaction.

2. $lim_{f_w/f_s \to \infty}$: Corresponds to the opposite case, that is, as if the fluid were incompressible with respect to the structure. Here it is possible to break down the problem into the two fundamentals proposed by Chopra.

3.7 Height of the reservoir

In this section, the effect of the filling degree of the reservoir on the dynamic behaviour of the system is studied. In general, the depth of a reservoir dam at a given time depends on two factors, the first related to the flows that are taxed in the water course on which the structure is located, and the second with the operating conditions of the reservoir (power generation, drinking water consumption, flood control, etc.)

With the intention of covering a range of situations close to that which occurs in practice, 3 scenarios were considered for each case study.

- The first corresponds to a totally full reservoir, associated with a flood event that supposes a filling level above the normal operation level. $H_e = H$.
- The second belongs to an intermediate point between the first and the last. $H_e = 0.85H$
- The last scenario supposes the opposite situation, that is to say, to a minimum volume, that the norms normally establish in the order of a 65 % of the height of the dam, based on the ecological flow, necessary to protect the fish fauna. $H_e = 0.65H$

The results of the simulations are presented in Figure 3.20. In general, the period of the coupled system increases with the water level, due to a greater amount of mass in the system, for the same rigidity. On the other hand, amplifications at high frequencies increase for intermediate fill values. In both cases, the amplifications for the first peak remain or decrease with respect to the full dam.

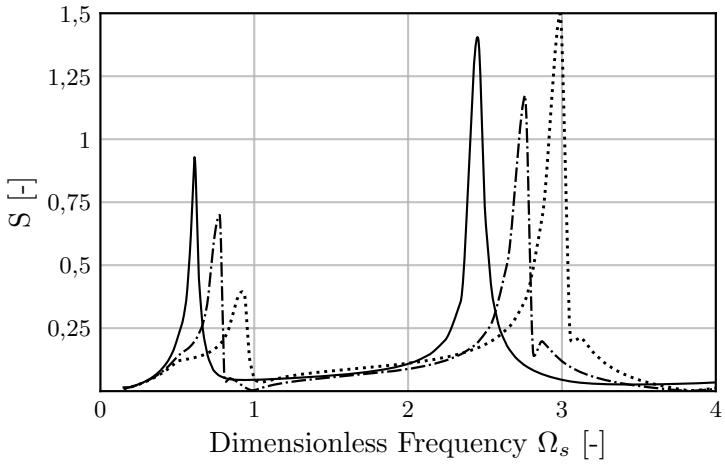

(a) Lumiei Dam

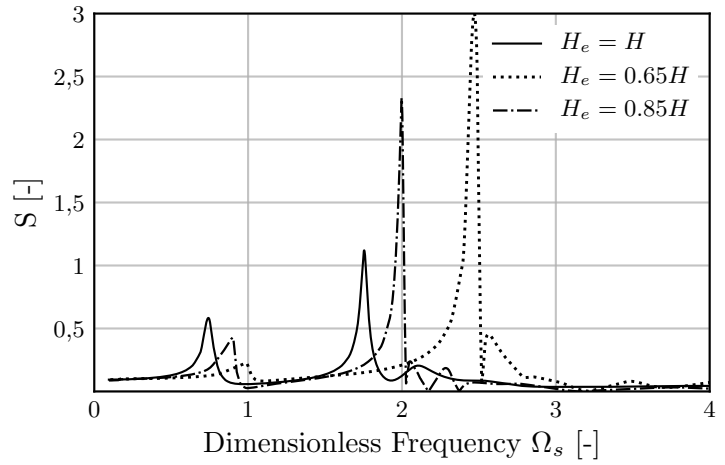

(b) Pertusillo Dam

Fig. 3.20: 2D Models - Effect of reservoir depth

3.8 Vertical vibration

The next boundary condition to be evaluated is the direction in which the oscillation occurs. Although normally the most important vibrations are developed perpendicular to the master section of the dam, there are vertical accelerations caused by these.

Figure 3.21 shows a direct comparison between the amplifications generated by horizontal and vertical oscillations, respectively. The former are clearly superior, by an order of magnitude.

In addition, it is evident that the same modes of vibration are activated for both directions of oscillation, as observed in the peaks that coincide on the axis Ω_s.

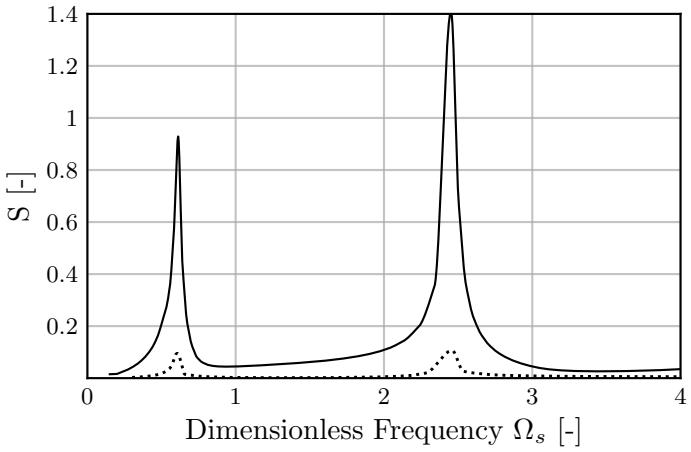

(a) Lumiei Dam

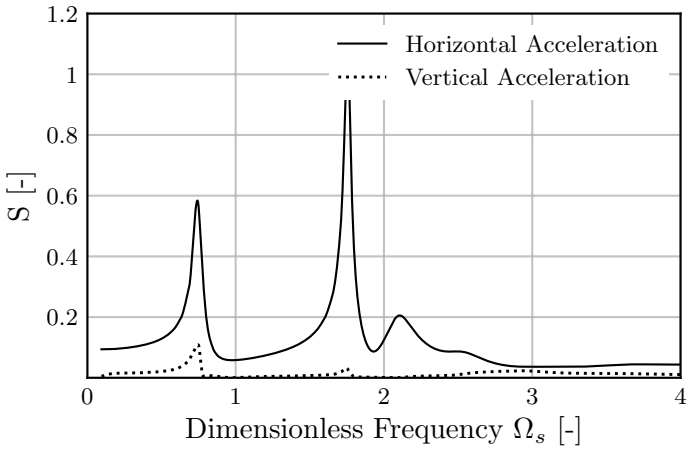

(b) Pertusillo Dam

Fig. 3.21: 2D Models - Effect of oscillation direction

3.9 Dissipation of energy by the sediments in the reservoir bed

This section presents the effects of energy absorption caused by the presence of deformable sediments in the reservoir bed. Numerous models exist in literature, of diverse relative complexity, for the simulation of the phenomenon.

In the present investigation, it was chosen to evaluate the process by means of an acoustic surface with an assigned impedance, as a function of assigned values of the dissipation coefficient α_r. Five notable values were chosen, presented in Table 3.8.

α_r	**Acoustic impedance**
1.00	∞
0.90	27.36×10^6 kg/s* m^2
0.70	79.30×10^5 kg/s* m^2
0.50	42.00×10^5 kg/s* m^2
0	14.00×10^5 kg/s* m^2

Table 3.8: Correspondence between values of α_r and acoustic impedances

Figure 3.22 shows the effect for each value of α_r for each dam. In the case of the more flexible dam, Lumiei, no changes are observed in the periods of the coupled system. For the Pertusillo dam moderate variations are detected.

Though its determination is complex. is safe to say that considering an average value of α_r seems to be enough in order to simulate realistic pressures.

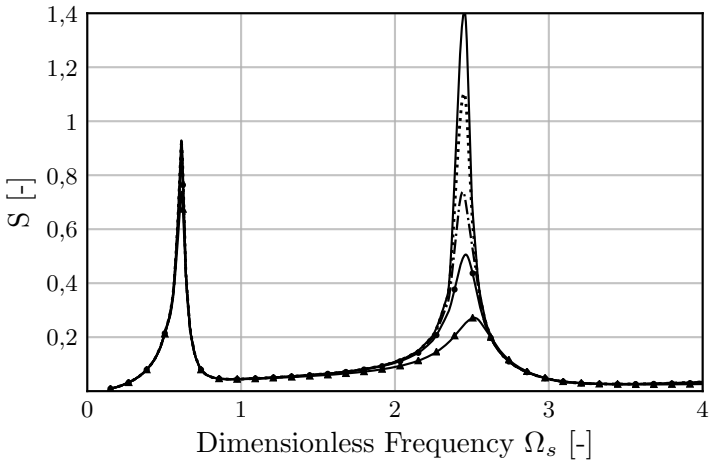

(a) Lumiei Dam

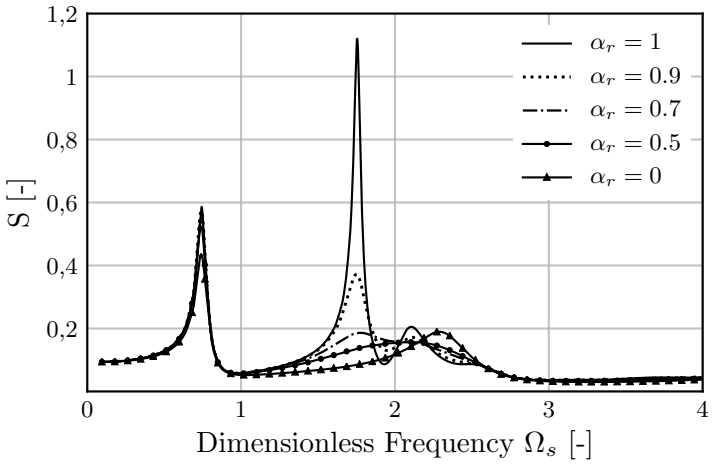

(b) Pertusillo dam

Fig. 3.22: 2D Models - Effect of sediments energy absorption

3.10 Three-dimensional models

Three-dimensional models of the case studies were built, respecting the geometries of the reservoirs. Through a process analogous to the one followed for the two-dimensional models, the convergence of the calculation meshes, the influence of the location and the types of elements used were studied. Figure 3.23 shows the first vibrating mode of each dam. It is observed that the fundamental mechanism is different in both cases.

Lumiei, presents an antisymmetric mode with respect to the main section on the ridge. This is particularly interesting for transverse vibrations, in the tangential sense to the horizontal arcs. On the other hand, Pertusillo presents a symmetrical way in the radial sense, typical of a structure of high flexibility fixed on its extremes.

In Table 3.9 the fundamental frequencies of empty dams, reservoirs and coupled systems are presented. Lumiei goes from being the most flexible dam to being the most rigid. Pertusillo, also increases its rigidity considerably.

Dam	**Model**	f_s	f_w	f_a	$(f_s - f_a)/f_s$
Lumiei	L_3	6.887 Hz	2.885 Hz	2.885 Hz	58.11 %
Pertusillo	P_3	4.773 Hz	4.655 Hz	3.521 Hz	26.23 %

Table 3.9: 3D Models - Natural frequencies of the dam-reservoir system

From the amplifications represented in Figure 3.25 it is understood that if the dams are considered rigid, the main mechanism is similar to the two-dimensional case, but with certain differences due to the geometry of the acoustic domain. On the other hand, if they are considered flexible, the amplifications are slightly higher with respect to the two-dimensional case, eliminating the peaks corresponding to higher values of Ω_s. This means that it is the first mode of the coupled system that is activated most effectively.

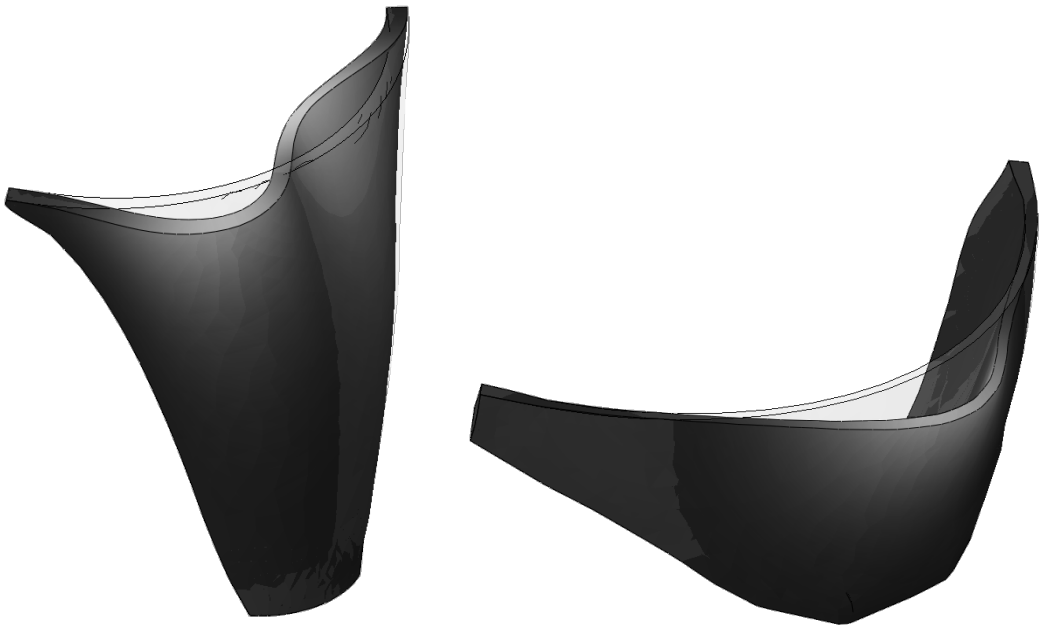

(a) Lumiei (b) Pertusillo

Fig. 3.23: 3D Models - First vibration mode

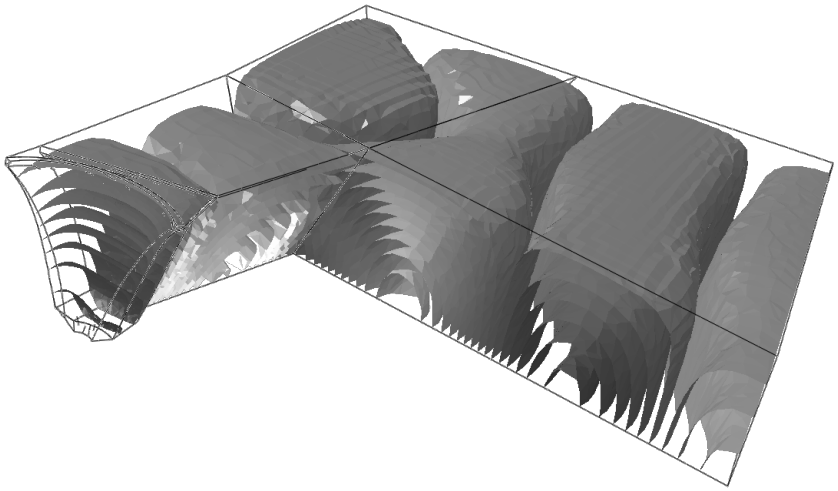

(a) Lumiei Dam

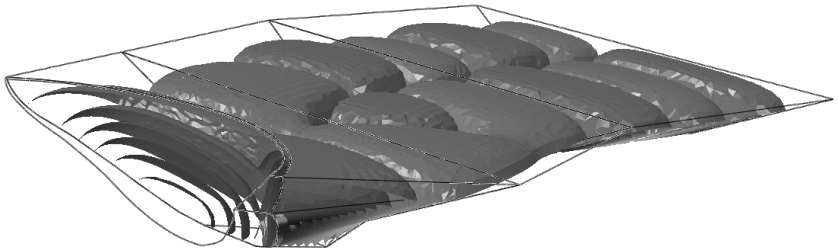

(b) Pertusillo Dam

Fig. 3.24: 3D Models - Transmission of acoustic waves within the reservoir

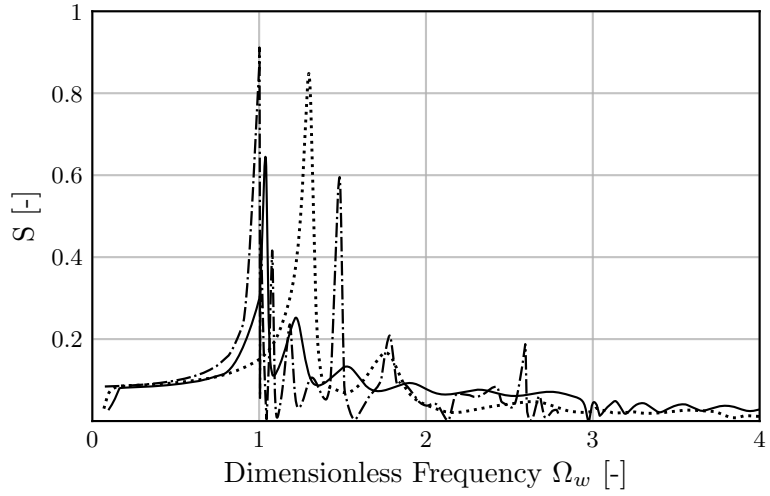

(a) Rigid dams

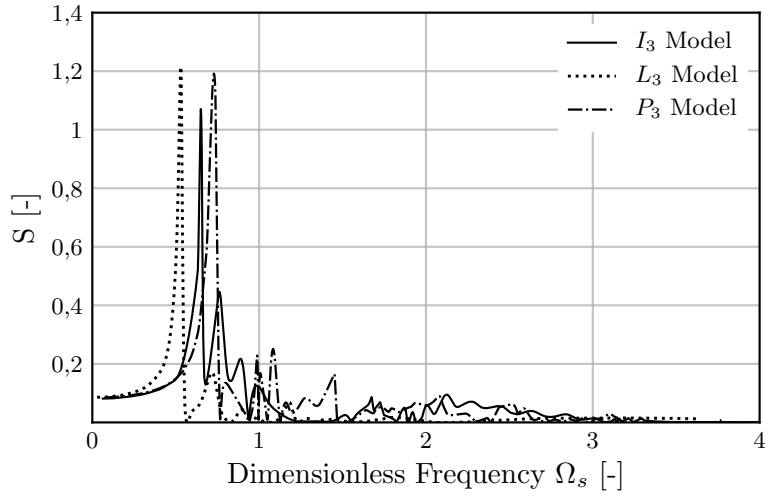

(b) Flexible dams

Fig. 3.25: 3D Models - Hydrodynamic thrusts in Sweep Analysis

3.11 Added Masses

In order to obtain an idea of the precision of the method in comparison with the classics, simulations were performed by adding point masses to the two-dimensional models, in such a way to simulate the hydrodynamic forces. These masses were calculated according to the Westergaard model, introduced in Section 1.2.2.1.

Figure 3.26 shows the differences between both procedures. In general, the aggregate point masses are on the safety side, overestimating the hydrodynamic thrusts. The amplifications are similar for frequencies less than f_w, but diverge for higher values. This is because the masses are calculated using the Westergaard model, which is limited to the aforementioned range. Therefore, for frequencies greater than f_w the method loses precision and although, for rapid estimates it is a useful procedure, it must always be supported by some more detailed numerical method such as that proposed in the present investigation.

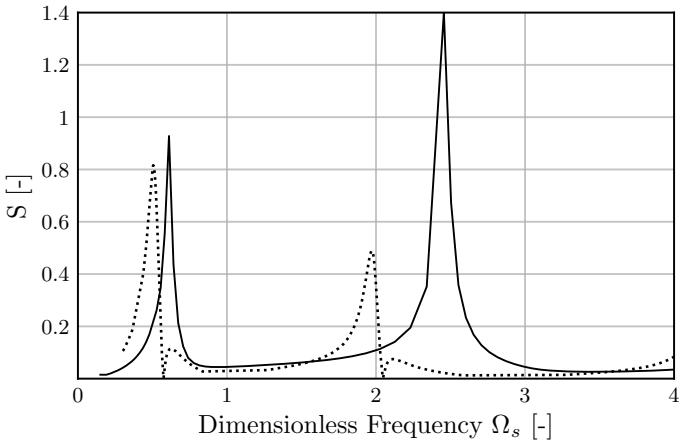

(a) Lumiei Dam

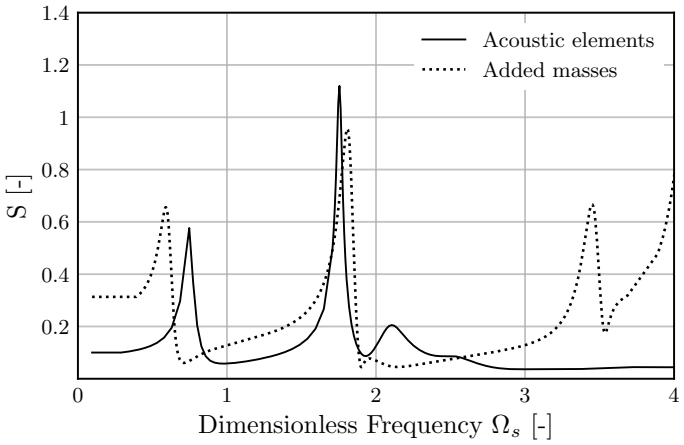

(b) Pertusillo Dam

Fig. 3.26: 2D Model - Added masses method

3.12 Rock mesh

For modelling the foundation rock and surrounding terrain, a parametric analysis was performed, considering 4 parameters; the 3 dimensions of the terrain portion and the ratio $K_t = E_c/E_f$, that is, the elastic modulus of the concrete divided by the elastic modulus of the foundation rock. The dam was considered fixed to the terrain through the abutments, and the rock was considered fixed in space through fixed links located on its contour. In this way, varying the value of the parameters above mentioned, different models of different dimensions were considered. Under static load for the dam and the terrain, stresses and strains were monitored. The aim was to find suitable ratios of $H/L/B$ such that the portion of terrain modelled did not influence the behaviour of the dam through local effects.

The following conclusions are drawn from this analysis:

- Quadratic elements converge quicker to a stable solution.
- Tetrahedral elements are more suitable to model geometric irregularities.
- 3 elements seem to be the lower limit to catch up the bending behaviour of the dam on the radial direction (through the thickness).
- In agreement with the USA code recommendations [14], if $K_t \geq 1$ a terrain portion of $H_t = B_t = L_t = H$, where H is the height of the dam, seems to be enough to avoid local effects. If $0{,}25 \leq K_t \leq 0{,}5$ a portion with $H_t = B_t = L_T = 2H$ is required.

3.13 Joints modelling

Given that dams are built deep into foundation rocks, with important excavation volumes, perimeter joints can be considered as fixed on the terrain in the tangential direction. Still, their tensile strength is limited, not being able to transmit tensile stresses during dynamic events. However, in order to limit computational cost and favour convergence, in this research the perimeter joints are considered as completely fixed on the foundation. By doing so, the possibility of sliding is discarded, which actually is a good approximation to reality, but tensile stresses become unrealistic high on the upstream face of the dam. However, the accurate description of stress distribution is not the main scope of this research, but to check the capability of metamodels to estimate selected EDPs for linear and non-linear models with an acceptable precision. On the other hand, joints opening and sliding between cantilevers are simulated with a Hard contact algorithm, with a mean value of the friction coefficient μ of 1.0.

Figures 3.27 and 3.28 compare stresses distribution in linear and non linear models. As explained above, non linear model results in a slight increment of tensile and compressive stresses. Figures 3.29 and 3.30 gives an analogous comparison for dynamic loads. The same trend is identified. Figure 3.31 shows the maximum joints opening for static and for the reference dynamic input. Crest displacements, on the other hand, have a higher range of variation. For the monolithic model, an absolute value of 16 cm is reported, whereas a value of 35 cm is reported for the jointed model.

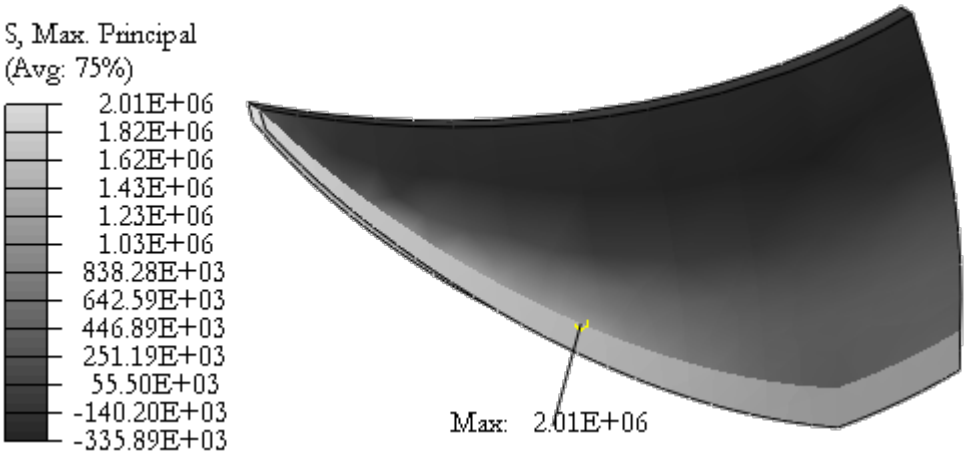

(a) Tensile Stresses

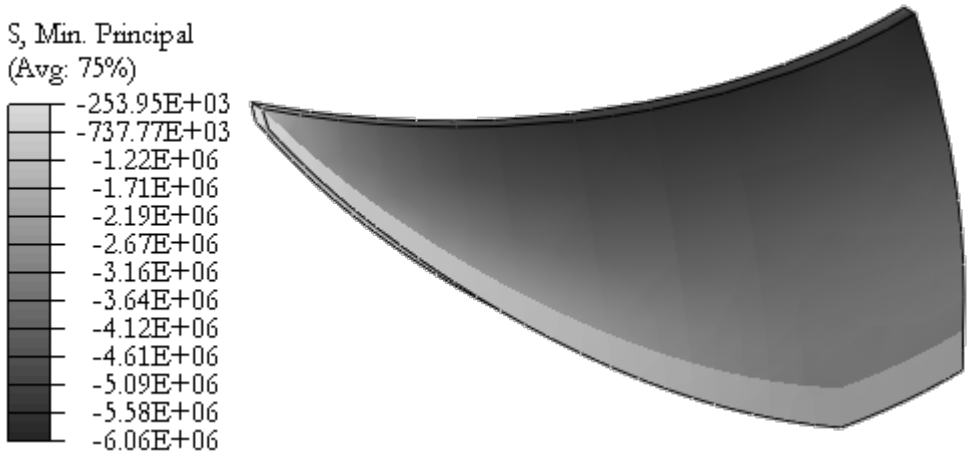

(b) Compressive Stresses

Fig. 3.27: Persutillo Monolithic Dam - Stresses for Static Loads

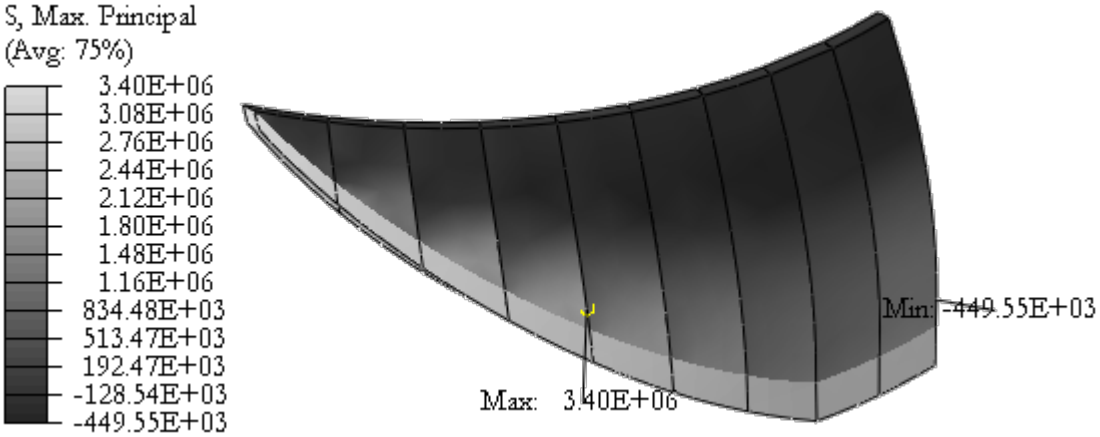

(a) Tensile Stresses

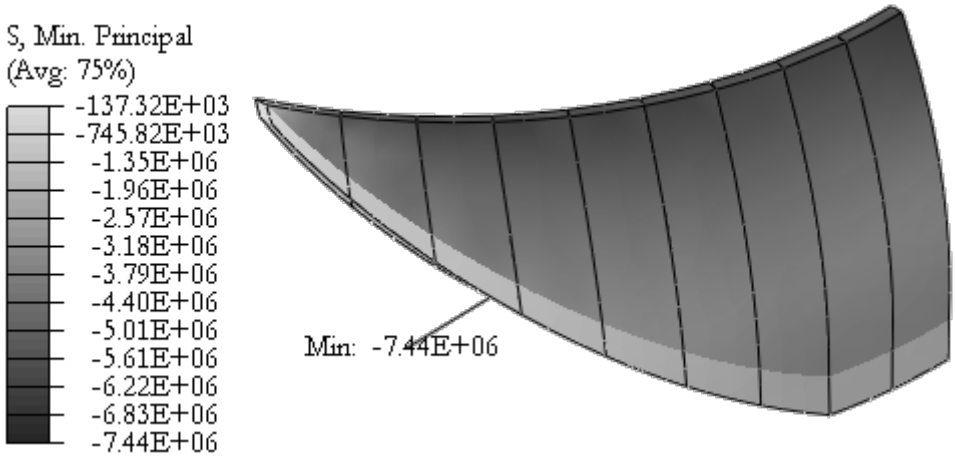

(b) Compressive Stresses

Fig. 3.28: Persutillo Jointed Dam - Stresses for Static Loads

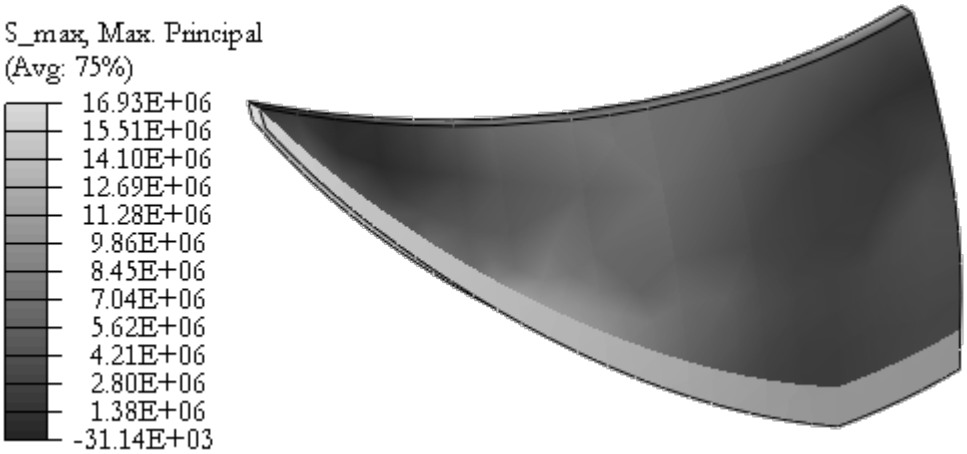

(a) Tensile Stresses

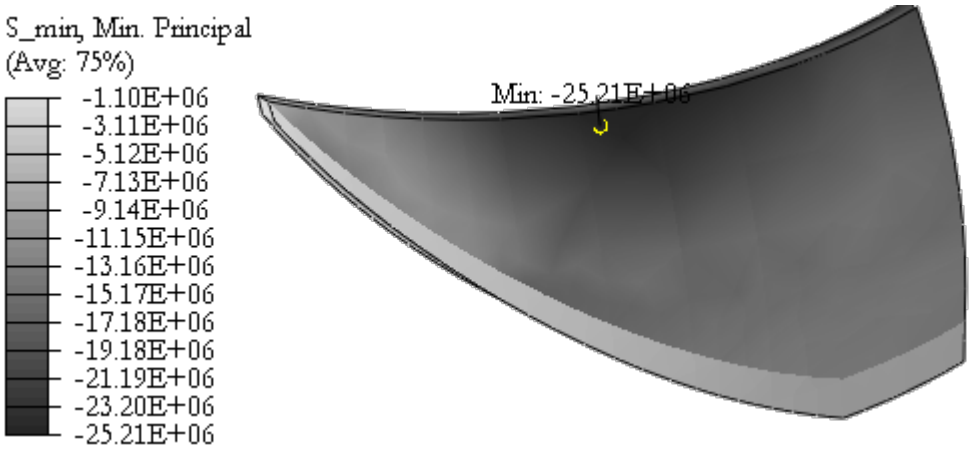

(b) Compressive Stresses

Fig. 3.29: Persutillo Monolitic Dam - Stresses for Dynamic Loads

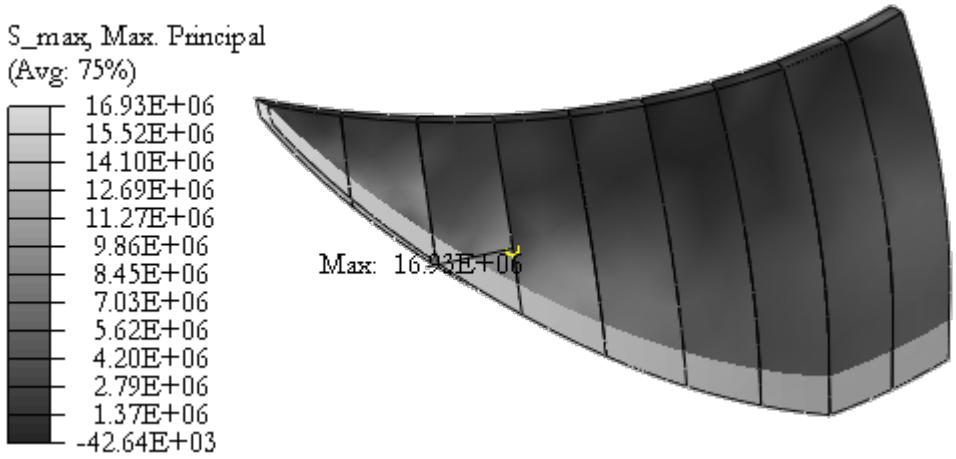

(a) Tensile Stresses

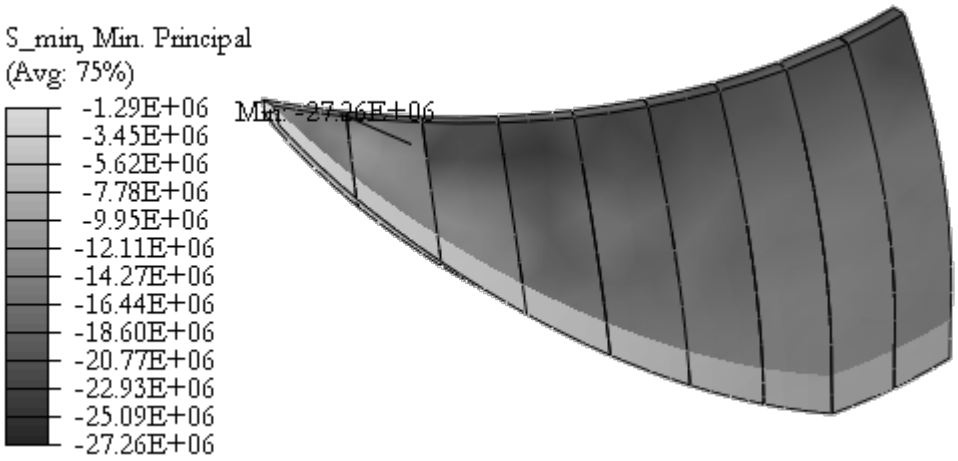

(b) Compressive Stresses

Fig. 3.30: Persutillo Jointed Dam - Stresses for Dynamic Loads

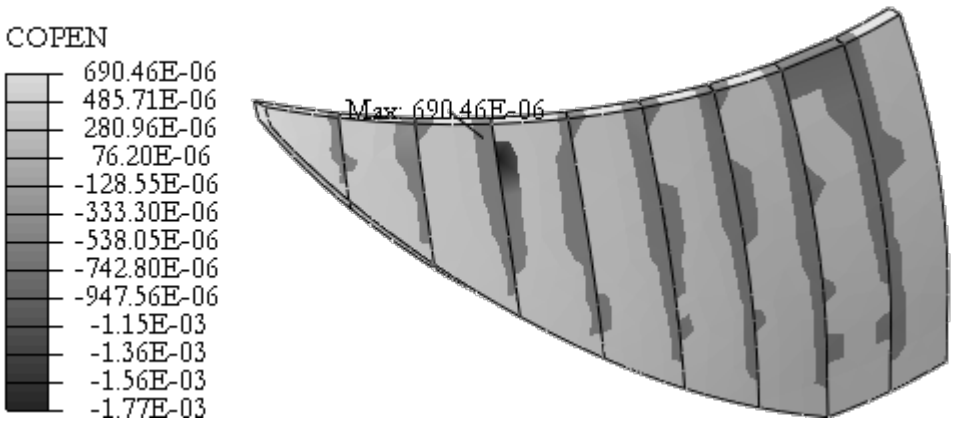

(a) Joint opening for Static Loads

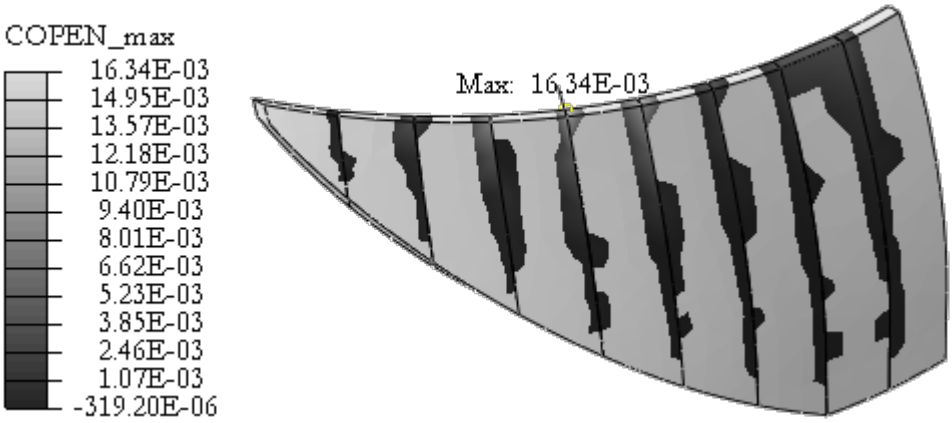

(b) Joint opening for Dynamic Loads

Fig. 3.31: Pertusillo Jointed Dam - Joints openings

3.14 Deterministic reference analysis

Deterministic analyses are carried on for the models reported in Table 3.10. Their reservoir are constructed with acoustic elements using results obtained in the FSI study as guidance. Quadratic elements are used both for the structure and terrain.

Three loads are imposed to the dam, two statics and one dynamic; own weight, hydrostatic with a full reservoir and the strong motion record depicted in 3.32. Maximum principal tensile and compressive stresses and maximum crown accelerations and displacements are monitored for the linear models. For the jointed models, joints sliding and opening are monitored in top of the mentioned linear EDPs.

Code	Dam	Joints
A	Lumiei	No
B	Pertusillo	No
C	Lumiei	Yes
D	Pertusillo	Yes

Table 3.10: Models used for Uncertainty analysis

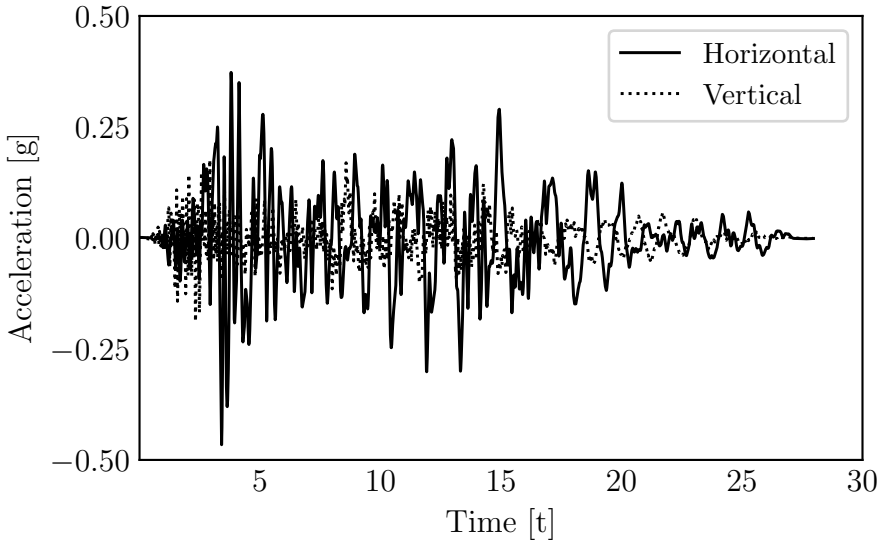

Fig. 3.32: Dinar Strong Motion record

3.15 Sensitivity analysis

A bound variation of ±20% is considered for each input factor. This are selected through a careful review of the results obtained until this point. Input parameters and their design space are described in Table 3.11.

Symbol	DL	Mean	UL
E_c	28×10^3 MPa	35×10^3 MPa	42×10^3 MPa
ν_c	0.18	0.22	0.26
ρ_c	2000 kgm3	2500 kgm3	3000 kgm3
μ	0.80	1.00	1.20
ζ_c	0.04	0.05	0.06
E_c	25.2×10^3 MPa	31.5×10^3 MPa	37.8×10^3 MPa
ν_f	0.18	0.22	0.26
α_r	0.40	0.50	0.60

Table 3.11: Bound variation of input parameters for SA

E_c: Concrete elasticity modulus, ν_c: Concrete Poisson ratio, ρ_c: Concrete mass density, μ: Concrete coefficient of friction, ζ_c: Concrete critical damping ratio, E_c: Foundation elasticity modulus, ν_f: Foundation Poisson ratio, α_r: Reservoir coefficient of reflectivity.

Results are reported in form of tornado plots, for each model in for each monitored EDP. It is clear that different EDPs are influenced more or less by different input parameter, thus there is no a clear trend between input and outputs a priori. Also, variability range of joints opening is wider for the model with less joints, and narrower for joints slippage. Crest displacement is more variable for jointed models. Yet, again the range is bigger for the model with less joints.

Three design factors are selected for the Lumiei dam and five for the Pertusillo dam. They are summarized in Table 3.12.

Model	Factors
A	E_c, E_f, ρ_c
B	E_c, E_f, ρ_c, ζ_c, α_r
C	E_c, ρ_c, μ
D	E_c, ρ_c, ζ_c, α_r, μ

Table 3.12: Factors selected for DOE

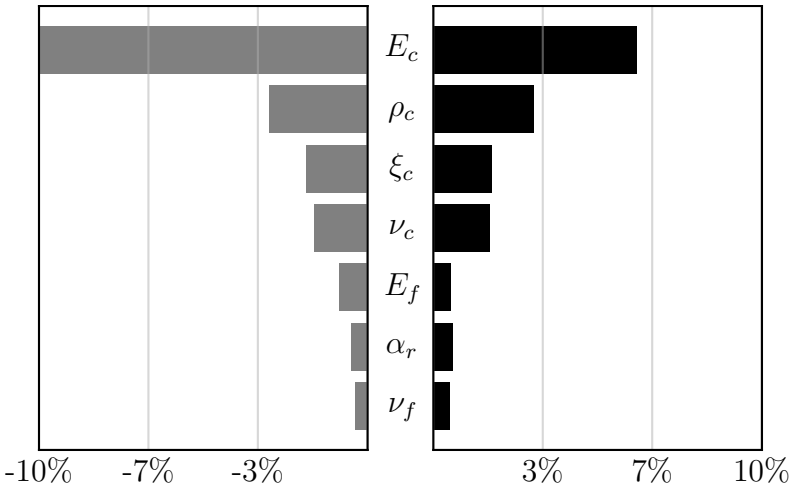

(a) Maximum Crest Displacement

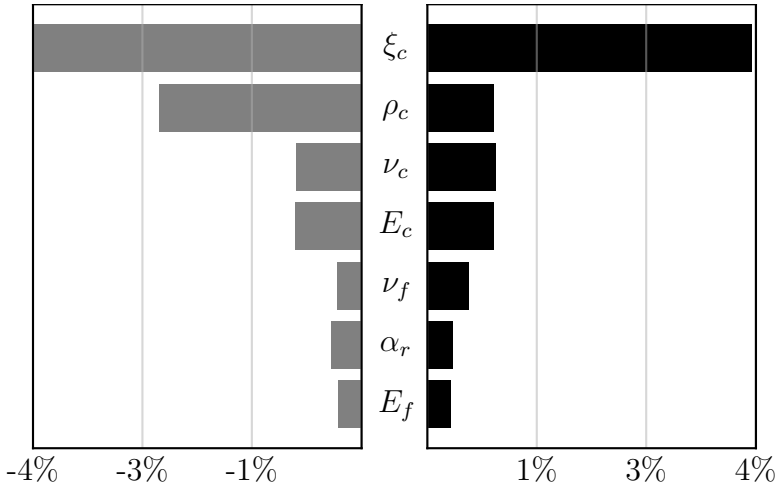

(b) Maximum Crest Acceleration

Fig. 3.33: Tornado Diagrams - Model A

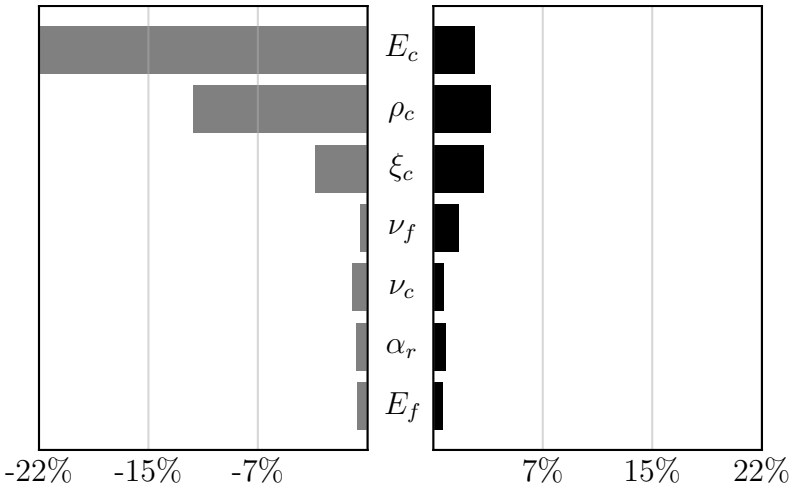

(c) Maximum Principal Tensile Stress

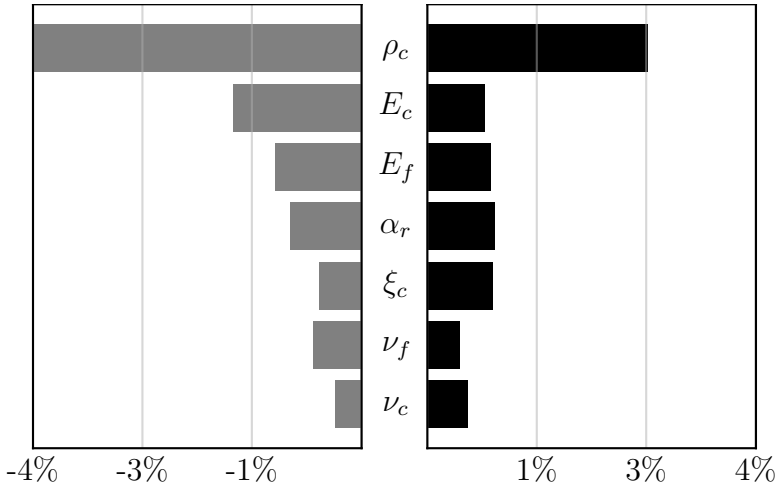

(d) Maximum Principal Compresive Stress

Fig. 3.33: Tornado Diagrams - Model A

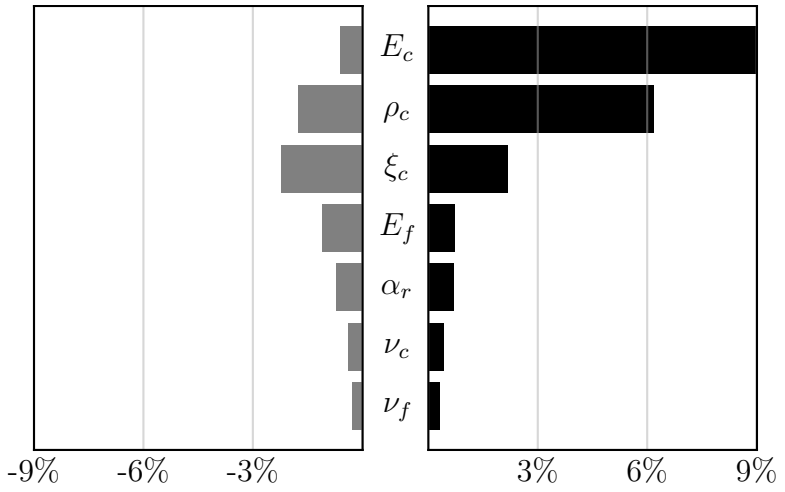

(a) Maximum Crest Displacement

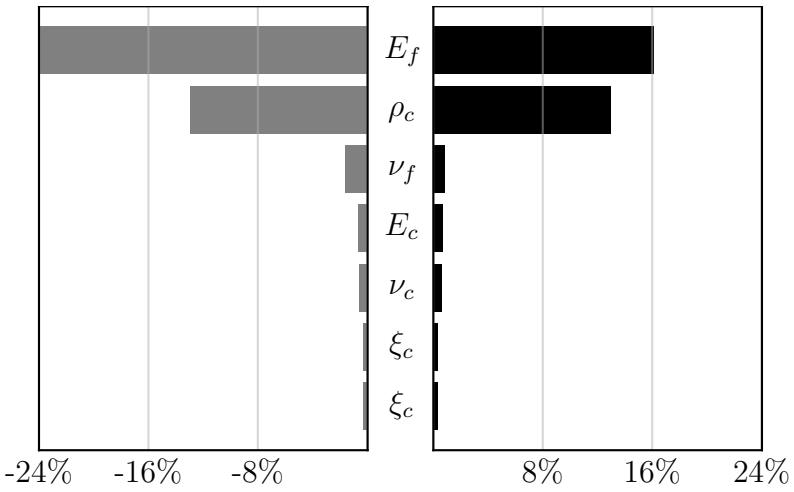

(b) Maximum Crest Acceleration

Fig. 3.34: Tornado Diagrams - Model B

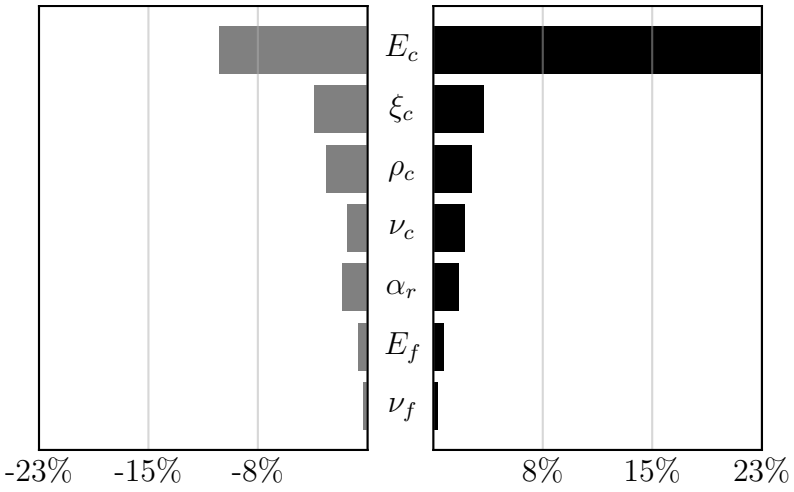

(c) Maximum Principal Tensile Stress

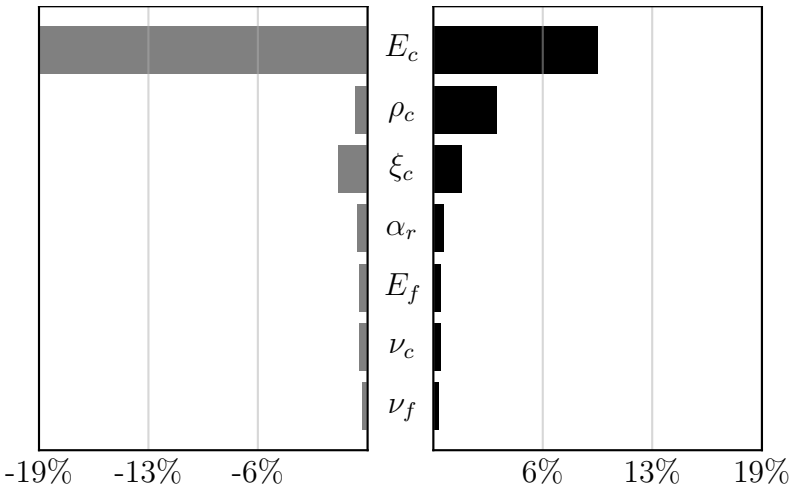

(d) Maximum Principal Compresive Stress

Fig. 3.34: Tornado Diagrams - Model B

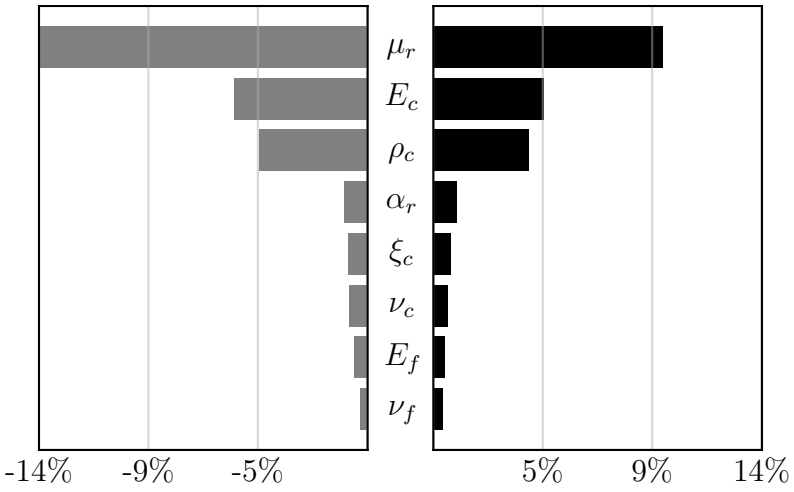

(a) Maximum Crest Displacement

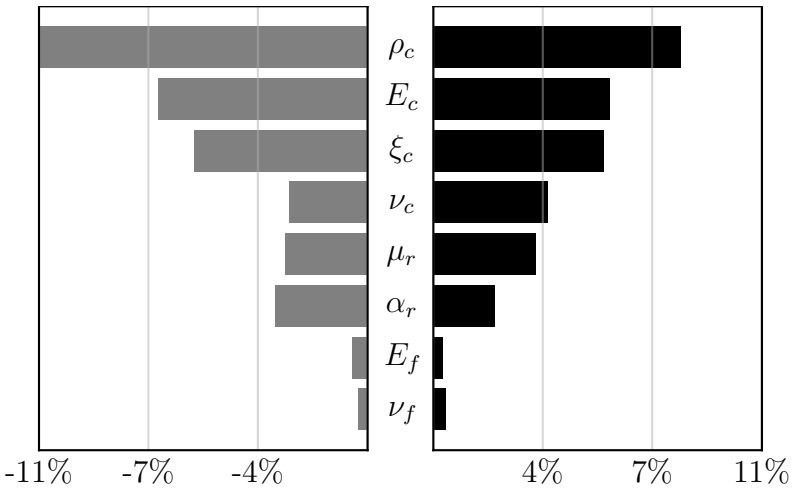

(b) Maximum Crest Acceleration

Fig. 3.35: Tornado Diagrams - Model C

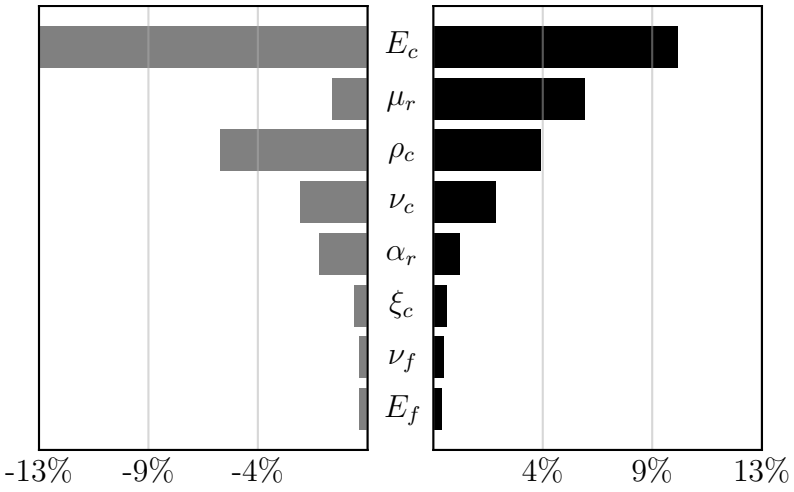

(c) Maximum Joints Opening

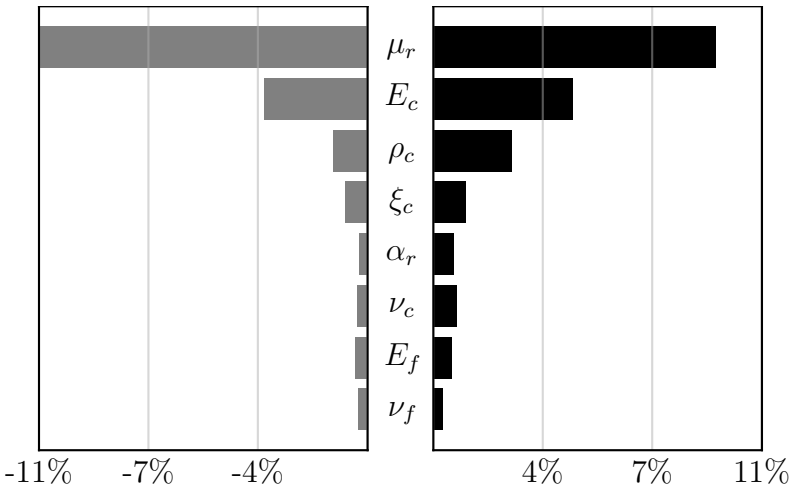

(d) Maximum Joints Slippage

Fig. 3.35: Tornado Diagrams - Model C

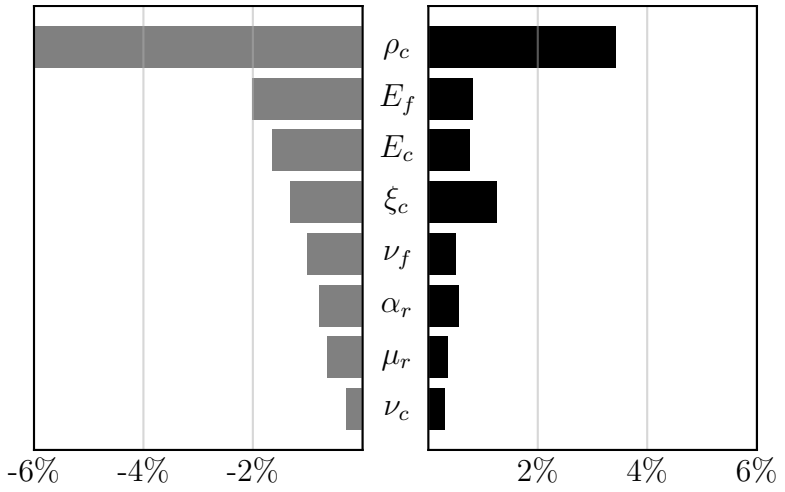

(a) Maximum Crest Displacement

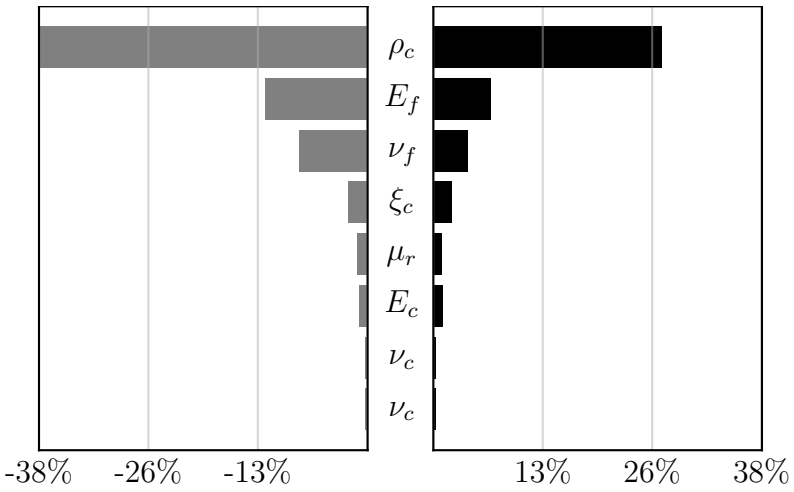

(b) Maximum Crest Acceleration

Fig. 3.36: Tornado Diagrams - Model D

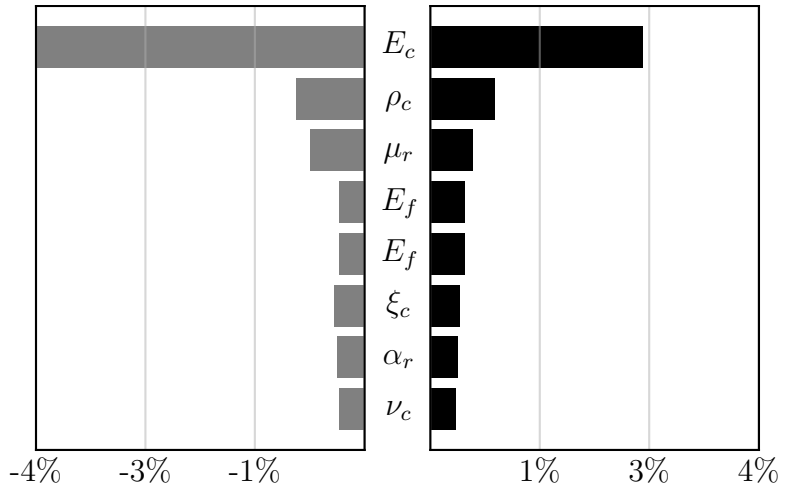

(c) Maximum Joints Opening

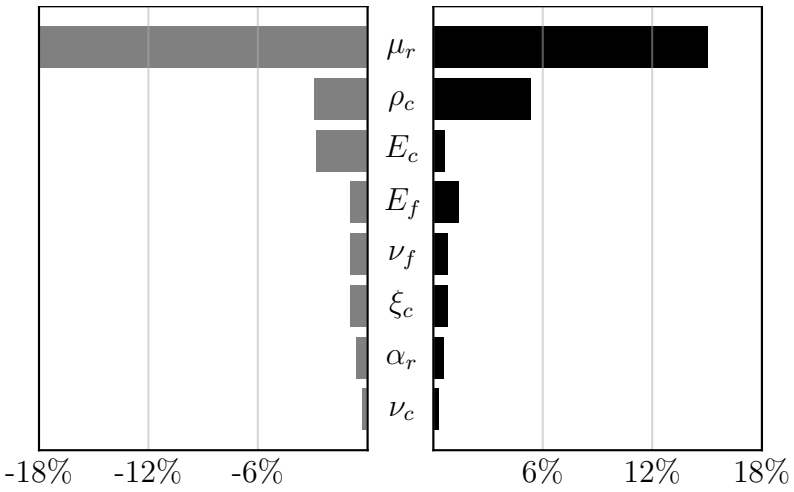

(d) Maximum Joints Slippage

Fig. 3.36: Tornado Diagrams - Model D

3.16 Design of experiments

In this section, the five DOEs in study are applied in order to obtain the design factor combinations.

The amount of experiments for each model and DOE technique is summarized on Table 3.13. For each DOE procedure there is a maximum degree of polynomial that can be fitted trough least squares. Whenever is possible, linear, quadratic and cubic polynomials are fitted, in order to further understand the effect of the polynomial degree. Figure 3.51 depicts the rate of grow of N_{DOE} for the 5 DOEs presented. It is clear that Full Factorial designs are not feasible for an important number of factors. FFD3 reaches the thousand experiments for $k = 8$.

Model	**FFD3**	**FFD2**	**BBOX**	**CCD**	**PBD**
A	27	8	13	15	4
B	243	32	41	43	8
C	27	8	13	15	4
D	243	32	41	43	8

Table 3.13: Amount of DOE experiments for each model

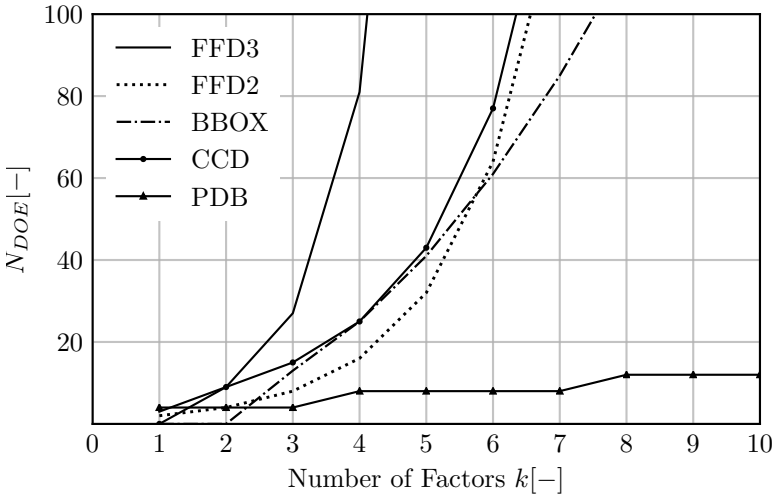

Fig. 3.37: Number of experiments required by each DOE technique

3.17 Sampling for uncertainty analysis

LHS, Halton and Sobol sequences are used to sample input factors in this research. Distributions patterns are depicted in Figure 3.38. It is clear that Halton and Sobol schemes produce much more consistent samples, and consequently the design space can be covered with less data points.

1000 samples were collected with each scheme for the linear models. The uniformity of distribution were checked using the mean of the output of every sample. These are reported in Figures 3.39 and 3.40. LHS needs a higher number of experiments to stabilize around the mean of the design space. Sobol and Halton need around 250 simulations only.

On the other hand, for non linear models only Halton sequence was utilized, because of its efficiency. This is represented in Figures 3.41 and 3.42. Also in this case, the sampling mean stabilizes with around 250 simulations, even for the case of $k = 5$.

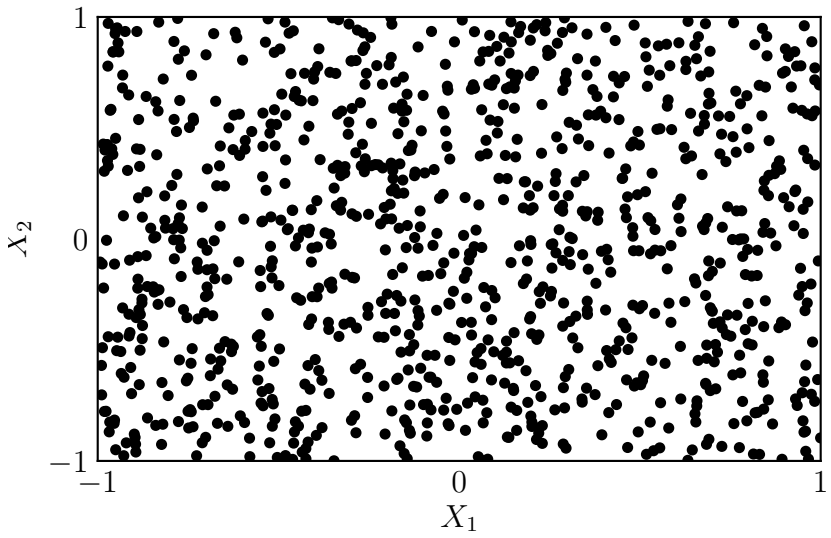

(a) Monte Carlo Sampling

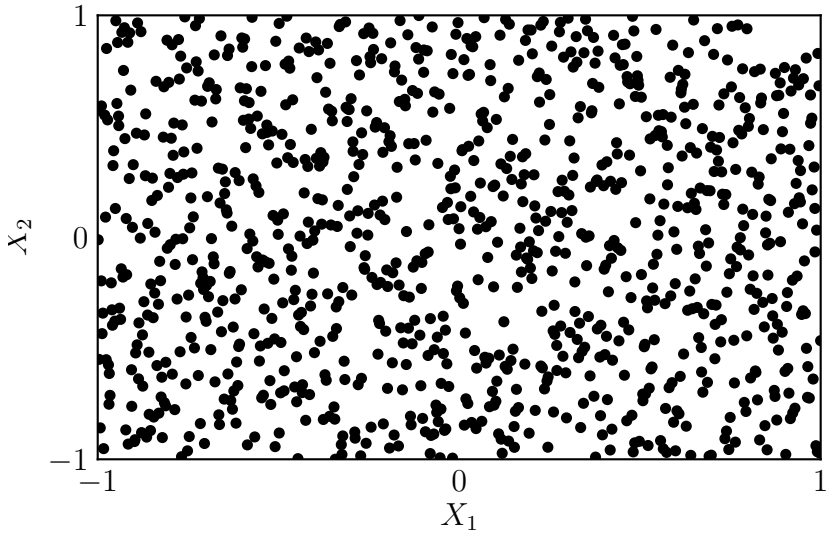

(b) Latin Hypercube Sampling

Fig. 3.38: Sampling sequences

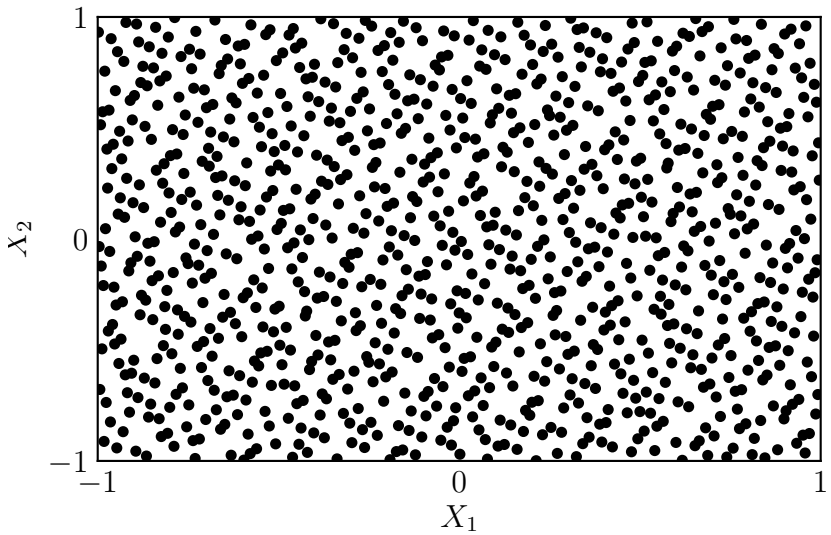

(c) Halton Sampling

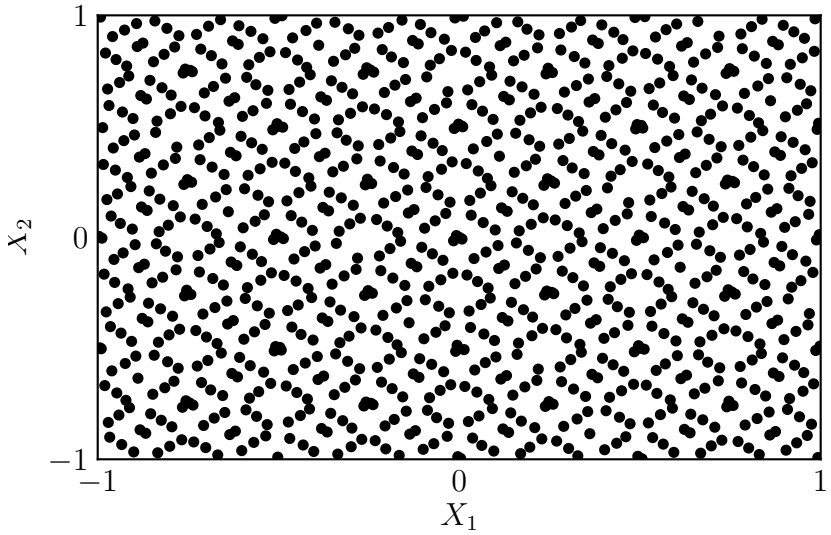

(d) Sobol Sampling

Fig. 3.38: Sampling sequences

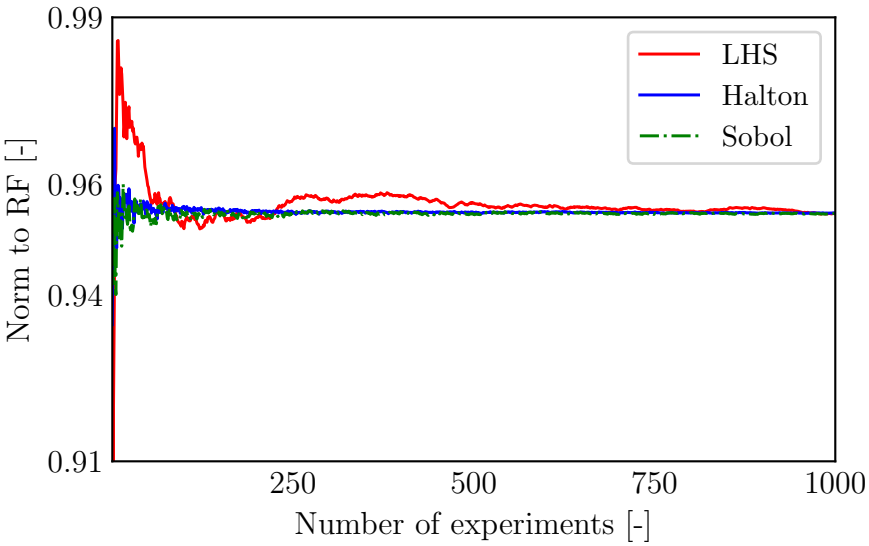

(a) Maximum crest displacement

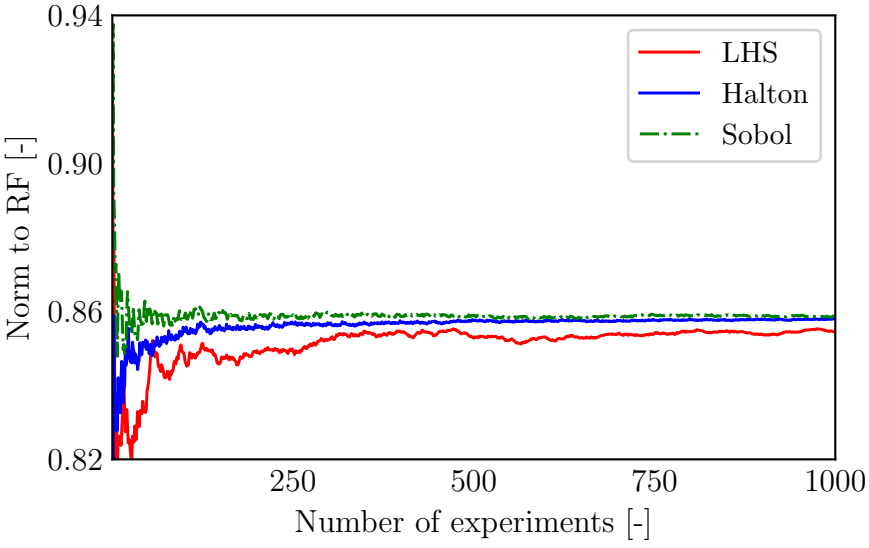

(b) Maximum tensile stress

Fig. 3.39: Model A - EDPs sampling convergence

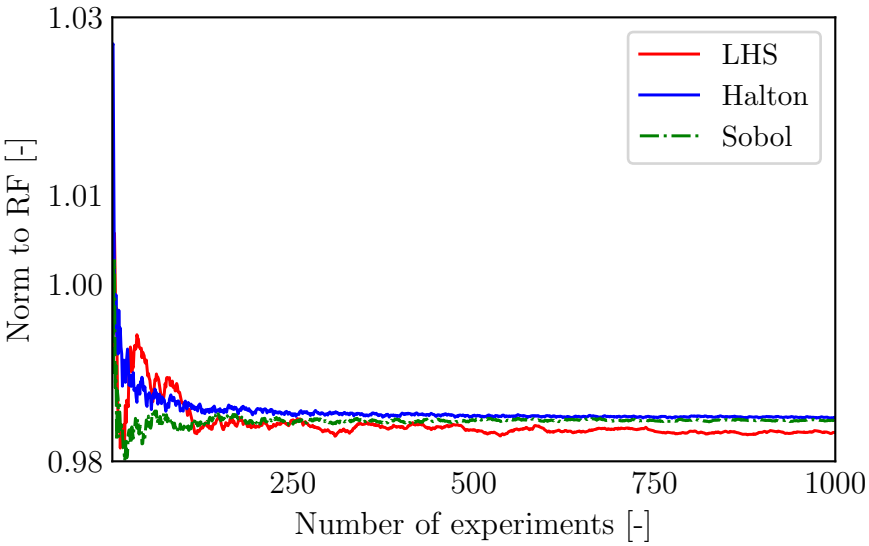

(a) Maximum crest displacement

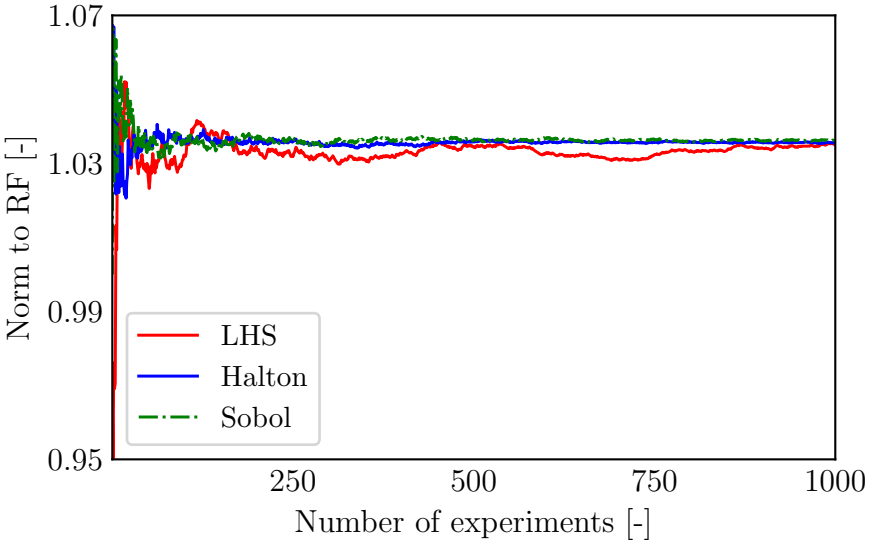

(b) Maximum tensile stress

Fig. 3.40: Model B - EDPs sampling convergence

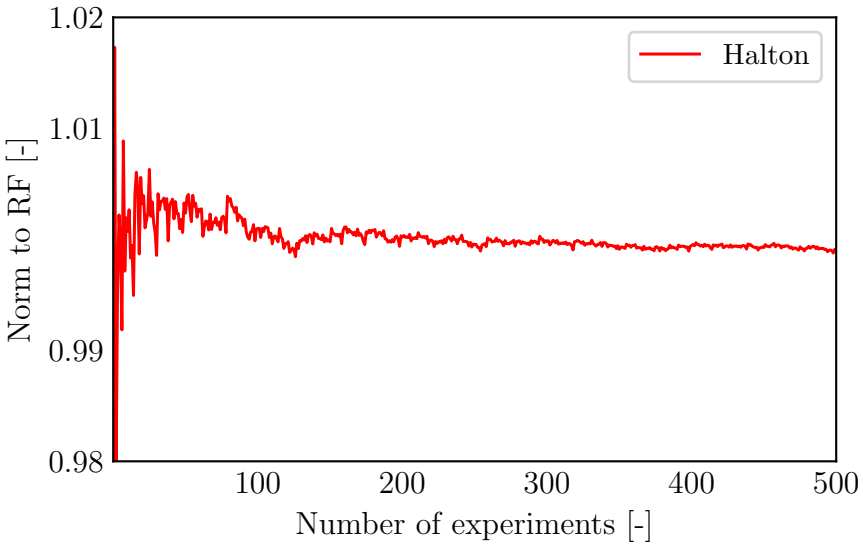

(a) Maximum joints opening

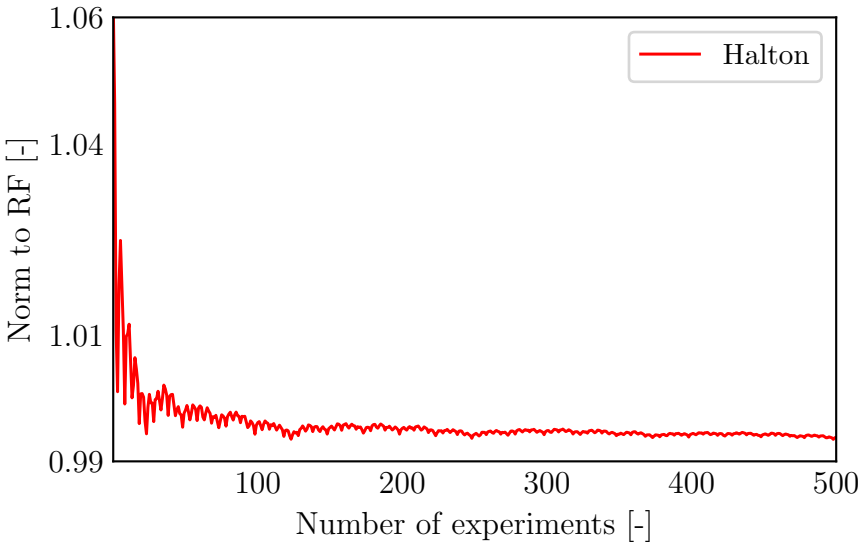

(b) Maximum joints slippage

Fig. 3.41: Model C - EDPs sampling convergence

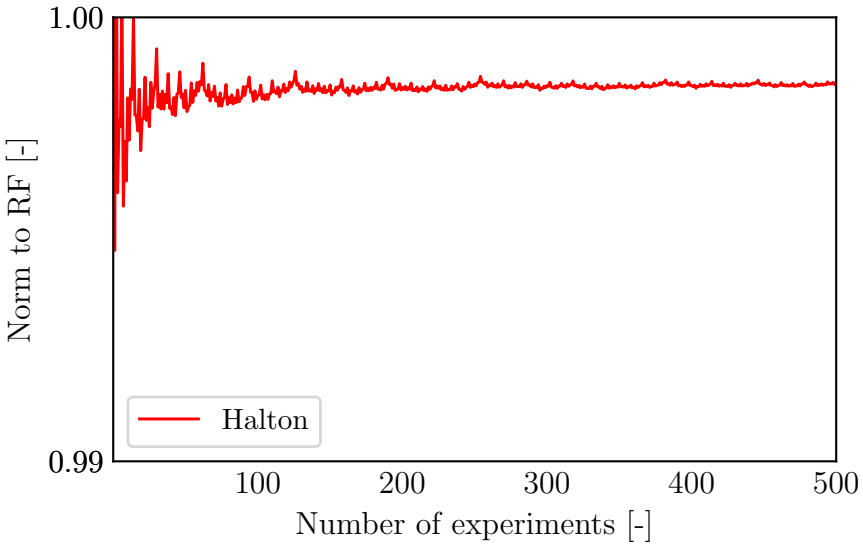

(a) Maximum joints opening

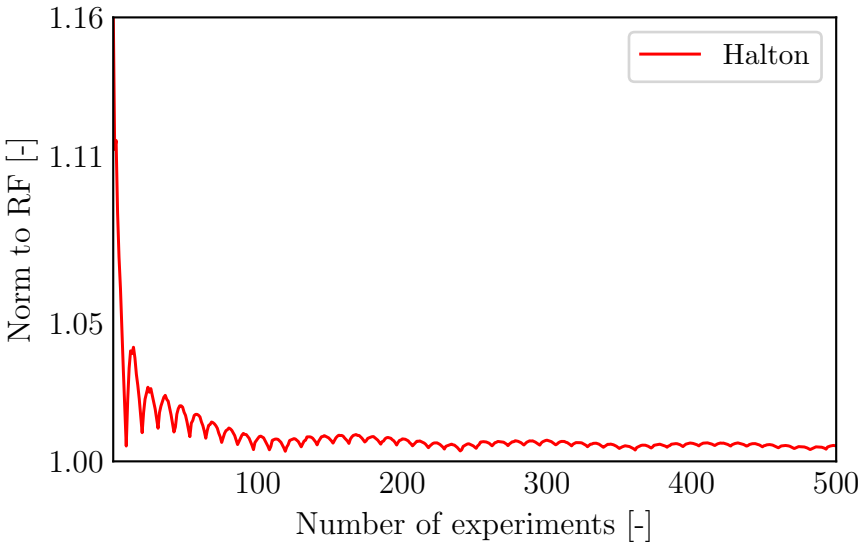

(b) Maximum joints slippage

Fig. 3.42: Model D - EDPs sampling convergence

3.18 Validation of metamodels

Using the outputs EDPs obtained at the DOE simulation points, one metamodel for each DOE technique and for each EDP was constructed and fitted with least squares on the DOE step. The coefficients are not reported here for the sake of brevity. Using this fitted polynomials, outputs corresponding to a big number of samples, generated on the previous section, are estimated for validation.

Considering that the number of metamodels is equal to the product of DOE procedures, EDPs responses and possible polynomials degrees, it would be cumbersome to report all the combinations here. Hence, not all of them will be reported, but only the quadratic version of them, whenever possible, and the linear version otherwise.

Estimations are reported in a series of scatter plots. The abscissas correspond to predicted values, whereas the actually observed values are on the ordinate. The closer the scatter points are to the 45 degrees line, the more accurate the prediction is.

Slippage of joints seems to be the most disperse EDP, followed by crest accelerations, joint openings, and tensile stresses. Displacements are the least disperse values, and can be accurately predicted.

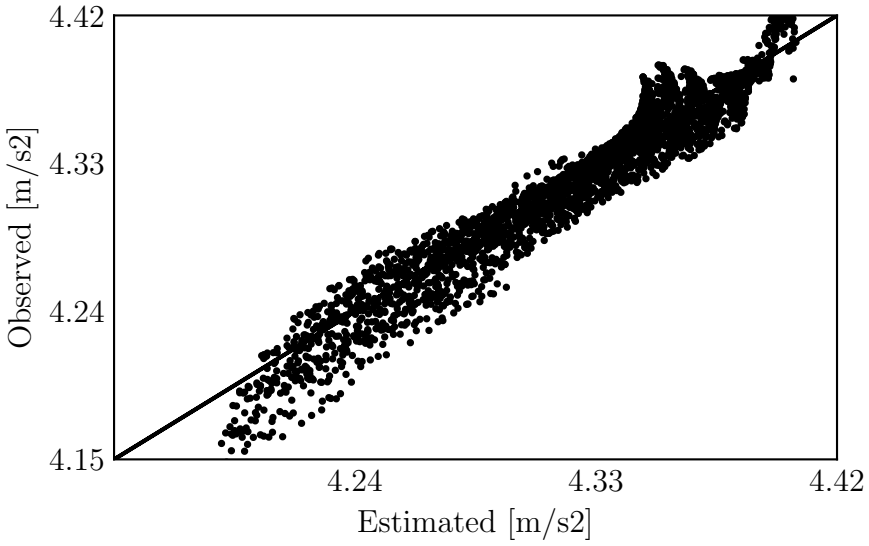

(a) Quadratic FFD3

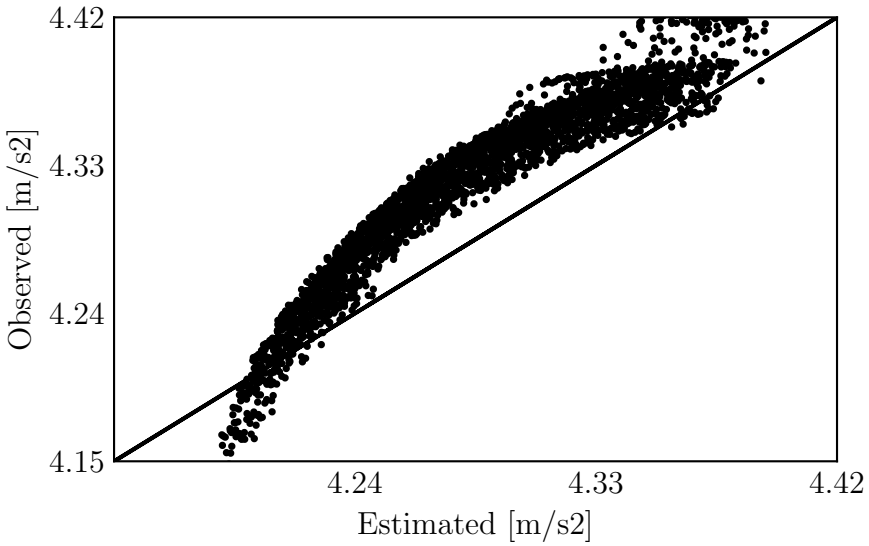

(b) Quadratic FFD2

Fig. 3.43: Model A - Maximum Crest Acceleration estimation

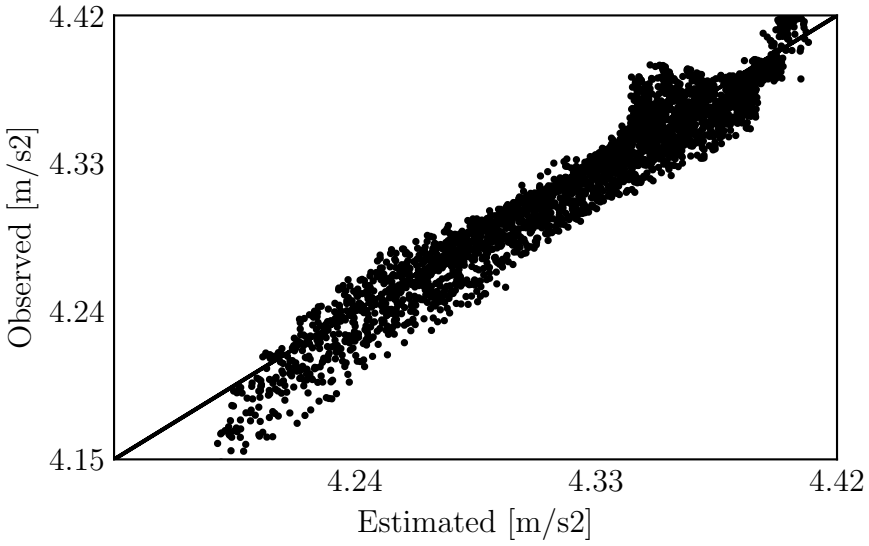

(c) Quadratic BOXB

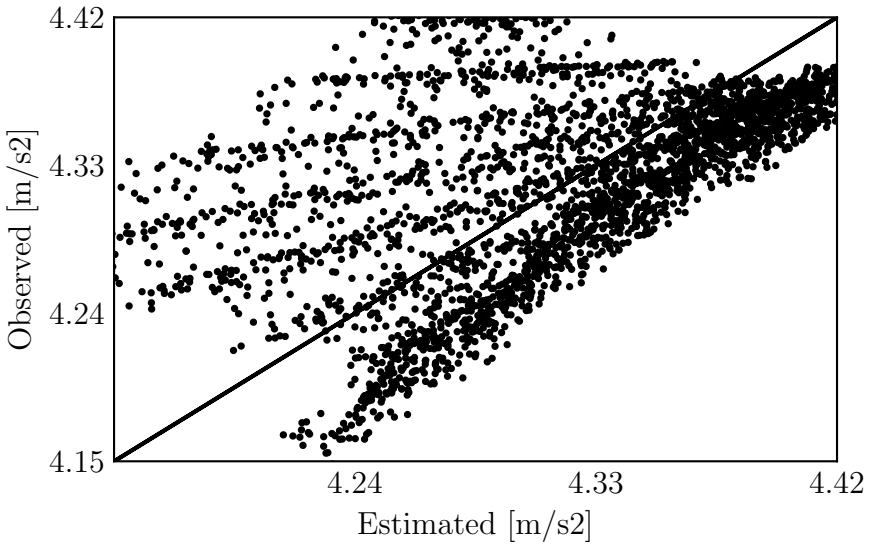

(d) Quadratic CCD

Fig. 3.43: Model A - Maximum Crest Acceleration estimation

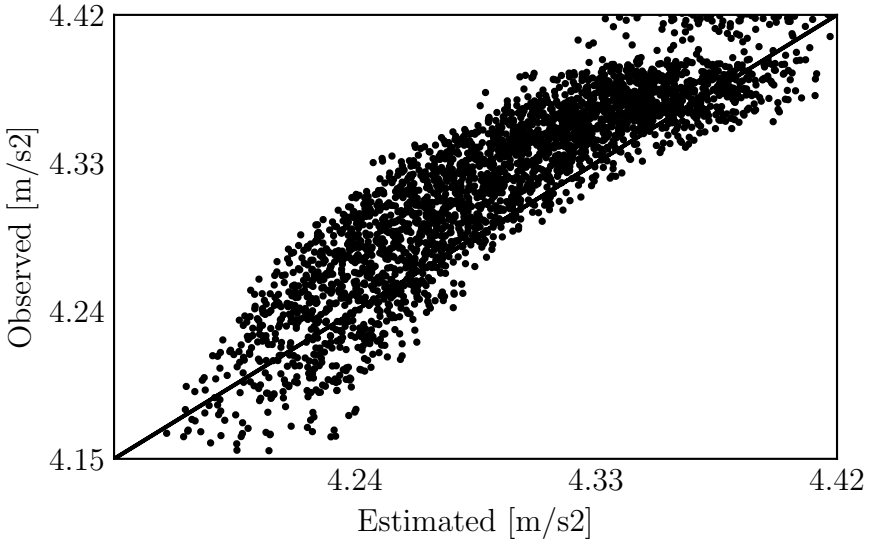

(e) Linear PBD

Fig. 3.43: Model A - Maximum Crest Acceleration estimation

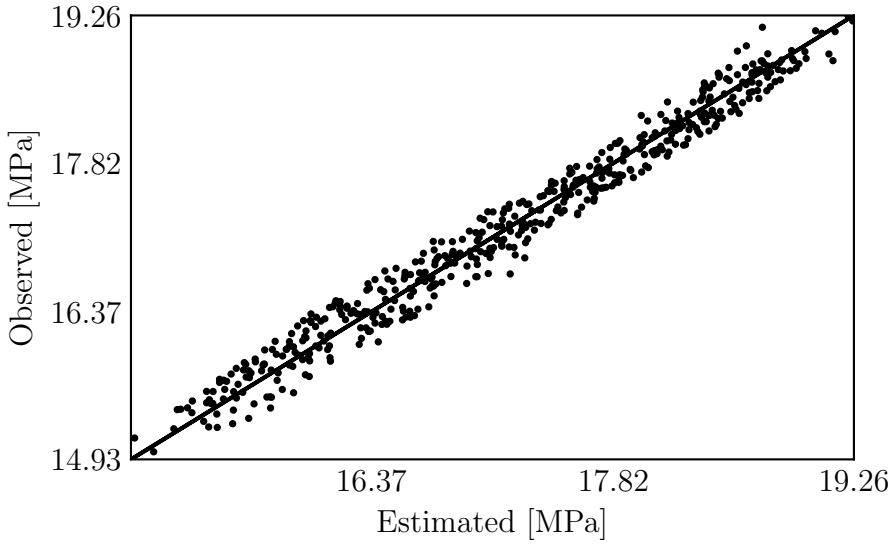

(a) Quadratic FFD3

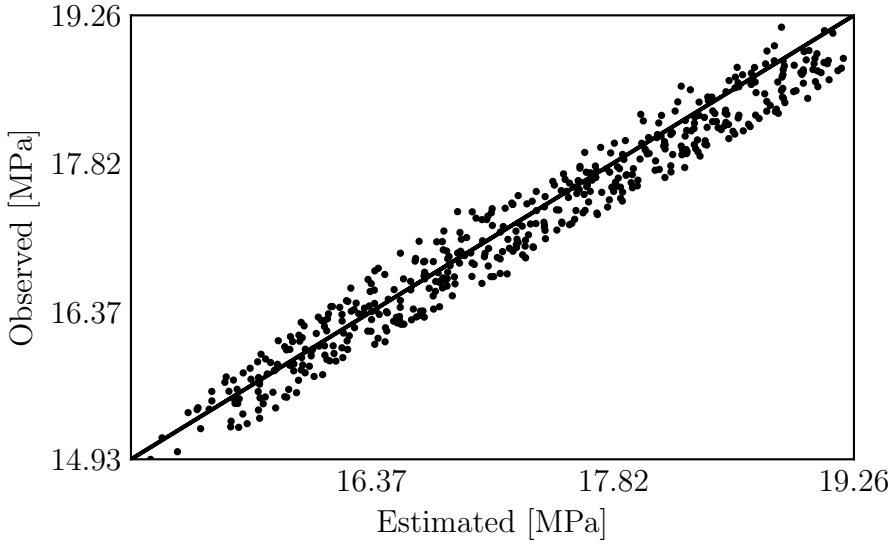

(b) Quadratic FFD2

Fig. 3.44: Model B - Maximum Tensile Stress estimation

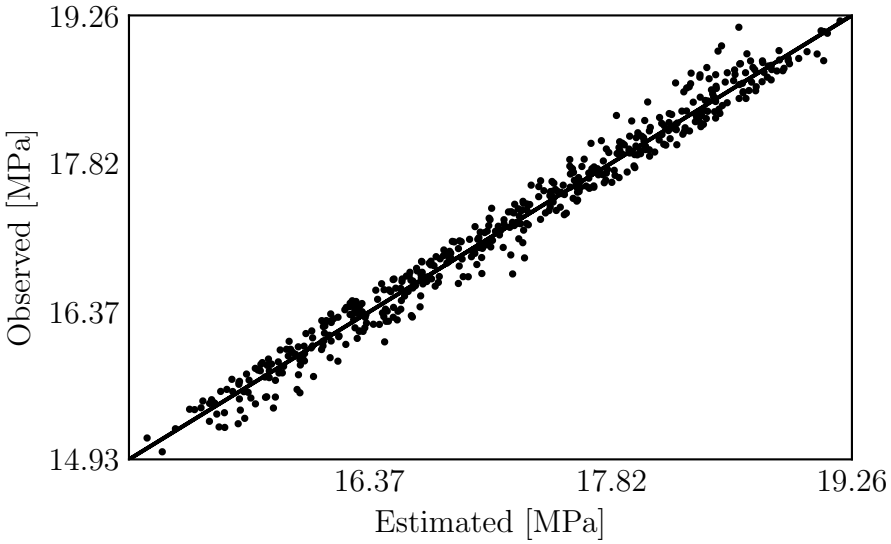

(c) Quadratic BOXB

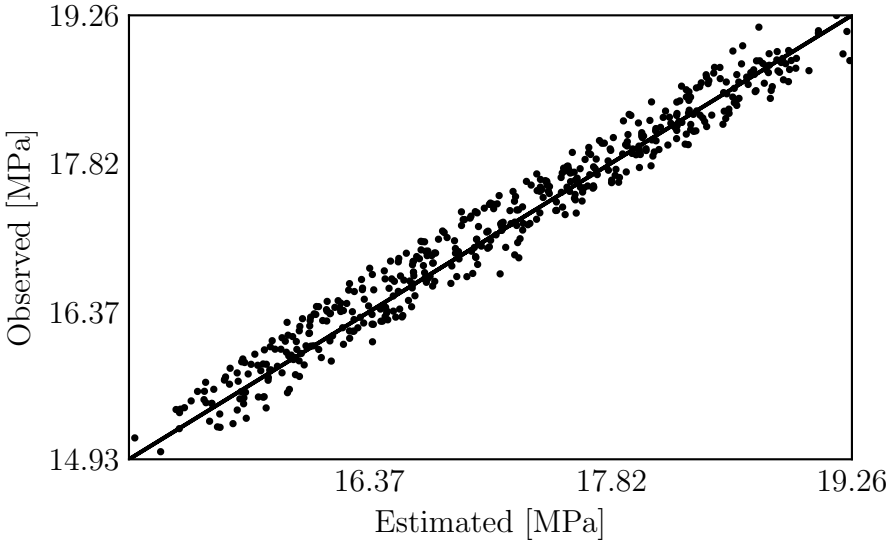

(d) Quadratic CCD

Fig. 3.44: Model B - Maximum Tensile Stress estimation

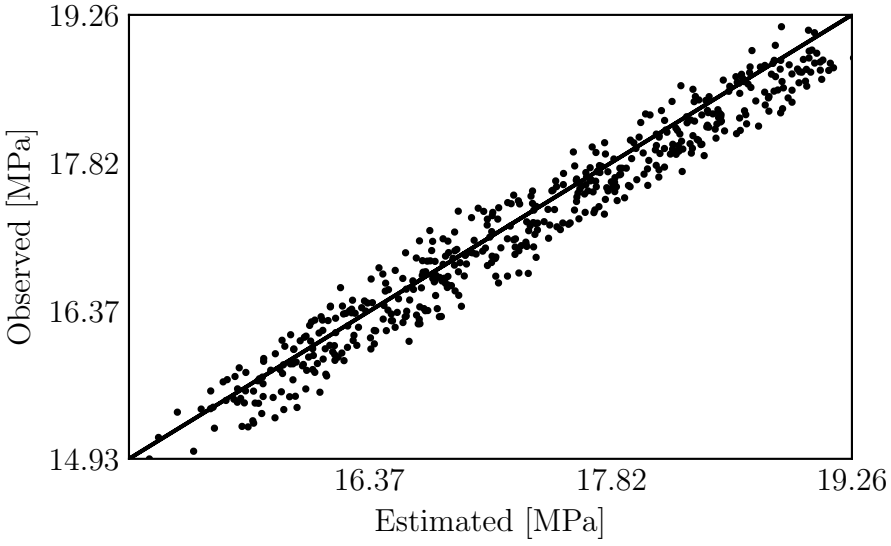

(e) Linear PBD

Fig. 3.44: Model B - Maximum Tensile Stress estimation

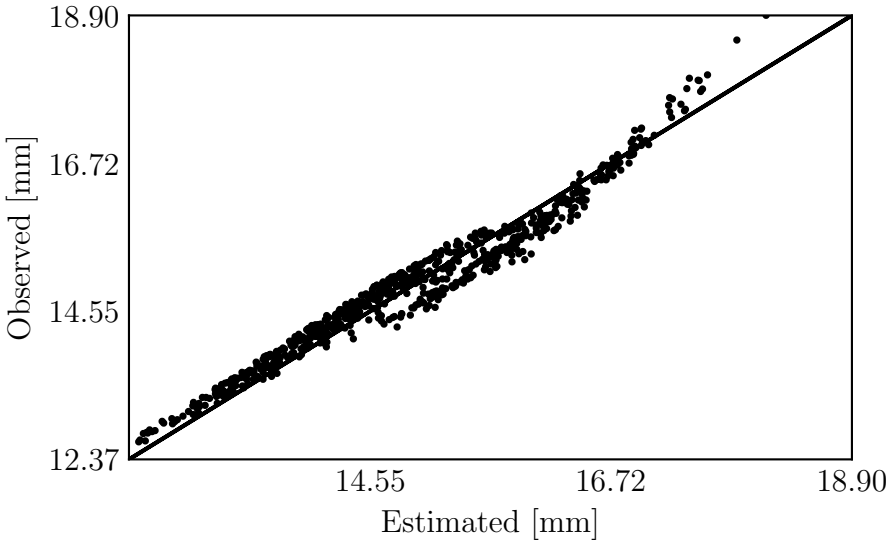

(a) Quadratic FFD3

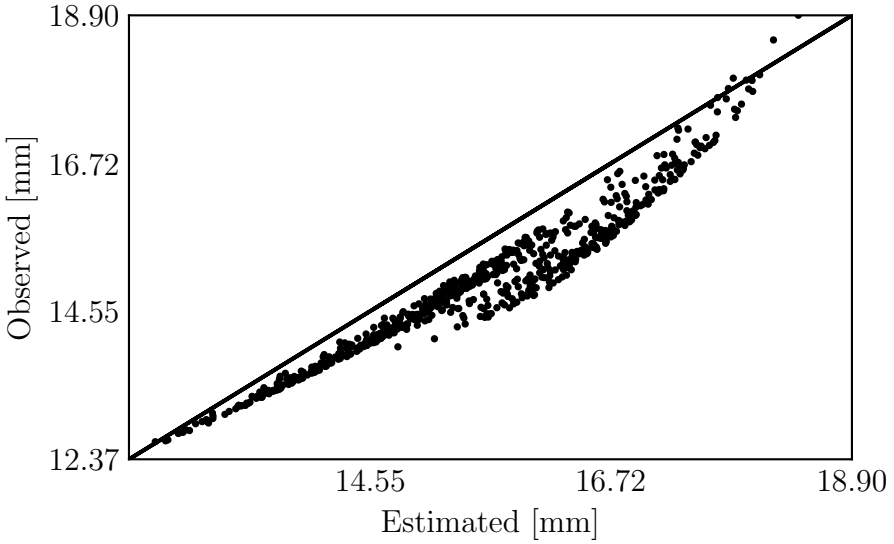

(b) Quadratic FFD2

Fig. 3.45: Model C - Maximum Joints Opening

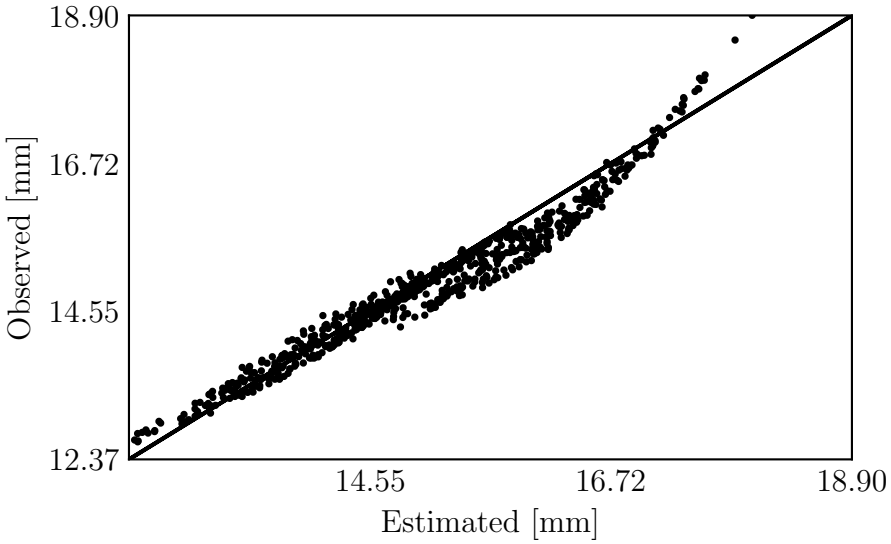

(c) Quadratic BOXB

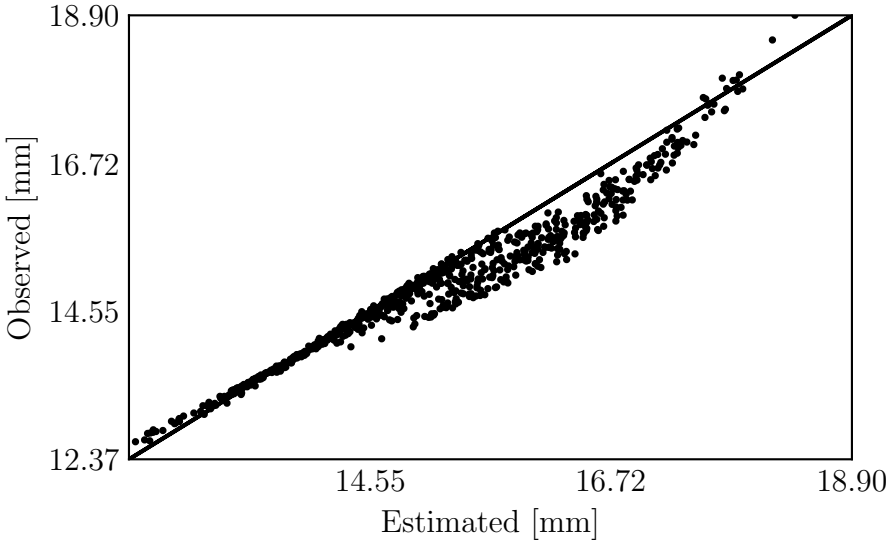

(d) Quadratic CCD

Fig. 3.45: Model C - Maximum Joints Opening

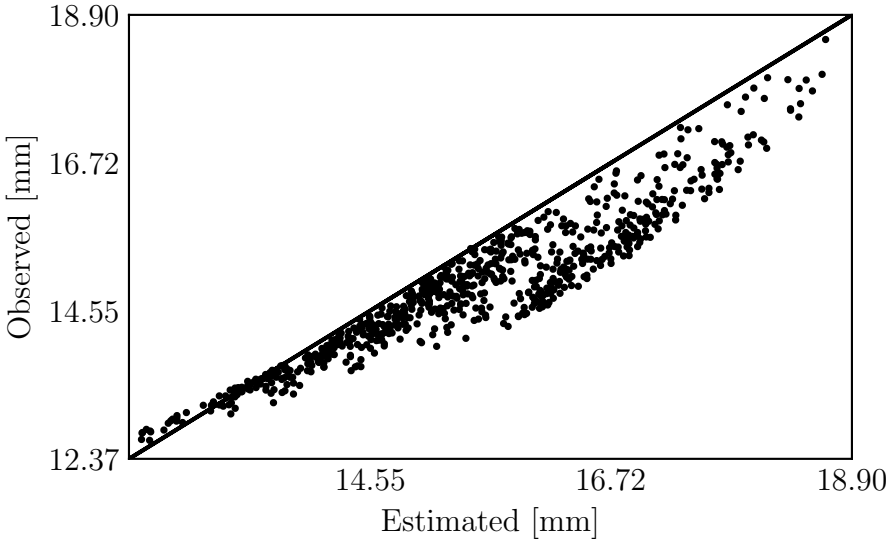

(e) Linear PBD

Fig. 3.45: Model C - Maximum Joints Opening

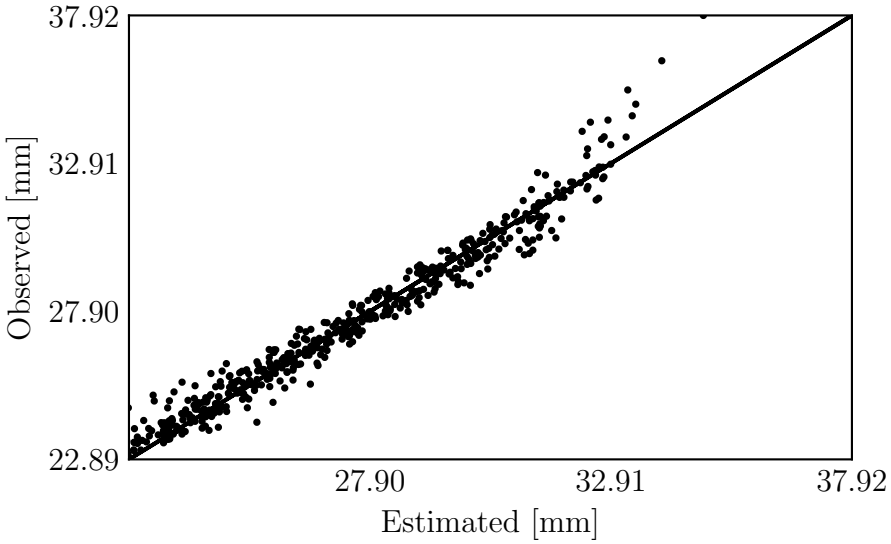

(a) Quadratic FFD3

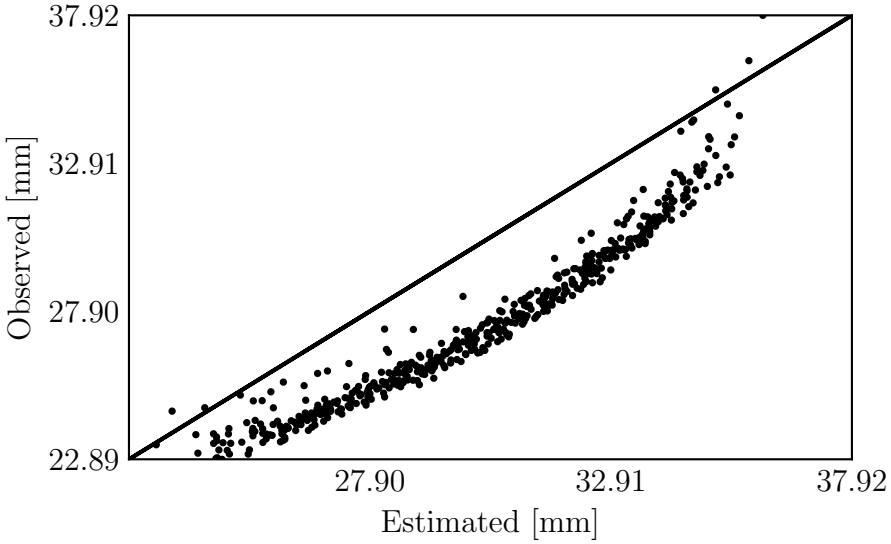

(b) Quadratic FFD2

Fig. 3.46: Model D - Maximum Joints Slippage

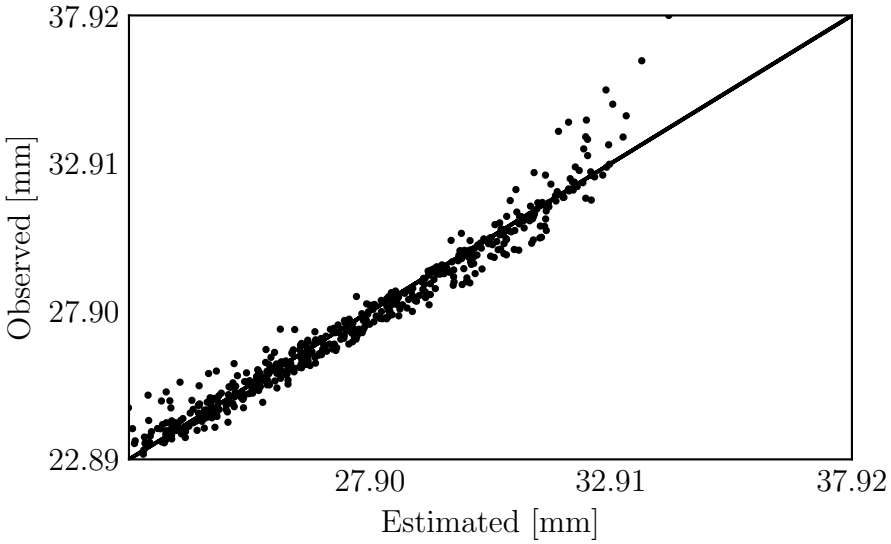

(c) Quadratic BOXB

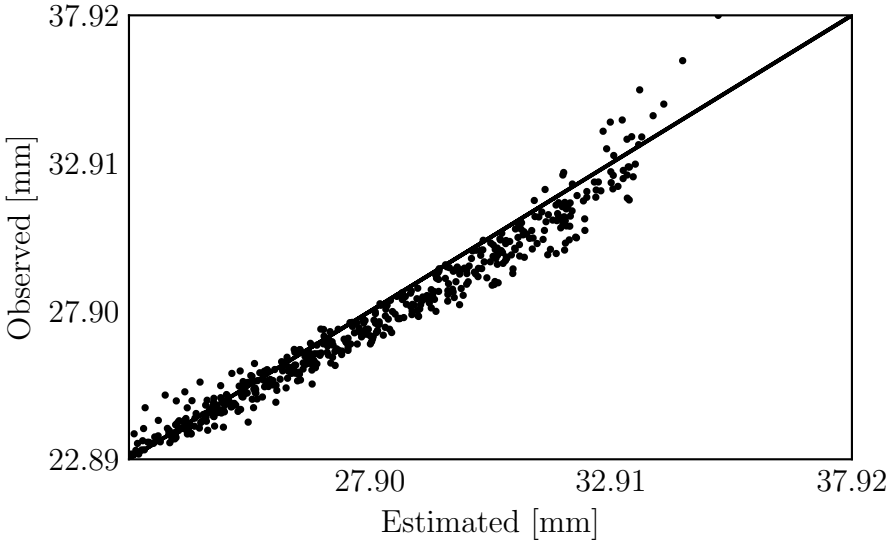

(d) Quadratic CCD

Fig. 3.46: Model D - Maximum Joints Slippage

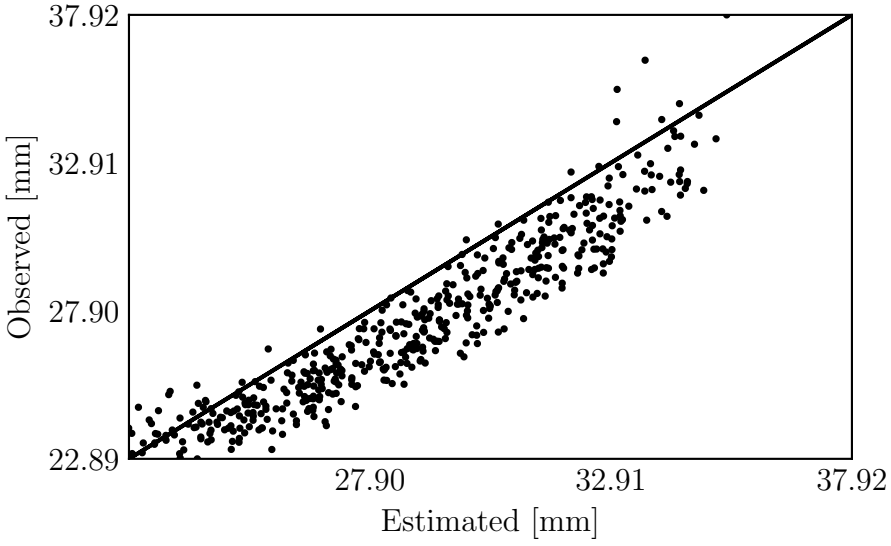

(e) Linear PBD

Fig. 3.46: Model D - Maximum Joints Slippage

3.18.1 Goodness of fitting

The R^2 Normal Regression Parameter is used to asses the goodness of fitness (GOF) of the multi-linear metamodels.

In general FFD3 gives the most accurate metamodels, for every EDP. Yet, as explained before, the amount of experiments it requires simply makes it impractical for several variables. On the other hand, FFD2 is not satisfactory for non linear models. It fails to predict acceleration in linear models as well. This is because, as the DOE only considers extreme values, cannot estimate the curvature of the hipersurface response. CCD fails to predict accelerations for linear models as well. The reason is not clear. It would seem that the acceleration EDP generates a particularly curve RSM with a high curvature. PBD behaves surprisingly well for the number of experiments it requires. Using only 8 design points, it can roughly describe the distribution of joints opening and slippage. This is specially useful for quick evaluations of as a check tool. Box Behnken design seems to be the most accurate for the number of experiments method, reaching the same order of accuracy as FFD3. It can describe the curvature of every RSM in this research. For this reason, it is concluded this is the recommended DOE technique for arch dams.

Next the R^2 parameter is presented for each EDP estimated on the previous section.

Quadratic polynomials have better accuracy compared to the correspondent linear versions depending on the DOE technique. In general, their capacity for estimating is similar for linear models. Also, cubic polynomials are not better predictors in any case. This is caused by the *overfitting* effect, which means that the model commits so much to the sample data that it trades-off its capacity for adapting to the new samples used for validation.

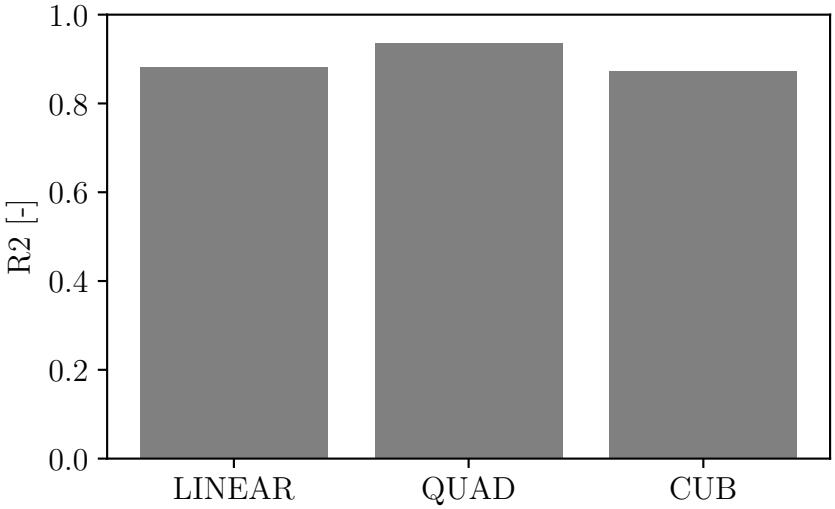

(a) FFD3

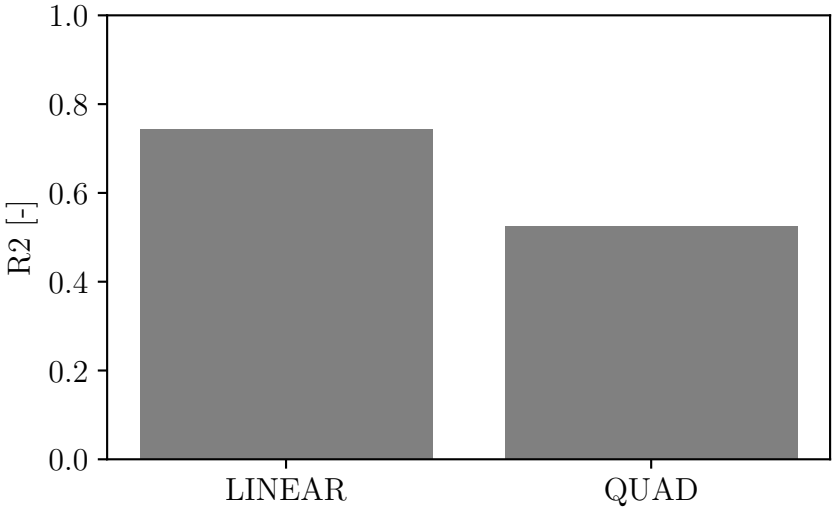

(b) FFD2

Fig. 3.47: Model A - GOF of DOEs for Maximum Crest Acceleration

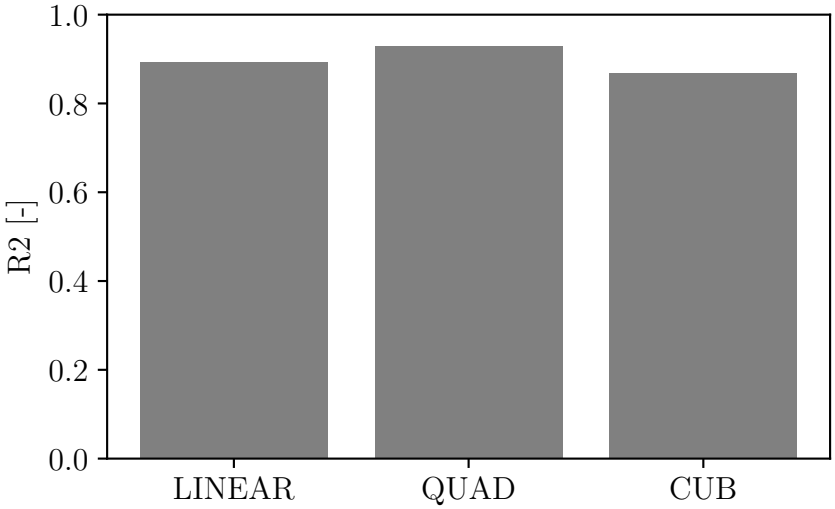

(c) BOXB

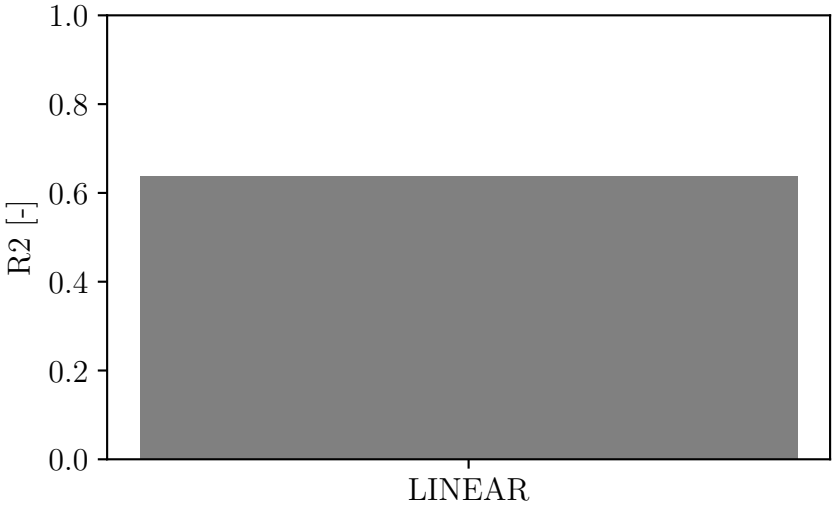

(d) PBD

Fig. 3.47: Model A - GOF of DOEs for Maximum Crest Acceleration

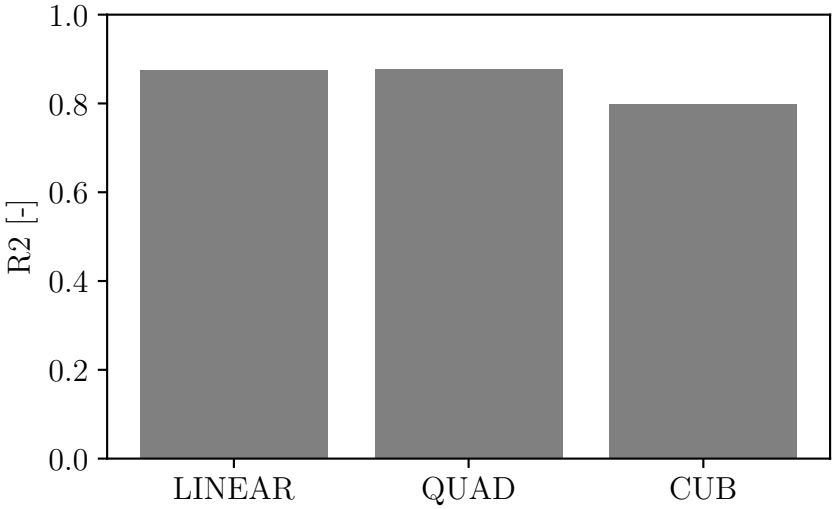

(a) FFD3

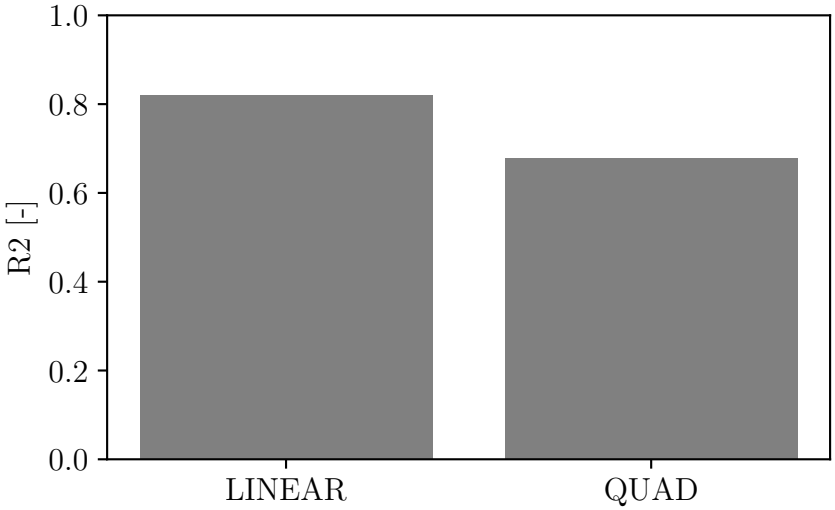

(b) FFD2

Fig. 3.48: Model B - GOF of DOEs for Maximum Tensile Stress

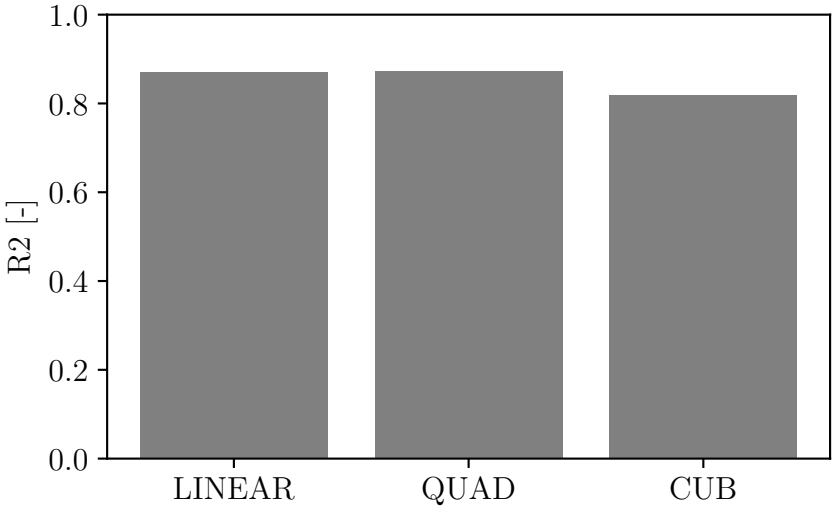

(c) BOXB

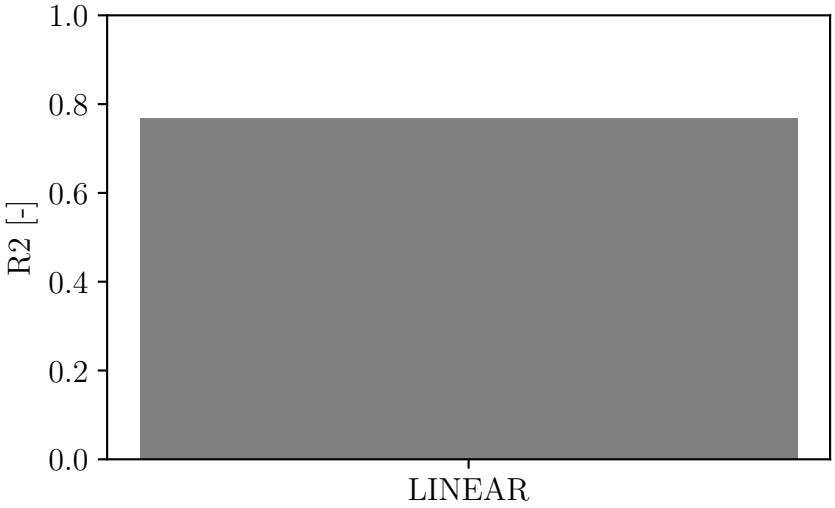

(d) PBD

Fig. 3.48: Model B - GOF of DOEs for Maximum Tensile Stress

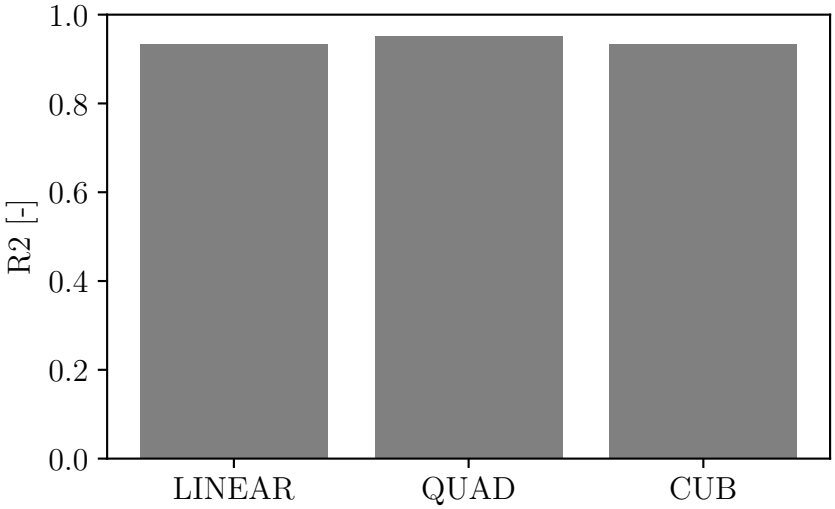

(a) FFD3

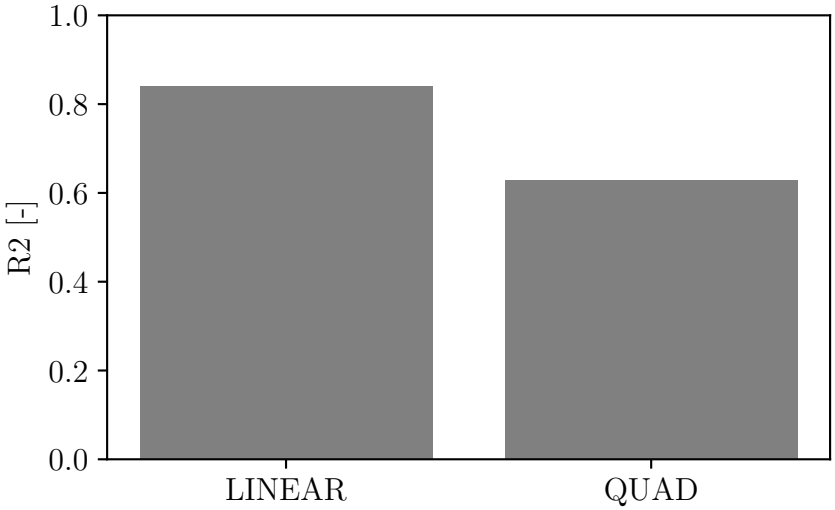

(b) FFD2

Fig. 3.49: Model C - GOF of DOEs for Maximum Joints Opening

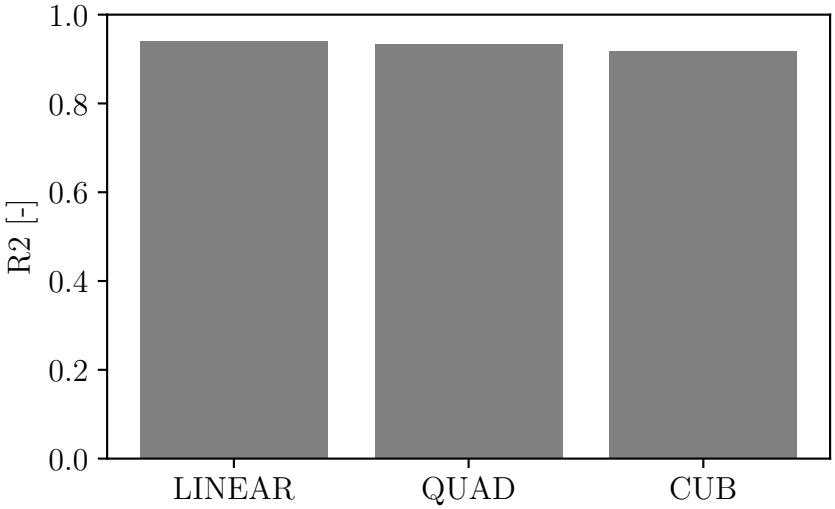

(c) BOXB

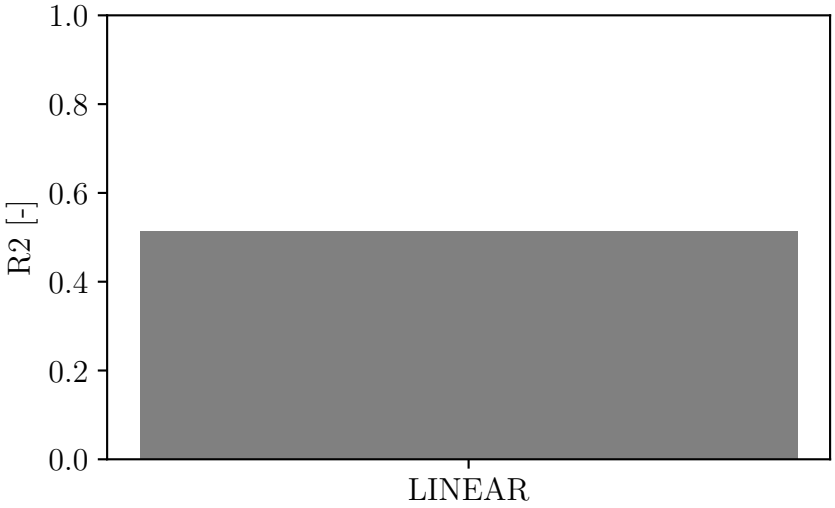

(d) PBD

Fig. 3.49: Model C - GOF of DOEs for Maximum Joints Opening

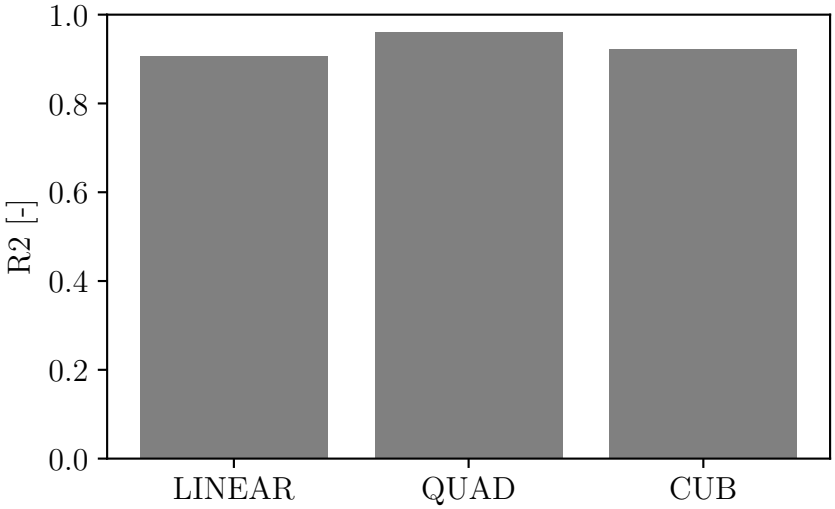

(a) FFD3

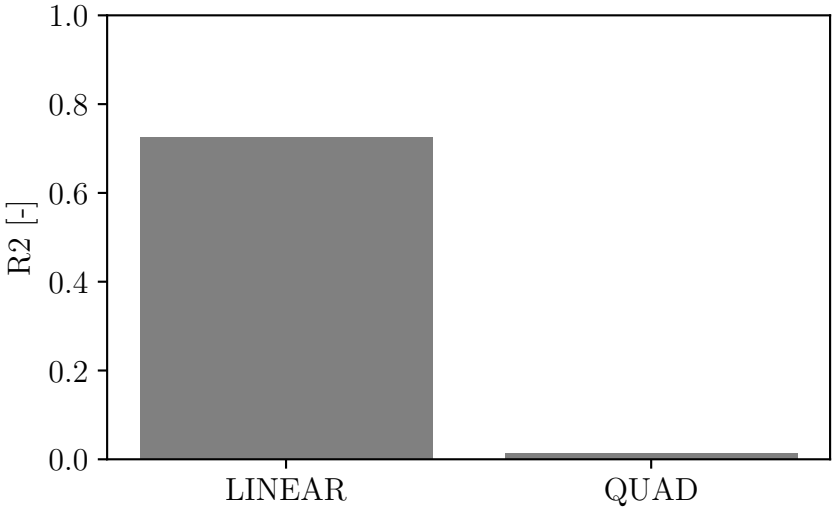

(b) FFD2

Fig. 3.50: Model D - GOF of DOEs for Maximum Joints Slippage

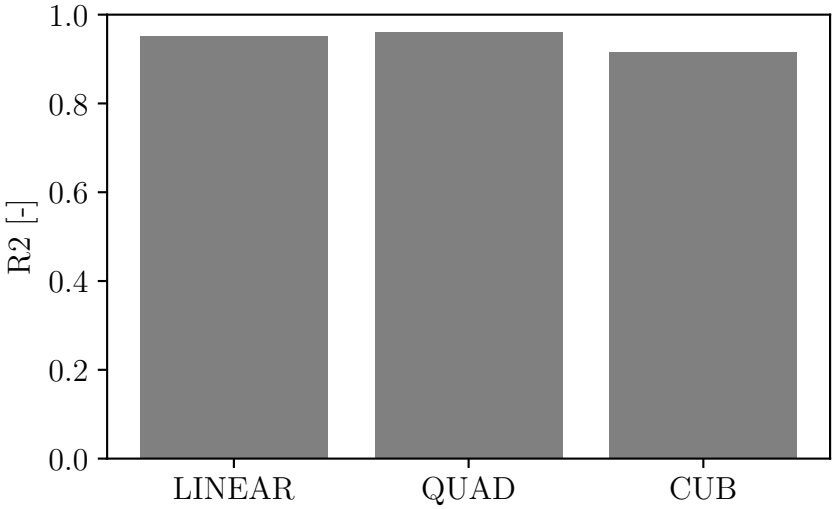

(c) BOXB

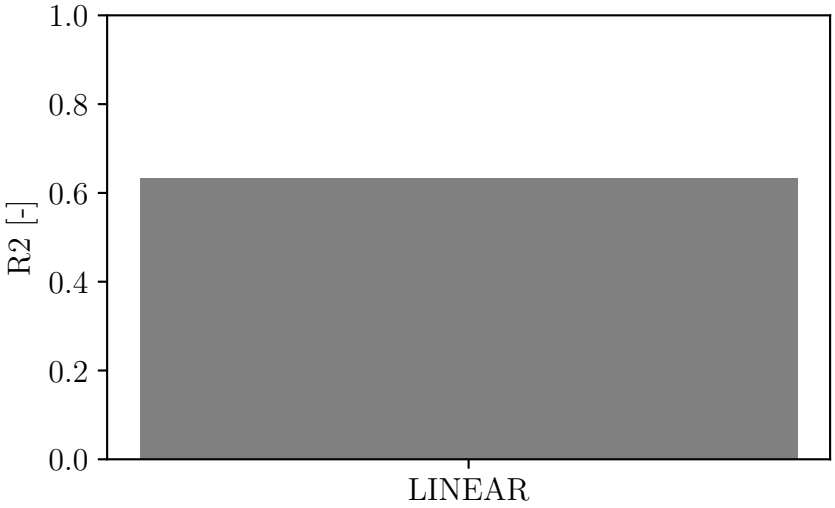

(d) PBD

Fig. 3.50: Model D - GOF of DOEs for Maximum Joints Slippage

3.18.2 Application of RSM in uncertainty analysis

Once a metamodel is fitted and validated, it can be used in any uncertainty quantification. As a brief example, 100×10^3 analysis are performed on a BBOX metamodel, to find out the probability of exceedance of the maximum crest displacement, and compared with the one obtained from the 3000 FE simulations.

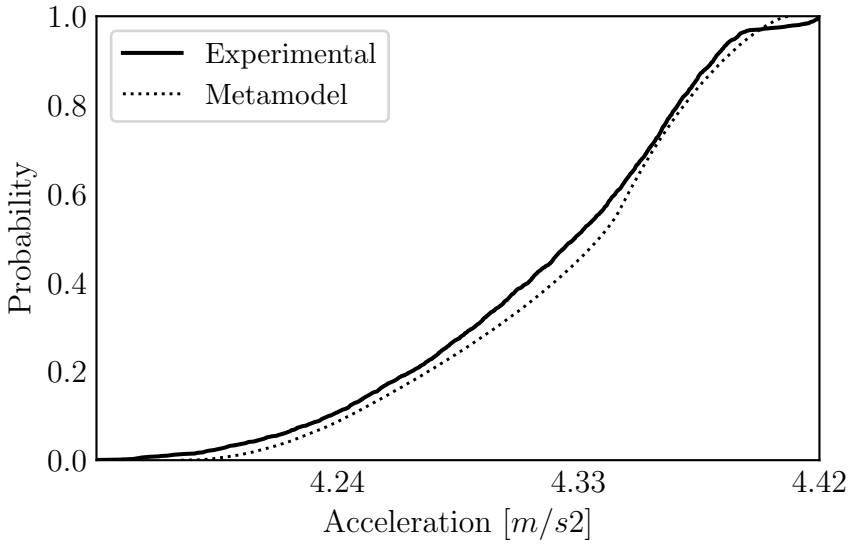

Fig. 3.51: Model A - CDF of Maximum crest displacement of experiments required by each DOE technique

With this simple example it becomes clear that metamodels developed with Box Behnken technique are specially suited for estimating structural responses of dam-reservoir coupled systems. For uncertainty analysis, the calculation time with metamodels is negligible compared to the corresponding for FE models, and the resultant precision is considered to be acceptable.

This allows to conclude that metamodels constitute a valid an powerful tool for arc dams safety probabilistic evaluation.

4. Conclusions

The present investigation is based on the use of metamodels for uncertainty analysis of concrete arch dams. The Response Surface Method is presented and proposed for the task.

In order to evaluate its applicability, two case studies were taken into consideration. As a previous step, aspects regarding to simulation of fluid structure interaction and non linear joints has been studied in depth, in order to develop finite element models suited for a big number of deterministic analysis, required for validation of the metamodels. Acoustic finite elements were introduced and their usage has been studied in known problems from dam literature. After that, restrictive hypothesis were removed one by one, to evaluate their effects on the resultant thrust over the dam.

In particular, the need to introduce three-dimensional models for curved dams is evident, because the behaviour of these is strongly dependent on mechanisms that act in space. The effect of the energy absorption in the bottom of the reservoir is another important characteristic, since it significantly reduces the pressures on the face of the structure. Although it is difficult to measure, it seems sufficient to consider an intermediate value of acoustic impedance. The effect of two commonly ignored conditions, the relative depth of the reservoir and the direction of the oscillation imposed on the structure were also analyzed. The first one turned out to be of medium importance, since it modifies the periods of the coupled system and induces important variations in the amplification of the hydrodynamic thrust. The second can be ignored safely for curved dams. In addition to these other factors were studied, related to the numerical simulation of the phenomenon under study. It was found that the beating of acoustic waves occurs when no energy dissipation mechanism is considered. The effect of joints between cantilevers was also analyzed. The increment on structural displacements resulting from their inclusion is notorious. Nevertheless, perimeter joints were not modelled, in order to reduce computational effort required on the next

phase.

At a later stage, four models were considered, two monolithic and their jointed versions. Two static loads and a strong motion were imposed as loads to the structure. A sensitivity analysis was executed, to identify primary factors corresponding to different outputs. It turned out that input factors affect different structural outputs in a well differentiated manner. Next, different Design of Experiment techniques were adopted, and after carrying on the simulation at those design points, linear, quadratic and cubic polynomials metamodels were fitted. Over seven thousand deterministic analysis were run in order to provide a framework for validation. Precision were discussed for different metamodels, output responses and polynomial degrees. In general, it was found that the Box Behnken design of experiments technique is well suited for building metamodels for arc dams. The obtained level of precision was roughly equal to the achieved with full factorial designs. It was also found that all the selected output parameters, namely, maximum crest displacement, maximum crest acceleration, maximum principal tensile stress, maximum principal compressive stress, maximum joint opening and maximum joint slippage were satisfactorily estimated by quadratic Response Surface metamodels developed with Box Benhken design. The probability of exceedance of the maximum acceleration at the crest of an arch dam was calculated as an example application.

Finally, it is concluded that the proposed method is consistent for uncertainty modelling of both linear and non linear arc dams and other large coupled systems as well. The main advantage they provided is to save computational effort on a great amount. Metamodels are not exclusive of structural engineering, and can be used in any applied science to estimate responses of complex systems, to improve designs, check prototypes, identify important input factors interactions, among other uses.

Bibliography

[1] International Comission on Large Dams - ICOLD, *General Synthesis Number of Dams by Country Members*, 2019. [Online]. Available: `https://www.icold-cigb.org/article/GB/world%7B%5C_%7Dregister/general%7B%5C_%7Dsynthesis/number-of-dams-by-country-members` (visited on 01/01/2019).

[2] Ministero delle Infrastrutture e dei Trasporti, "Norme tecniche per la progettazione e la costruzione degli sbarramenti di ritenuta (dighe e traverse)," *Decreto Ministeriale 26 Giugno 2014*, vol. 1, p. 156, 2014.

[3] Parlamento Italiano, "Conversione in legge, con modificazioni, del decreto-legge 29 marzo 2004, n. 79, recante disposizioni urgenti in materia di sicurezza di grandi dighe," 2004.

[4] M. A. Hariri-Ardebili, "Mcs-based response surface metamodels and optimal design of experiments for gravity dams," *Structure and Infrastructure Engineering*, vol. 14, no. 12, pp. 1641–1663, 2018.

[5] M. U. of Science and Technology, "Probabilistic engineering design," *Missouri University of Science and Technology*,

[6] M. D. McKay, R. J. Beckman, and W. J. Conover, "Comparison of three methods for selecting values of input variables in the analysis of output from a computer code," *Technometrics*, vol. 21, no. 2, pp. 239–245, 1979.

[7] J. Halton and G. Smith, "Radical inverse quasi-random point sequence, algorithm 247," *Commun. ACM*, vol. 7, p. 701, 1964.

[8] I. M. Sobol', "On the distribution of points in a cube and the approximate evaluation of integrals," *Zhurnal Vychislitel'noi Matematiki i Matematicheskoi Fiziki*, vol. 7, no. 4, pp. 784–802, 1967.

[9] R. A. Fisher, *The design of experiments*. Oliver and Boyd; Edinburgh; London, 1937.

[10] G. E. Box and D. W. Behnken, "Some new three level designs for the study of quantitative variables," *Technometrics*, vol. 2, no. 4, pp. 455–475, 1960.

[11] G. Box and D. Behnken, "Simplex-sum designs: A class of second order rotatable designs derivable from those of first order," *The Annals of Mathematical Statistics*, vol. 31, no. 4, pp. 838–864, 1960.

[12] R. L. Plackett and J. P. Burman, "The design of optimum multifactorial experiments," *Biometrika*, vol. 33, no. 4, pp. 305–325, 1946.

[13] G. E. Box and K. B. Wilson, "On the experimental attainment of optimum conditions," *Journal of the Royal Statistical Society: Series B (Methodological)*, vol. 13, no. 1, pp. 1–38, 1951.

[14] United States Army Corps of Engineers - USACE, "Time-history dynamic analysis of concrete hydraulic structures," no. EM 1110-2-6051, p. 401, 2003.

[15] H. M. Westergaard, "Water pressures on dams during earthquakes," *Transaction American Society of Civil Engineering - ASCE*, vol. 95, pp. 418–433, 1933.

[16] Ministry of Construction, "The River Law n. 167 – Legal Framework for River and Water Management in Japan," *River Bureau*, no. 4, 1964.

[17] T. Von Kármán, "Discussion of water pressures on dams during earthquakes," *Transaction American Society of Civil Engineering - ASCE*, vol. 98, pp. 434–436, 1933.

[18] Ministero delle Infrastrutture e dei Trasporti, "Regolamento Italiano Dighe," *D.P.R. n. 1.363*, 1959.

[19] C. N. Zangar, "Hydrodynamic pressures on dams due to horizontal earthquake effects," *Technical Information Office*, no. 11, 1952.

[20] Ministero delle Infrastrutture e dei Trasporti, "Regolamento Italiano Dighe," *Decreto Ministeriale 24 Marzo 1982*, 1982.

[21] G. W. Housner, "Dynamic pressures on accelerated fluid containers," *Bulletin of the seismological society of America*, vol. 47, no. 1, pp. 15–35, 1957.

[22] A. T. Chwang and G. W. Housner, "Hydrodynamic pressures on sloping dams during earthquakes. part 1. momentum method," *Journal of Fluid Mechanics*, vol. 87, no. 2, pp. 335–341, 1978.

[23] P. P. Kulmaci, "Methode pratique pour la dètermination de l'action de l'eau sour le construction hydrotechnique massive, sommises aux oscillations," – *Reveu de la Riviste National pour la recherche scientifique*, vol. 74, 1964.

[24] A. K. Chopra, "Hydrodynamic pressures on dams during earthquakes," *Journal of the Engineering Mechanics Division*, vol. 93, no. 6, pp. 205–224, 1967.

[25] S. Kotsubo, "Dynamic water pressure on dams during earthquakes," in *Second world conference on earthquake engineering*, 1960, pp. 799–814.

[26] H. Brahtz and C. Heilbron, "Discussion of water pressures on dams during earthquakes," *Trans. ASCE*, vol. 98, pp. 452–460, 1933.

[27] J. Bustamante, E. Rosenblueth, I. Herrera, and A. Flores, "Presion hidrodinamica en presas y depositos," *Boletin Sociedad Mexicana de Ingenieria Sismica*, vol. 1, no. 2, 1963.

[28] C.-C. Chen, "The effect of dynamic fluid pressure on a dam during earthquakes," *Journal of Applied Mathematics and Mechanics*, vol. 25, no. 1, pp. 211–219, 1961.

[29] A. Chopra, "Earthquake analysis of arch dams, factors to be considered," *Journal of Structural Engineering*, vol. 138, no. 2, pp. 205–214, 2012.

[30] L. Zhang and A. K. Chopra, "Computation of spatially varying ground motion and foundation-rock impedance matrices for seismic analysis of arch dams," vol. 91, no. 6, 1991.

[31] G. Fenves and A. K. Chopra, "Effects of reservoir bottom absorption on earthquake response of concrete gravity dams," *Earthquake engineering & structural dynamics*, vol. 11, no. 6, pp. 809–829, 1983.

[32] Y. Ghanaat and B. B. Redpath, "Measurements of reservoir-bottom reflection coefficient at seven concrete damsites," 1995.

[33] Y. Calayir, A. Dumanoğlu, and A. Bayraktar, "Earthquake analysis of gravity dam-reservoir systems using the eulerian and lagrangian approaches," *Computers & structures*, vol. 59, no. 5, pp. 877–890, 1996.

[34] M. Akköse, S. Adanur, A. Bayraktar, and A. A. Dumanoğlu, "Elastoplastic earthquake response of arch dams including fluid–structure interaction by the lagrangian approach," *Applied Mathematical Modelling*, vol. 32, no. 11, pp. 2396–2412, 2008.

[35] G. Gladwell and G. Zimmermann, "On energy and complementary energy formulations of acoustic and structural vibration problems," *Journal of sound and vibration*, vol. 3, no. 3, pp. 233–241, 1966.

[36] A. Craggs, "The transient response of a coupled plate-acoustic system using plate and acoustic finite elements," *Journal of Sound and Vibration*, vol. 15, no. 4, pp. 509–528, 1971.

[37] Ministero delle Infrastrutture e dei Trasporti, "Norme tecniche per le costruzioni," *Decreto Ministeriale 14 Gennaio 2008*, 2008.

[38] Bundesamt für Wasser und Geologie, "Documentation de base pour la verification des ouvrages d'accumulation aux sèismes," 2003.

[39] United States Bureau of Reclamation - USBR, "Best Practices in dam and Leeve safety risk analysis," 2012.

[40] Federal Emergency Management Agency - FEMA, "Federal Guidelines for Dam Safety," no. April, 2004.

[41] Ministry of Land Infrastructure and Transport - MILT, "Draft of Guidelines for seismic safety evaluation of Dams," 2005.

[42] A. K. Chopra, P. Chakrabarti, and S. Gupta, "Earthquake response of concrete gravity dams including hydrodynamic and foundation interaction effects," CALIFORNIA UNIV BERKELEY EARTHQUAKE ENGINEERING RESEARCH CENTER, Tech. Rep., 1980.

[43] H. Tan and A. K. Chopra, "Dam-foundation rock interaction effects in earthquake response of arch dams," *Journal of Structural Engineering*, vol. 122, no. 5, pp. 528–538, 1996.

[44] S. Küçükarslan, "Dynamic analysis of dam–reservoir-foundation interaction in time domain," *Computational Mechanics*, vol. 33, no. 4, pp. 274–281, 2004.

[45] A. Bayraktar, E. Hançer, and M. Akköse, "Influence of base-rock characteristics on the stochastic dynamic response of dam–reservoir–foundation systems," *Engineering Structures*, vol. 27, no. 10, pp. 1498–1508, 2005.

[46] J.-T. Wang and A. K. Chopra, "Linear analysis of concrete arch dams including dam–water–foundation rock interaction considering spatially varying ground motions," *Earthquake Engineering & Structural Dynamics*, vol. 39, no. 7, pp. 731–750, 2010.

[47] M. Hariri-Ardebili and H. Mirzabozorg, "A comparative study of seismic stability of coupled arch dam-foundation-reservoir systems using infinite elements and viscous boundary models," *International Journal of Structural Stability and Dynamics*, vol. 13, no. 06, p. 1 350 032, 2013.

[48] M. K. Poul and A. Zerva, "Nonlinear dynamic response of concrete gravity dams considering the deconvolution process," *Soil Dynamics and Earthquake Engineering*, vol. 109, pp. 324–338, 2018.

[49] B. Ellingwood and P. B. Tekie, "Fragility analysis of concrete gravity dams," *Journal of infrastructure systems*, vol. 7, no. 2, pp. 41–48, 2001.

[50] Federal Energy Regulatory Commission - FERC, "Engineering Guidelines for the evaluation of Hydropower Projects," 1999.

[51] D. T. Lau, B. Noruziaan, and A. Razaqpur, "Modelling of contraction joint and shear sliding effects on earthquake response of arch dams," *Earthquake engineering & structural dynamics*, vol. 27, no. 10, pp. 1013–1029, 1998.

[52] M. Hariri-Ardebili, H. Mirzabozorg, and M. Kianoush, "Seismic analysis of high arch dams considering contraction-peripheral joints coupled effects," *Open Engineering*, vol. 3, no. 3, pp. 549–564, 2013.

[53] M. Alembagheri and M. Ghaemian, "Seismic performance evaluation of a jointed arch dam," *Structure and Infrastructure Engineering*, vol. 12, no. 2, pp. 256–274, 2016.

[54] J. de Araújo and A. M. Awruch, "Probabilistic finite element analysis of concrete gravity dams," *Advances in Engineering Software*, vol. 29, no. 2, pp. 97–104, 1998.

[55] P. B. Tekie and B. R. Ellingwood, "Seismic fragility assessment of concrete gravity dams," *Earthquake engineering & structural dynamics*, vol. 32, no. 14, pp. 2221–2240, 2003.

[56] S. Mirzahosseinkashani and M. Ghaemian, "Seismic fragility assessment of concrete gravity dams," in *Proceedings of the 29th annual USSD conference, Nashville, Tennessee, US*, 2009.

[57] Y. Ghanaat, P. S. Hashimoto, O. Zuchuat, and R. P. Kennedy, "Seismic fragility of mühleberg dam using nonlinear analysis with latin hypercube simulation," in *Proceeding, 31th USSD Annual Meeting and Conf*, 2011.

[58] Y. Ghanaat, R. Patev, and A. Chudgar, "Seismic fragility analysis of concrete gravity dams," in *Proceedings of the 15th world conference on earthquake engineering, Lisbon, Portugal*, 2012.

[59] ——, "Seismic fragility for risk assessment of concrete gravity dams," in *Proceeding of the USSD Annual Conference*, 2015, pp. 645–60.

[60] M. Alembagheri and M. Seyedkazemi, "Seismic performance sensitivity and uncertainty analysis of gravity dams," *Earthquake Engineering & Structural Dynamics*, vol. 44, no. 1, pp. 41–58, 2015.

[61] M. Hariri-Ardebili and V. Saouma, "Sensitivity and uncertainty quantification of the cohesive crack model," *Engineering Fracture Mechanics*, vol. 155, pp. 18–35, 2016.

[62] X. Yao, A. Elnashai, and J. Jiang, "Analytical seismic fragility analysis of concrete arch dams," in *Proceedings of the 15th World Conference on Earthquake Engineering*, 2012.

[63] H. Zhong, H. J. Li, and Y. L. Bao, "Seismic risk analysis of an arch dam," in *Applied mechanics and materials*, Trans Tech Publ, vol. 353, 2013, pp. 2020–2023.

[64] M. A. Hariri-Ardebili, V. E. Saouma, and K. A. Porter, "Quantification of seismic potential failure modes in concrete dams," *Earthquake Engineering & Structural Dynamics*, vol. 45, no. 6, pp. 979–997, 2016.

[65] T. W. Simpson, J. Poplinski, P. N. Koch, and J. K. Allen, "Metamodels for computer-based engineering design: Survey and recommendations," *Engineering with computers*, vol. 17, no. 2, pp. 129–150, 2001.

[66] L. Faravelli, "Response-surface approach for reliability analysis," *Journal of Engineering Mechanics*, vol. 115, no. 12, pp. 2763–2781, 1989.

[67] M. R. Rajashekhar and B. R. Ellingwood, "A new look at the response surface approach for reliability analysis," *Structural safety*, vol. 12, no. 3, pp. 205–220, 1993.

[68] S. K. Saha, V. Matsagar, and S. Chakraborty, "Uncertainty quantification and seismic fragility of base-isolated liquid storage tanks using response surface models," *Probabilistic Engineering Mechanics*, vol. 43, pp. 20–35, 2016.

[69] K. Hacıefendioğlu, H. B. Başağa, and S. Banerjee, "Probabilistic analysis of historic masonry bridges to random ground motion by monte carlo simulation using response surface method," *Construction and Building Materials*, vol. 134, pp. 199–209, 2017.

[70] S. De Grandis, M. Domaneschi, and F. Perotti, "A numerical procedure for computing the fragility of npp components under random seismic excitation," *Nuclear Engineering and Design*, vol. 239, no. 11, pp. 2491–2499, 2009.

[71] J. Park and P. Towashiraporn, "Rapid seismic damage assessment of railway bridges using the response-surface statistical model," *Structural Safety*, vol. 47, pp. 1–12, 2014.

[72] Q. Guo, L. Pei, Z. Zhou, J. Chen, and F. Yao, "Response surface and genetic method of deformation back analysis for high core rockfill dams," *Computers and Geotechnics*, vol. 74, pp. 132–140, 2016.

[73] M. E. Kartal, H. B. Başağa, and A. Bayraktar, "Probabilistic nonlinear analysis of cfr dams by mcs using response surface method," *Applied Mathematical Modelling*, vol. 35, no. 6, pp. 2752–2770, 2011.

[74] USGS, "USGS.gov — Science for a changing world," [Online]. Available: `https://www.usgs.gov/` (visited on 01/01/2019).

[75] Dassault Systèmes Simulia Corporation, "Coupled fluid-structural medium analysis," *Abaqus Theory Manual*, p. 2.9.1,

[76] H. M. Koh, J. K. Kim, and J.-H. Park, "Fluid–structure interaction analysis of 3-d rectangular tanks by a variationally coupled bem–fem and comparison with test results," *Earthquake engineering & structural dynamics*, vol. 27, no. 2, pp. 109–124, 1998.

[77] X. Liu, Y. Xu, G. Wang, and C. Zhang, "Seismic response of arch dams considering infinite radiation damping and joint opening effects," *Earthquake Engineering and Engineering Vibration*, vol. 1, no. 1, pp. 65–73, 2002.

[78] Hibbett, Karlsson, and Sorensen, "Abaqus/standard: User's manual," vol. 1, 1998.

[79] H. M. Hilber, T. J. Hughes, and R. L. Taylor, "Improved numerical dissipation for time integration algorithms in structural dynamics," *Earthquake Engineering & Structural Dynamics*, vol. 5, no. 3, pp. 283–292, 1977.

[80] N. M. Newmark *et al.*, "A method of computation for structural dynamics," 1959.

[81] J. P. Den Hartog, "Mechanical vibrations," 1985.